P-04-207

Oskarshamn site investigation

Drill hole KSH01A

Uniaxial compression test of intact rock

Lars Jacobsson
SP Swedish National Testing and Research Institute

May 2004

Svensk Kärnbränslehantering AB
Swedish Nuclear Fuel
and Waste Management Co
Box 5864
SE-102 40 Stockholm Sweden
Tel 08-459 84 00
+46 8 459 84 00
Fax 08-661 57 19
+46 8 661 57 19

ISSN 1651-4416
SKB P-04-207

Oskarshamn site investigation

Drill hole KSH01A

Uniaxial compression test of intact rock

Lars Jacobsson
SP Swedish National Testing and Research Institute

May 2004

Keywords: Rock mechanics, Uniaxial compressive strength, Uniaxial compression test, Elasticity parameters, Post-failure behaviour.

Abstract

Uniaxial compression tests, containing the complete loading response beyond compressive failure, so called post-failure tests, were carried out on 20 water saturated specimens of intact rock from borehole KSH01A in Simpevarp. The cylindrical specimens were taken from drill cores at four depth levels ranging between 299–320 m, 398–414 m, 486–498 m and 699–709 m. Moreover, the rock types were Quartz monzodiorite (299–320 m and 699–709 m) and Fine-grained dioritoid (398–414 m and 486–498 m). The elastic properties, represented by the Young's modulus and the Poisson ratio, and the peak value of the axial stress were deduced from these tests. The wet density of the specimens was determined before the mechanical tests. The specimens were documented by photographing the specimens before and after the mechanical testing.

The measured densities for the water saturated specimens were in the range 2,770–2,840 kg/m^3 and had a mean value of 2,798 kg/m^3. The peak values of the axial compressive stress were in the range 109.3–246.8 MPa with a mean value of 171.2 MPa. The elastic parameters were determined at load corresponding to 50% of the failure load and it was found that Young's modulus was in the range 66.0–103.9 GPa with a mean value of 80.8 GPa and the Poisson ratio was in the range of 0.17–0.33 with a mean value of 0.26. It should be remarked some results have been excluded in the summary above as some specimens contained defects (cracks) and a few data were judged to be not representative for the homogenous rock material. Furthermore, it was seen from the mechanical tests that the material in the specimens responded in a brittle way.

Contents

1 Introduction

Uniaxial compression tests, with loading beyond the failure point into the post-failure regime, have been conducted on water-saturated specimens sampled from borehole KSH01A in Simpevarp, see map in Figure 1-1. These tests belong to one of the activities performed as part of the site investigation nearby Oskarshamn lead by Swedish Nuclear Fuel and Waste Management Co (SKB). The tests were carried out in the material and rock mechanics laboratories at the department of Building Technology and Mechanics at Swedish National Testing and Research Institute (SP). All work is carried out in accordance with the activity plan AP PS 400-03-066 (SKB internal controlling document) and is controlled by SP-QD 13.1 (SP internal quality document).

SKB supplied SP with rock cores and they arrived at SP in May 2003 and were tested during March 2004. Cylindrical specimens were cut from the cores and selected based on the preliminary core logging with the strategy to primarily investigate the properties of the dominant rock type. The method description SKB MD 190.001, (SKB internal controlling document) was followed for the sampling and for the compression tests and the method description SKB MD 160.002, (SKB internal controlling document) was followed when the density was determined. As to the specimen preparation, the end surfaces on the specimens were grinded in order to comply with the required shape tolerances and then put in water and kept stored in water, with a minimum of 7 days, up to testing. This yields a water saturation, which is intended to resemble the in-situ moisture condition. The density was determined on each specimen and the uniaxial compression tests were carried out at this moisture condition. The specimens were photographed before and after the mechanical testing.

The uniaxial compression tests were carried out using radial strain as the feed back signal in order to obtain the complete response in the post-failure regime on brittle specimens as is described in the method description SKB MD 190.001, (SKB internal controlling document) and in the ISRM suggested method /1/. The axial ε_a and radial ε_r strains together with the axial stress σ_a were recorded during the tests. The peak value of the axial compressive stress σ_c was determined at each test. Furthermore, two elasticity parameters, Young's modulus E and Poisson ratio v, were deduced from the tangent properties at 50 % of the peak load. Diagrams with the volumetric and crack volumetric strain versus axial stress are reported. These diagrams can be used to determine crack initiation stress σ_i and the crack damage stress σ_d,
cf. /2, 3/.

Figure 1-1. *Location of the borehole at the Oskarshamn site.*

2 Objective and scope

The purpose of the testing is to determine the uniaxial compressive strength and the elastic properties, represented by the Young's modulus and the Poisson ratio, of a cylindrical intact rock core with a water content corresponding to the in-situ conditions. Furthermore, the loading is carried out into the post-failure regime in order to study the mechanical behaviour of the rock after cracking and thereby be able to determine the brittleness and residual strength.

The results from the tests are going to be used in the site descriptive rock mechanics model, which will be established for the candidate area selected for site investigations at Simpevarp.

3 Equipment

A circular saw with a diamond blade was used to cut the specimens to their final lengths. The surfaces were then grinded after cutting in a grinding machine in order to achieve a high-quality surface for the axial loading that complies with the required tolerances. The measurements of the specimen dimensions were made with a sliding calliper. Furthermore, the tolerances were checked by means of a dial indicator and a stone face plate. The specimen preparation is carried out in accordance with ASTM 4543-01 /4/.

The specimens and the water were weighted using a scale for weight measurement. A thermometer was used for the water temperature measurement. The calculated wet density was determined with an uncertainty of ± 4 kg/m^3.

The mechanical tests were carried out in a servo controlled testing machine specially designed for rock tests, see Figure 3-1. The system consists of a load frame, a hydraulic pump unit, a controller unit, a PC and various sensors. The communication with the controller unit is made by means of special testing software running on a PC that is connected to the controller. The load frame has a high stiffness and a fast responding actuator cf. the ISRM suggested method /1/. The stiffness of the various components in the loading chain in the load frame has been optimized in order to obtain a high total stiffness. This includes, the load frame, load cell, load platens and piston, as well as minimizing the amount of hydraulic oil in the cylinder. Furthermore, the sensors, the controller and the servo valve are fast responding components.

The axial load is determined using a load cell, which has a maximum capacity of 1.5 MN. The uncertainty of the load measurement is less than 1% according to the calibration results. The axial and circumferential (radial) deformations of the rock specimen were measured. The rock deformation measurement systems are based on miniature LVDTs which have a measurement range of +/– 2.5 mm. The LVDTs were calibrated by means of a special calibration tool using a micrometer and they displayed an accuracy of +/– 2.5 % within a +/– 2 mm range that was used in the tests.

Figure 3-1. *Rock testing system. From left: Digital controller unit, pressure cabinet (used for triaxial tests) and load frame. The PC with the test software (not shown in the picture) is placed on the left hand side of the controller unit.*

Two independent systems were used for the axial deformation measurement in order to obtain two comparative results. The first system (S1), see Figure 3-2, comprises two aluminium rings that are attached on the specimen placed at ¼ and ¾ of the specimen height. Two LVDTs mounted on the rings are used to measure the distance change between the rings on opposite sides of the specimen. As to the attachment, a rubber band made of thin rubber hose with 0.5 mm thickness is first mounted on the specimen right under where the rings are to be mounted. The rings have three adjustable spring-loaded screws each with a rounded tip pointing towards the specimen with 120 degrees division. The rings are mounted on the specimen with small round washers put in between the screws and the rubber band. The washers distribute the load from the screws on a larger surface on the rock and increase the friction to prevent the rings from sliding on the specimen surface during the test. The second system (S2), see Figure 3-3, consists of two aluminium plates that are clamped around the circular loading platens of steel on top and on bottom of the specimen. Two LVDTs, mounted on the plates, measure the distance change between these plates at opposite side of the specimen at corresponding positions as for the first measurement system (S1).

The radial deformation was obtained by using a chain mounted around the specimen at mid-height, see Figures 3-2 and 3-3. The change of the chain-opening gap was measured by means of one LVDT and the circumferential and thereby also the radial deformation could be obtained. See Appendix A.

The specimens were photographed with a 4.0 Mega pixel digital camera at highest resolution and the photographs were stored in a jpeg-format.

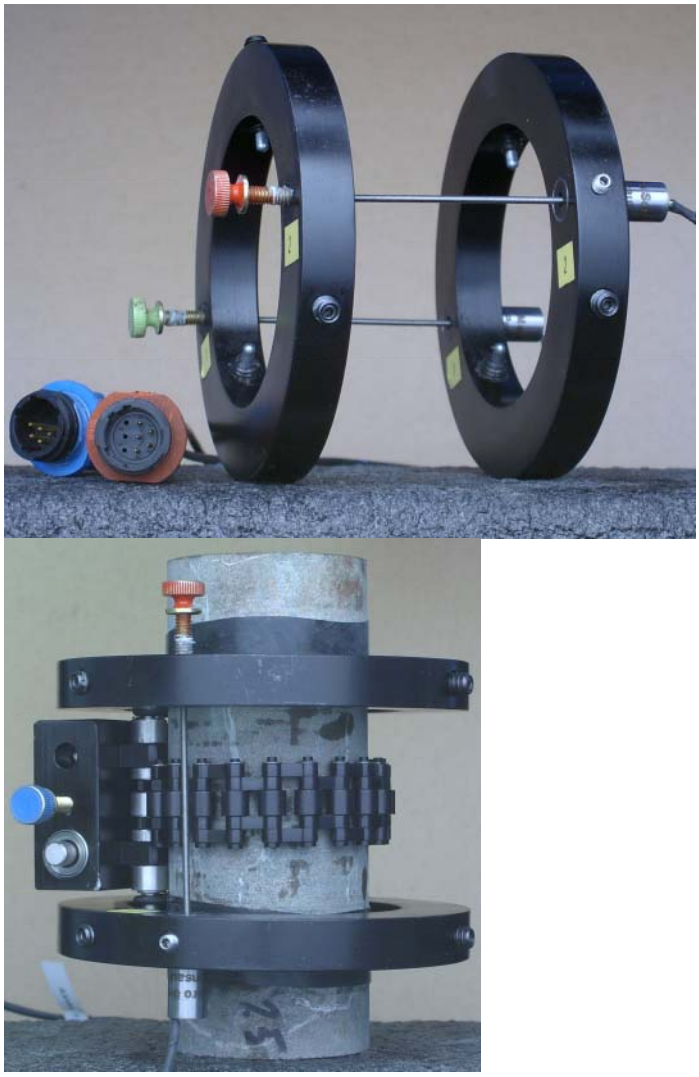

Figure 3-2. *Left: Rings and LVDTs for local axial deformation measurement. Right: Specimen with two rubber bands. Devices for local axial and circumferential deformation measurements attached on the specimen.*

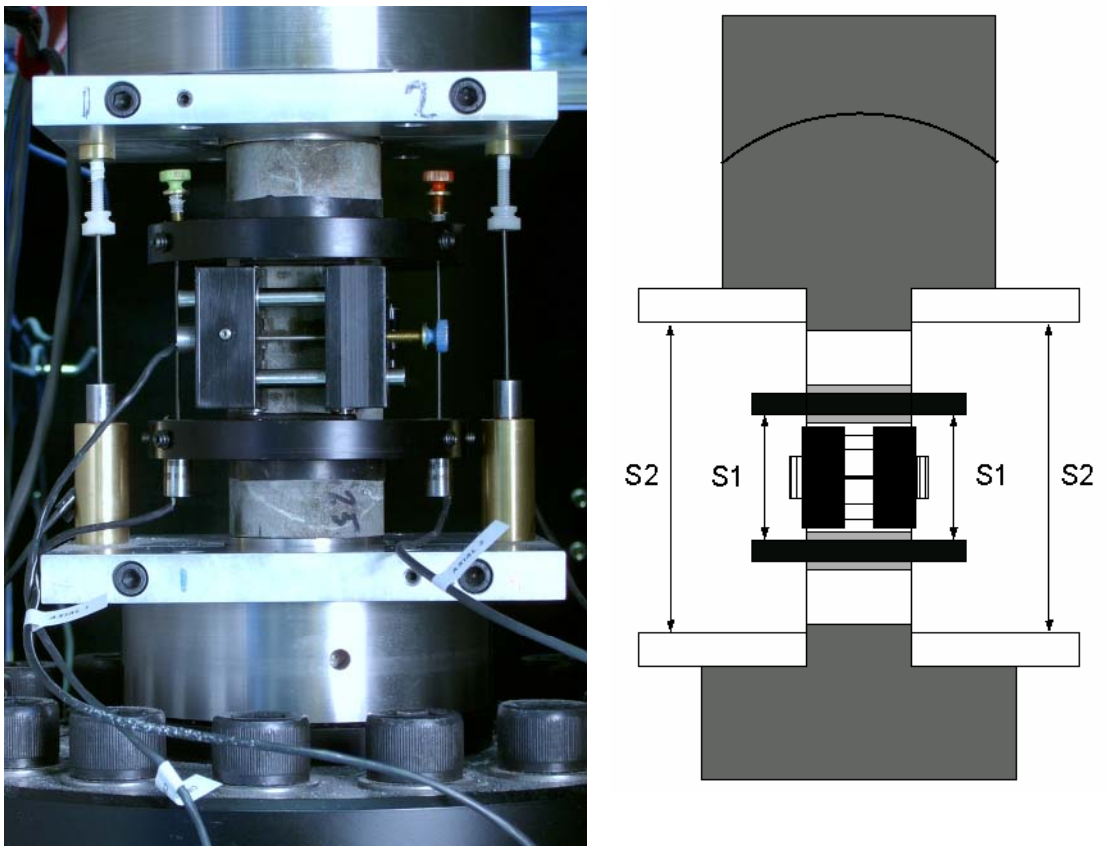

Figure 3-3. *Left: Specimen inserted between the loading platens. The two separate axial deformation measurement devices can be seen: system (S1) that measures the local axial deformation (rings) and system (S2) that measures the deformation between the aluminium plates (total deformation). Right: Principal sketch showing the two systems used for the axial deformation measurements.*

4 Execution

The water saturation and determination of the density of the wet specimens were made in accordance with the method description SKB MD 160.002, (SKB internal controlling document). This includes determination of density in accordance to ISRM /5/ and water saturation by SS EN 13755 /6/. The uniaxial compression test was carried out according to the method description SKB MD 190.001, (SKB internal controlling document). The test method is based on ISRM suggested method /1/.

4.1 Description of the samples

The rock type characterisation was made according to Stråhle /7/ using the SKB mapping (Boremap). The identification marks, upper and lower sampling depth (Secup and Seclow) and the rock type are shown in Table 4-1.

Table 4-1. Specimen identification, sampling depth and rock type for all specimens.

Identification	Secup (m)	Seclow (m)	Rock type
KSH01A-113-1	299.27	299.42	Quartz monzodiorite
KSH01A-113-3	301.66	301.81	Quartz monzodiorite
KSH01A-113-5	303.04	303.19	Quartz monzodiorite
KSH01A-113-7	311.21	311.36	Quartz monzodiorite
KSH01A-113-9	319.59	319.74	Quartz monzodiorite
KSH01A-113-14	398.85	399.00	Fine-grained dioritoid
KSH01A-113-15	401.48	401.63	Fine-grained dioritoid
KSH01A-113-17	413.16	413.31	Fine-grained dioritoid
KSH01A-113-18	413.46	413.61	Fine-grained dioritoid
KSH01A-113-19	414.44	414.59	Fine-grained dioritoid
KSH01A-113-21	486.05	486.20	Fine-grained dioritoid
KSH01A-113-22	488.18	488.33	Fine-grained dioritoid
KSH01A-113-23	491.95	492.10	Fine-grained dioritoid
KSH01A-113-24	494.81	494.96	Fine-grained dioritoid
KSH01A-113-25	495.57	495.72	Fine-grained dioritoid
KSH01A-113-28	699.67	699.82	Quartz monzodiorite
KSH01A-113-29	700.35	700.50	Quartz monzodiorite
KSH01A-113-30	702.38	702.53	Quartz monzodiorite
KSH01A-113-31	703.00	703.15	Quartz monzodiorite
KSH01A-113-32	703.15	703.30	Quartz monzodiorite

4.2 Testing

A step-by step description of the full test procedure is as follows:

Step	Activity
1	The drill cores were marked where the specimens are to be taken.
2	The specimens were cut to the specified length according to markings and the cutting surfaces were grinded.
3	The tolerances were checked: parallel and perpendicular end surfaces, smooth and straight sides of the specimen.
4	The diameter and height were measured three times each. The respectively mean value determines the dimensions that are reported.
5	The specimens were water saturated according to the method described in SKB MD 160.002, (SKB internal controlling document) and were stored for minimum 7 days in water whereupon the wet density was determined.
6	Digital photos were then taken of each specimen before the mechanical testing.
7	Devices for measuring axial and circumferential deformations were attached to the specimen.
8	The specimen was put in testing position in the load frame and centred between the loading platens.
9	The core on each LVDT was adjusted by means of a set screw to the right initial position. This was done so that the optimal range of the LVDTs can be used for the deformation measurement.
10	The frame piston was brought down into contact with the specimen with a force corresponding to 0.6 MPa axial stress.
11	A load cycle with loading to 5 MPa and unloading back to 0.6 MPa was conducted in order to settle possible contact gaps in the spherical seat in the piston and between the rock specimen and the loading platens.
12	The centring was checked again.
13	The deformation measurement channels were zeroed in the test software.
14	The loading was started and the initial loading rate was set to a radial strain rate of –0.025%/min. The loading rate was increased after reaching the post-failure region. This was done in order to prevent the total time for the test to become too long.
15	The test was stopped either manually when the test had proceeded large enough to obtain the post-failure loading envelope, or after severe cracking had occurred and it was judged that very little residual axial loading capacity was left in the specimen or when the radial deformation became too large. Some tests were restarted after a sudden radial expansion had occurred due to cracking leading to a complete unloading. Only tests with specimens, which were judged to have a major residual strength left, were restarted. In those cases the loading platen was then brought into contact again and applying a stress of 0.6 MPa before the test was restarted.
16	Digital photos were then taken of each specimen after the mechanical testing.

The temperature of the water was 18.4°C, which equals to a water density of 998.5 kg/m^3, when the determination of wet density of the rock specimens was carried out. Further, the specimens had been stored 7 days in water when the density was determined and between 19 and 27 days when the compression tests were carried out. The functionality of the system was checked, by carrying out tests on other cores with a similar type rock before the tests described in this report started. A check-list was filled in successively during the work in order to confirm that the different specified steps have been carried out. Moreover, comments were made upon observed things during the mechanical testing that are relevant for the interpretation of the results. The check-list form is a SP internal quality document.

4.3 Data handling

The test results were exported as text files from the test software and stored in a file server on the SP computer network after each completed test. The main data processing, in which the elastic moduli were computed and the peak stress was determined, has been carried out in the program MATLAB /8/. Moreover, MATLAB was used to produce the diagrams shown in Section 5.1 and in Appendix B. The summary of results in Section 5.2 with tables containing mean value and standard deviation of the different parameters and diagrams were produced using MS Excel. MS Excel was also used for reporting data to the SICADA database.

4.4 Analyses and interpretation

As to the definition of the different results parameters we begin with the axial stress σ_a, which is defined as

$$\sigma_a = \frac{F}{A}$$

where F is the axial force acting on the specimen and A is specimen cross section area. The peak value of the axial stress during a test is representing the uniaxial compressive strength σ_c in the results presentation.

The average value of the two axial displacement measurements on opposite sides of the specimen is used for the axial strain calculation, cf. Figure 3-3. In the first measurement system (S1), the recorded deformation represents a local axial deformation δ_{local} between the points at ¼ and ¾ height. A local axial strain is defined as

$$\varepsilon_{a,local} = \delta_{local}/L_{local}$$

where L_{local} is the distance between the rings before loading.

In the second measurement system (S2), the recorded displacement corresponds to a total deformation that, in addition to total rock deformation, also contains the local deformations that occur in the contact between the rock and the loading platens and further it also contains the deformation of the steel loading platens at each side of the

specimen ends. The average value of the two total deformation measurements on opposite sides of the specimen is defined as the total deformation δ_{total}. An axial strain based on the total of the deformation is defined as

$$\varepsilon_{a,total} = \delta_{total}/L_{total}$$

where L_{total} is the height of the rock specimen.

The radial deformation is measured by means of a chain mounted around the specimen at mid-height, cf. Figures 3-2 and 3-3. The change of chain opening gap is measured by means of one LVDT. This measurement is used to compute the radial strain ε_r, see Appendix A. Moreover, the volumetric strain ε_{vol} is defined as

$$\varepsilon_{vol} = \varepsilon_a + 2\varepsilon_r$$

The stresses and the strains are defined as positive in compressive loading and deformation. The elasticity parameters are defined by the tangent Young's modulus E and tangent Poisson ratio ν as

$$E = \frac{\sigma_a(0.55\sigma_c) - \sigma_a(0.45\sigma_c)}{\varepsilon_a(0.55\sigma_c) - \varepsilon_a(0.45\sigma_c)}$$

$$\nu = -\frac{\varepsilon_r(0.55\sigma_c) - \varepsilon_r(0.45\sigma_c)}{\varepsilon_a(0.55\sigma_c) - \varepsilon_a(0.45\sigma_c)}$$

The tangents were evaluated with values corresponding to an axial load between 45% and 55% of the axial peak stress σ_c.

Two important observations can be made from the results:

(i) The results based on the total axial deformation measurement (S2) display a lower axial stiffness, i.e. a lower value on Young's modulus, than in the case when the results are based on the local axial deformation measurement (S1). This is due to the additional deformations from the contact interface between the rock specimen and the steel loading platens and also due to the deformation of the loading platens themselves.

(ii) It can be seen that the response differs qualitatively between the results obtained with the local axial deformation measurement system (S1) and the system that measure total axial deformation (S2). In some cases the post-peak response obtained with the local deformation measurement system seems not to be physically correct. This can be due to a number of reasons, e.g. that a crack caused a localized deformation, see Figure 4-1. Another explanation could be that the rings attached to the specimens have slightly slipped or moved for example if a crack was formed nearby one of the attachment points.

It is reasonable to assume that results based on the local axial deformation measurement (S1) are fairly accurate up to the formation of the first macro cracks or up to the peak load, but not after. However, the results obtained with the total axial deformation measurement (S2) seem to be qualitatively correct after failure. We will therefore report the results based on the total axial deformation measurement, but carry out a correction of those results as described below in order to get overall good results.

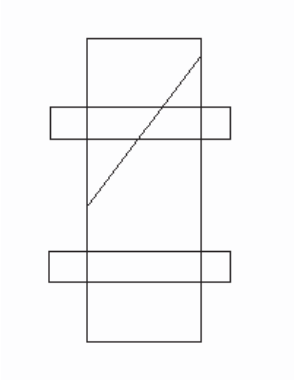

Figure 4-1. *Example of cracking that may cause results that are difficult to interpret with a local deformation measurement.*

The total axial deformation δ_{total} measured by (S2) is a summation of several deformations

$$\delta_{total} = \delta_{rock} + \delta_{system} \quad (1)$$

where

$$\delta_{system} = \delta_{interface} + \delta_{loading\ platens}$$

and δ_{rock} is the axial deformation of the whole rock specimen. Assume that the system deformation is proportional to the applied axial force F_a in the loading chain, i.e.

$$\delta_{system} = F_a/K_{system} \quad (2)$$

where K_{system} is the axial stiffness in the system (containing the interface between the rock and loading platens and the deformation of the loading platens). Combining (1) and (2) leads to

$$\delta_{rock} = \delta_{total} - F_a/K_{system} \quad (3)$$

where an expression of the axial deformation in the whole specimen is obtained. This can be viewed as a correction of the measurements made by system (S2). By using δ_{rock} to represent the axial deformation of the specimen that is based on a correction of the results of the total axial deformation will yield good results both in the loading range up to failure and also at loading after failure. However, it is noticed that K_{system} is not known and has to be determined.

It was previously suggested that the local axial deformation measurement represents the real rock deformation well up to the load where the macro cracks forms. Further, it is fair to assume that the axial deformation is homogenous at this part of the loading. Hence, we get

$$\delta_{rock} = \delta_{local} \cdot L_{total}/L_{local}$$

This yields representative values of the total rock deformation for the first part of the loading up to point where macro cracking is taking place. By rewriting (2) we get

$$K_{\text{system}} = \frac{F_{\text{a}}}{\delta_{\text{system}}} \tag{4}$$

It is now possible to determine δ_{system} up to the threshold of macro cracking. We will, however, compute the system stiffness based on the results between 45% and 55% of the axial peak stress σ_c. This means that the Young's modulus and the Poisson ratio will take the same values both when the data from the local axial deformation measurement (S1) and when the data from corrected total axial deformation are used. This means

$$K_{\text{system}} = \frac{F_{\text{a}}(0.55\sigma_{\text{c}}) - F_{\text{a}}(0.45\sigma_{\text{c}})}{\delta_{\text{system}}(0.55\sigma_{\text{c}}) - \delta_{\text{system}}(0.45\sigma_{\text{c}})} \tag{5}$$

where $\delta_{system} = \delta_{total} - \delta_{rock}$ according to (1). The results based on the correction according to (3) and (5) are presented in Section 5.1 whereas the original measured unprocessed data are reported in Appendix B.

A closure of present micro cracks will take place initially during axial loading. Development of new micro cracks will start when the load is further increased and axial stress reaches the crack initiation stress σ_i. The crack growth at this stage is as stable as increased loading is required for further cracking. A transition from a development of micro cracks to macro cracks will take place when the axial load is further increased. At a certain stress level the crack growth becomes unstable. The stress level when this happens is denoted the crack damage stress σ_d, cf. /2/. In order to determine the stress levels we look at the volumetric strain.

By subtracting the elastic volumetric strain $\varepsilon_{\text{vol}}^{\text{e}}$ from the total volumetric strain a volumetric strain corresponding to the crack volume $\varepsilon_{\text{vol}}^{\text{cr}}$ is obtained. This has been denoted calculated crack volumetric strain in the literature, cf. /2, 3/. We have thus

$$\varepsilon_{\text{vol}}^{\text{cr}} = \varepsilon_{\text{vol}} - \varepsilon_{\text{vol}}^{\text{e}}$$

Assuming linear elasticity leads to

$$\varepsilon_{\text{vol}}^{\text{cr}} = \varepsilon_{\text{vol}} - \frac{1-2\nu}{E}\sigma_{\text{a}}$$

where $\sigma_r = 0$ was used. Experimental investigations have shown that the crack initiation stress σ_i coincides with the onset of increase of the calculated crack volume, cf. /2, 3/. The same investigations also indicate that the crack damage stress σ_d can be defined as the axial stress at which the total volume starts to increase, i.e. when a dilatant behaviour is observed.

5 Results

The results of the individual specimens are presented in Section 5.1 and a summary of the results is given in Section 5.2. The reported parameters are based on both unprocessed raw data and processed data obtained from the testing and were reported to the SICADA database, FN 96. These data together with the digital photographs of the individual specimens were stored on a CD and handed over to SKB. The handling of the results follows SDP-508 (SKB internal controlling document) in general.

5.1 Description and presentation of the specimen

The cracking is shown in pictures taken on the specimens and comments on observed things that appeared during the testing are reported. The elasticity parameters have been evaluated by using the results from the local axial deformation measurements. The data from the adjusted total axial deformation measurements, cf. Section 4.4, are shown in this Section. Red rings are superimposed on the graphs indicating every five minutes of the progress of testing.

Diagrams showing the data from both the local and the total axial deformation measurements, system (S1) and (S2) in Figure 3-3, and the computed individual values of K_{system} used at the data corrections are shown in Appendix B. The diagrams actual radial strain rates versus the test time are also shown in Appendix B. The results for the individual specimens are as follows:

Specimen ID: KSH01A-113-1

Before mechanical test

After mechanical test

Diameter (mm)	Height (mm)	Density (kg/m^3)
50.1	126.4	2,770

Comments Vertical cracking of the specimen is observed.

Specimen ID: KSH01A−113−01

Youngs Modulus (E):	68.7	[GPa]
Poisson Ratio (ν):	0.312	[−]
Axial peak stress (σ_c):	158.3	[MPa]

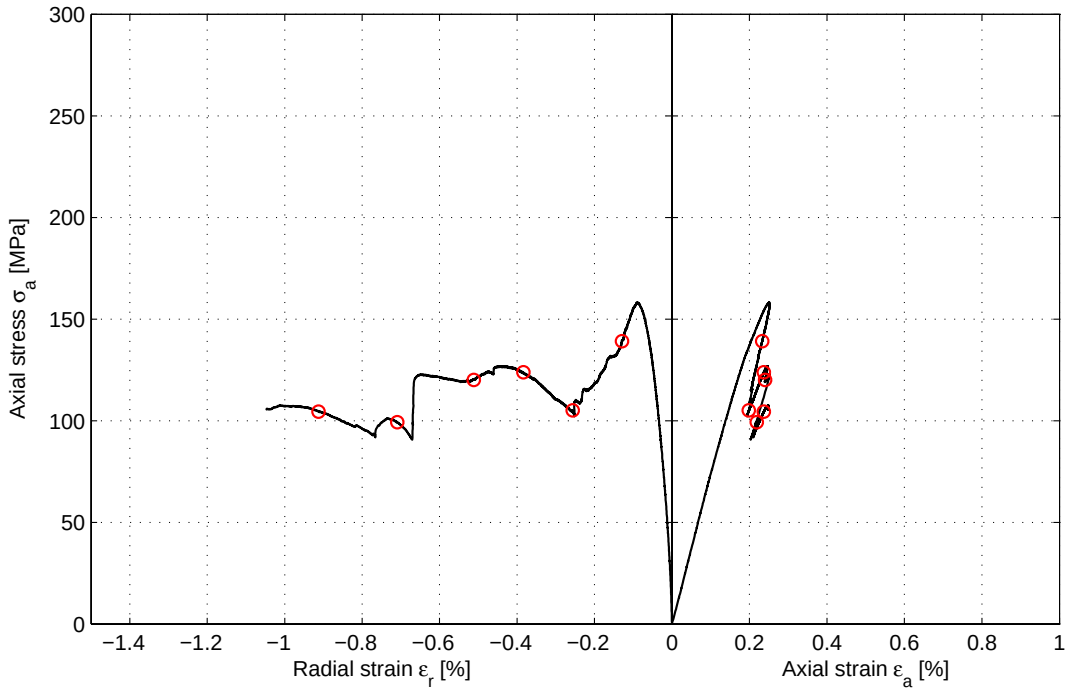

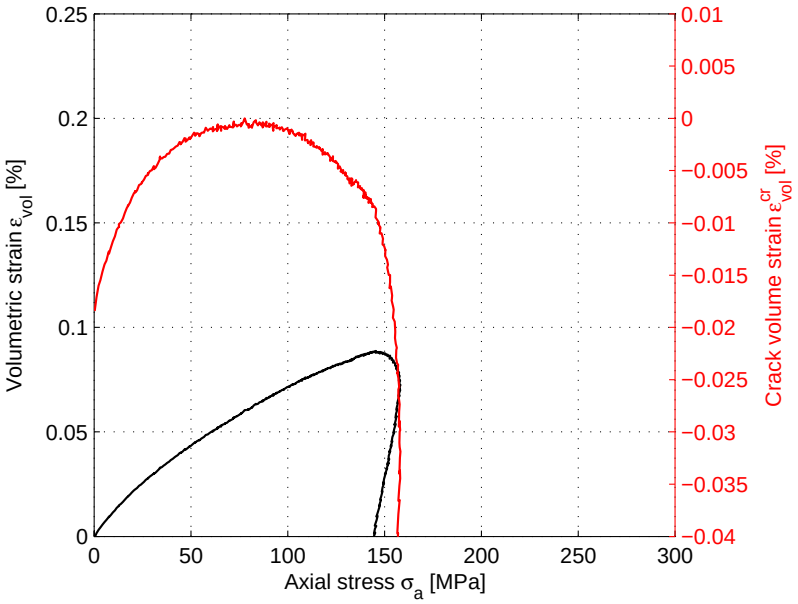

Specimen ID: KSH01A-113-3

Before mechanical test

After mechanical test

Diameter (mm)	**Height (mm)**	**Density (kg/m^3)**
50.2	126.5	2,770

Comments Spalling at one side of the specimen around mid-height is observed.

Specimen ID: KSH01A−113−03

Youngs Modulus (E):	66	[GPa]
Poisson Ratio (ν):	0.325	[−]
Axial peak stress (σ_c):	167.7	[MPa]

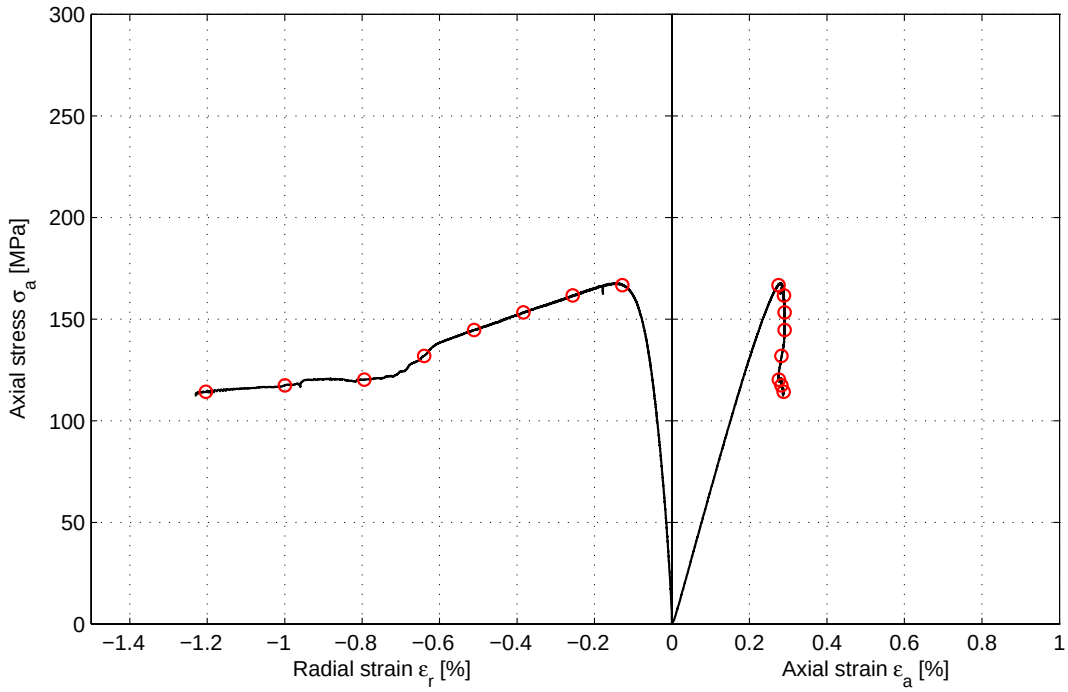

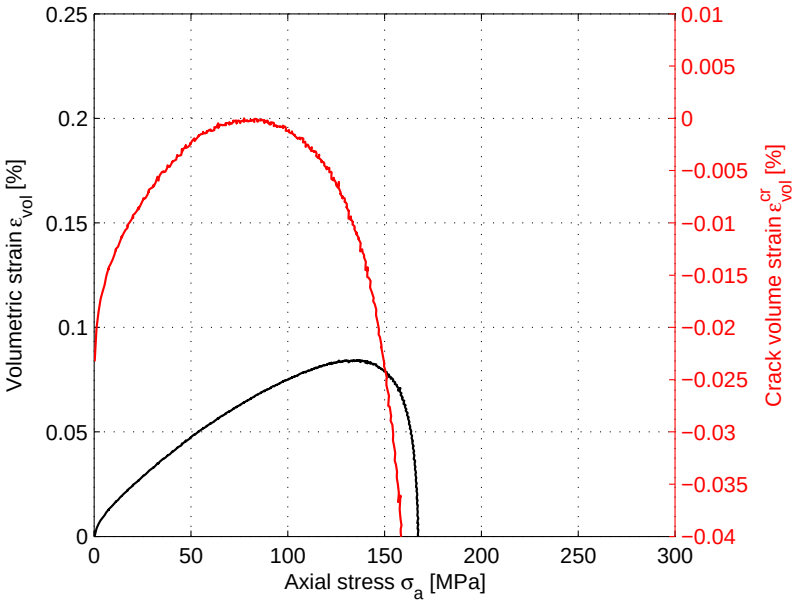

Specimen ID: KSH01A-113-5

Before mechanical test

After mechanical test

Diameter (mm)	Height (mm)	Density (kg/m^3)
50.2	126.6	2,780

Comments Spalling at one side of the specimen around mid-height is observed.

Specimen ID: KSH01A−113−05

Youngs Modulus (E):	66.7	[GPa]
Poisson Ratio (ν):	0.274	[−]
Axial peak stress (σ_c):	170.4	[MPa]

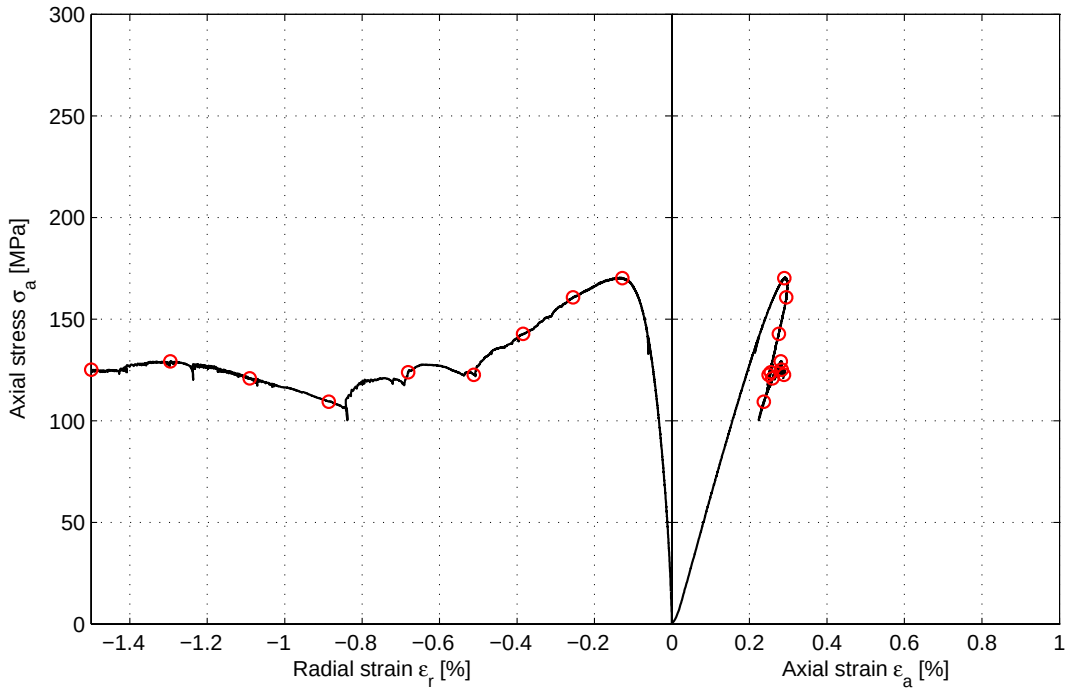

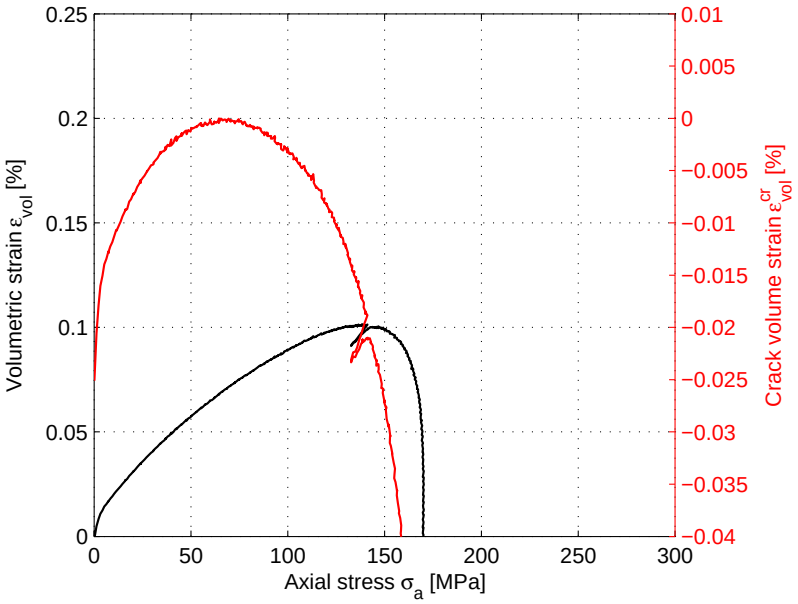

Specimen ID: KSH01A-113-7

Before mechanical test

After mechanical test

Diameter (mm)	**Height (mm)**	**Density (kg/m^3)**
50.2	126.5	2,790

Comments Spalling at one side of the specimen around mid-height is observed.

Specimen ID: KSH01A−113−07

Youngs Modulus (E):	82.9	[GPa]
Poisson Ratio (ν):	0.316	[−]
Axial peak stress (σ_c):	192.9	[MPa]

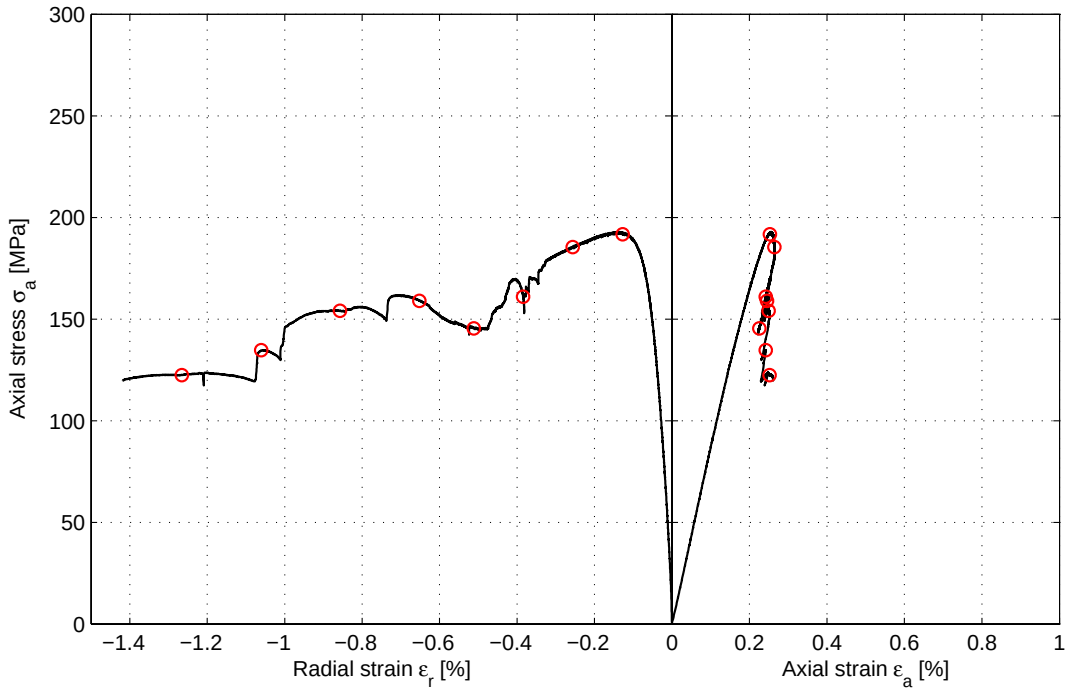

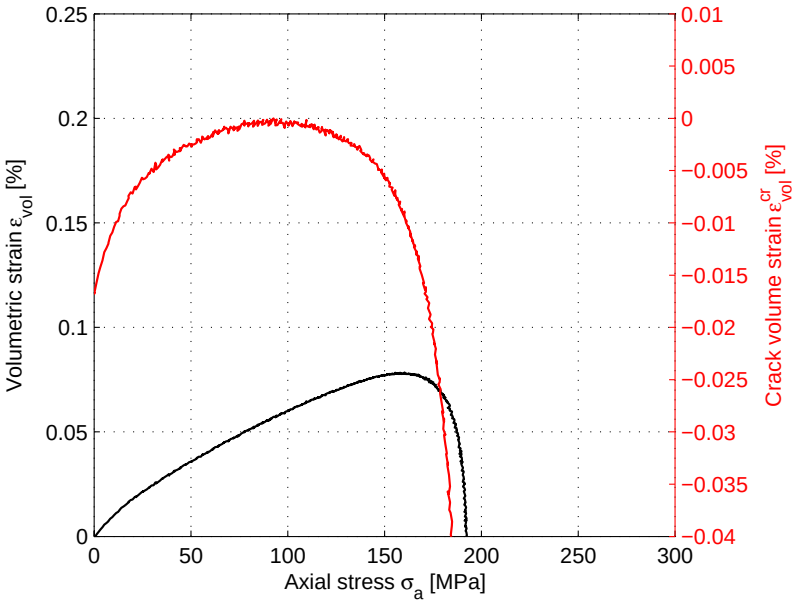

Specimen ID: KSH01A-113-9

Before mechanical test	After mechanical test
	
No picture	No picture

Diameter (mm)	**Height (mm)**	**Density (kg/m^3)**
50.1	127.3	2,810

Comments The specimen was totally damaged as the machine piston deformed the specimen with its full stroke. This happened when the radial deformation was let to progress to the very end of the range of the LVDT measuring the circumferential displacement. When it was at the end of the range of the LVDT the machine became uncontrollable.

Specimen ID: KSH01A−113−09

Youngs Modulus (E):	78.6	[GPa]
Poisson Ratio (ν):	0.333	[−]
Axial peak stress (σ_c):	186	[MPa]

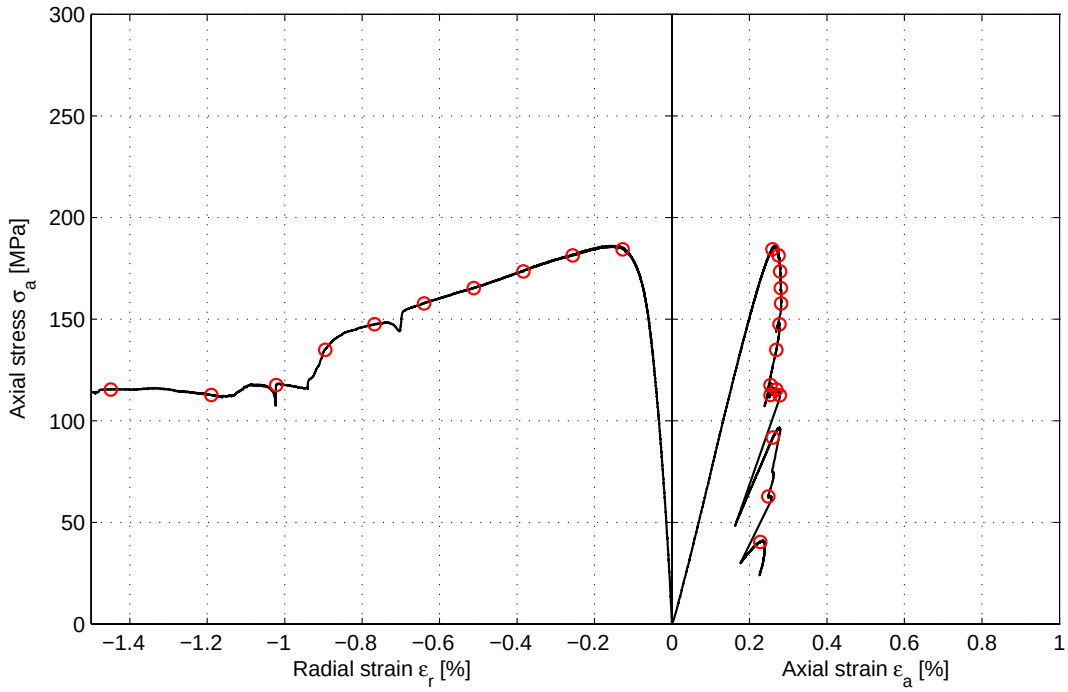

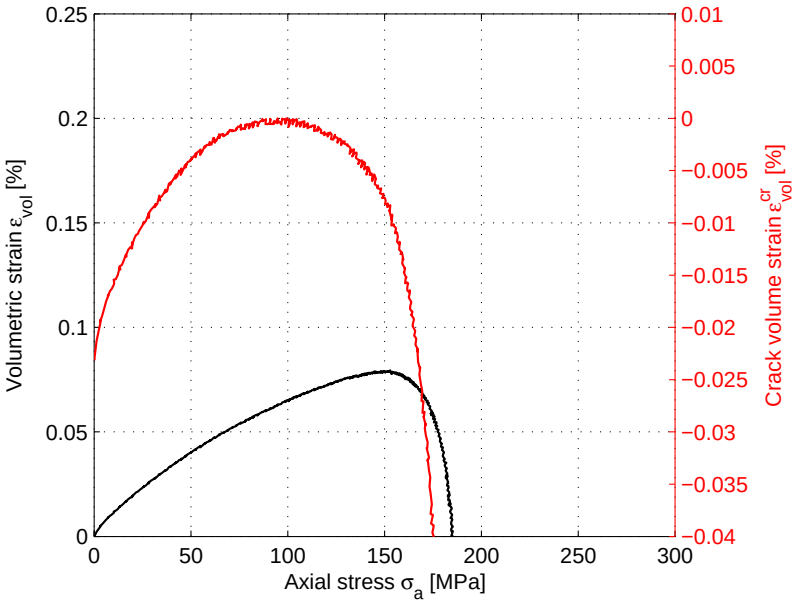

Specimen ID: KSH01A-113-14

Before mechanical test

After mechanical test

Diameter (mm)	Height (mm)	Density (kg/m^3)
50.1	127.6	2,780

Comments A diagonal crack was developed in a weakness zone. In addition a vertical crack is observed. The test was restarted two times due to load oscillations after a sudden cracking.

Specimen ID: KSH01A−113−14

Youngs Modulus (E):	81.7	[GPa]
Poisson Ratio (ν):	0.192	[−]
Axial peak stress (σ_c):	151.6	[MPa]

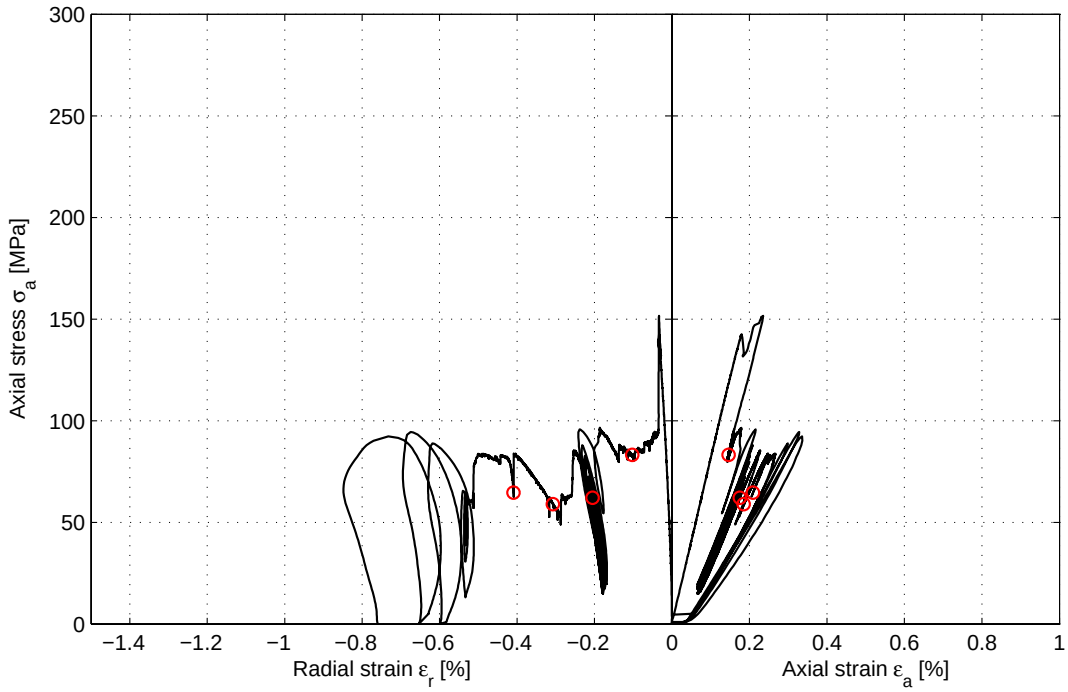

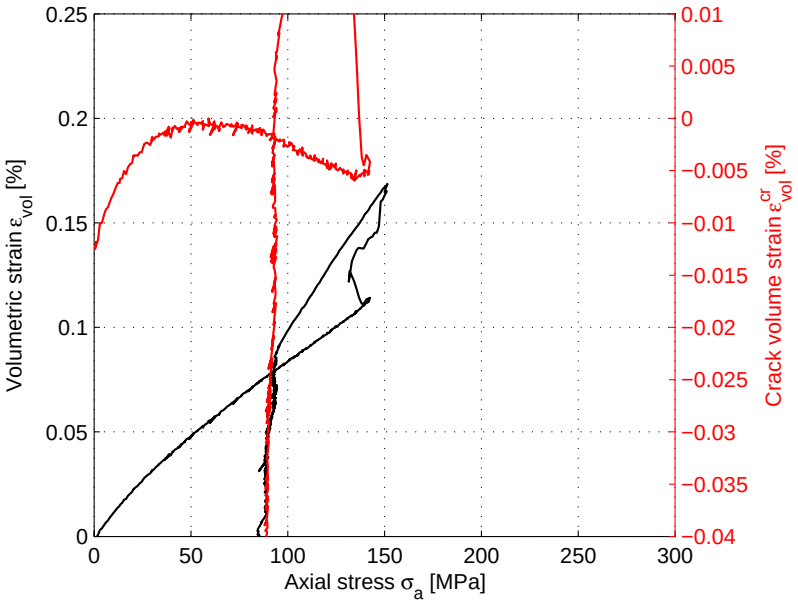

Specimen ID: KSH01A-113-15

Before mechanical test

After mechanical test

Diameter (mm)	Height (mm)	Density (kg/m^3)
50.1	127.4	2,780

Comments Several vertical cracks are observed. The test was restarted after a sudden large radial expansion leading to complete unloading.

Specimen ID: KSH01A−113−15

Youngs Modulus (E):	84.3	[GPa]
Poisson Ratio (ν):	0.249	[−]
Axial peak stress (σ_c):	246.8	[MPa]

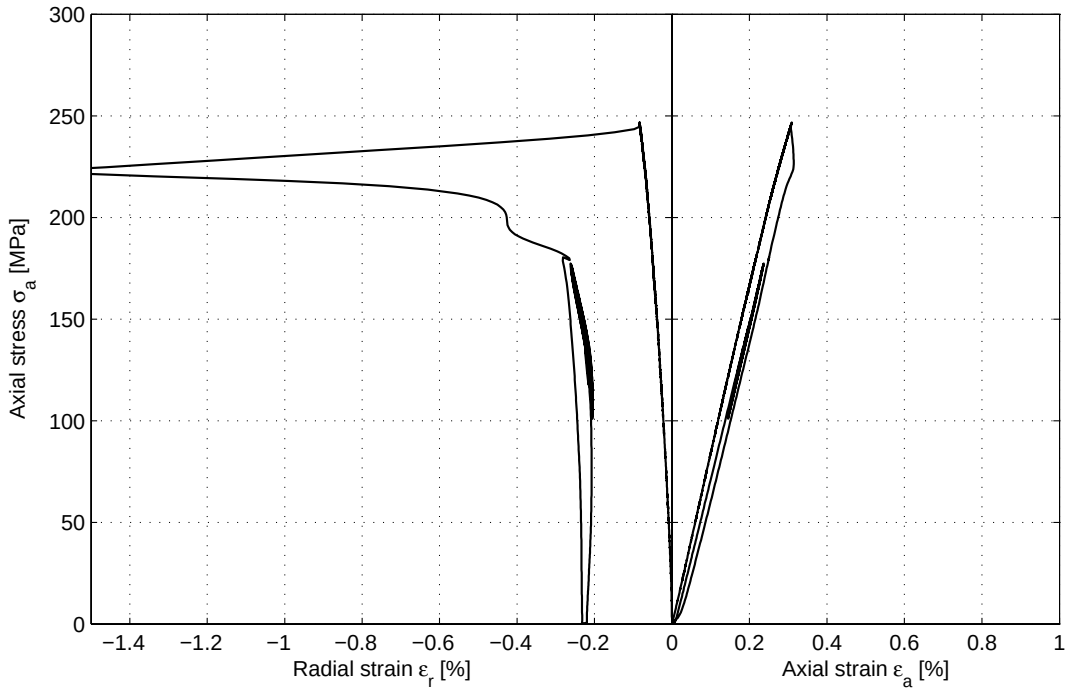

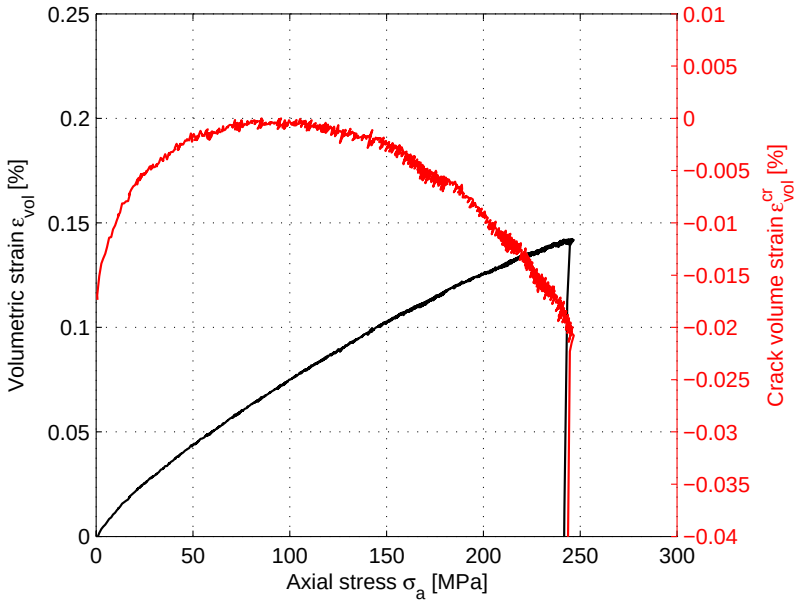

Specimen ID: KSH01A-113-17

Before mechanical test

After mechanical test

Diameter (mm)	Height (mm)	Density (kg/m^3)
49.6	117.9	2,780

Comments A shear type of failure was developed.

Specimen ID: KSH01A−113−17

Youngs Modulus (E):	78.5	[GPa]
Poisson Ratio (ν):	0.237	[−]
Axial peak stress (σ_c):	109.3	[MPa]

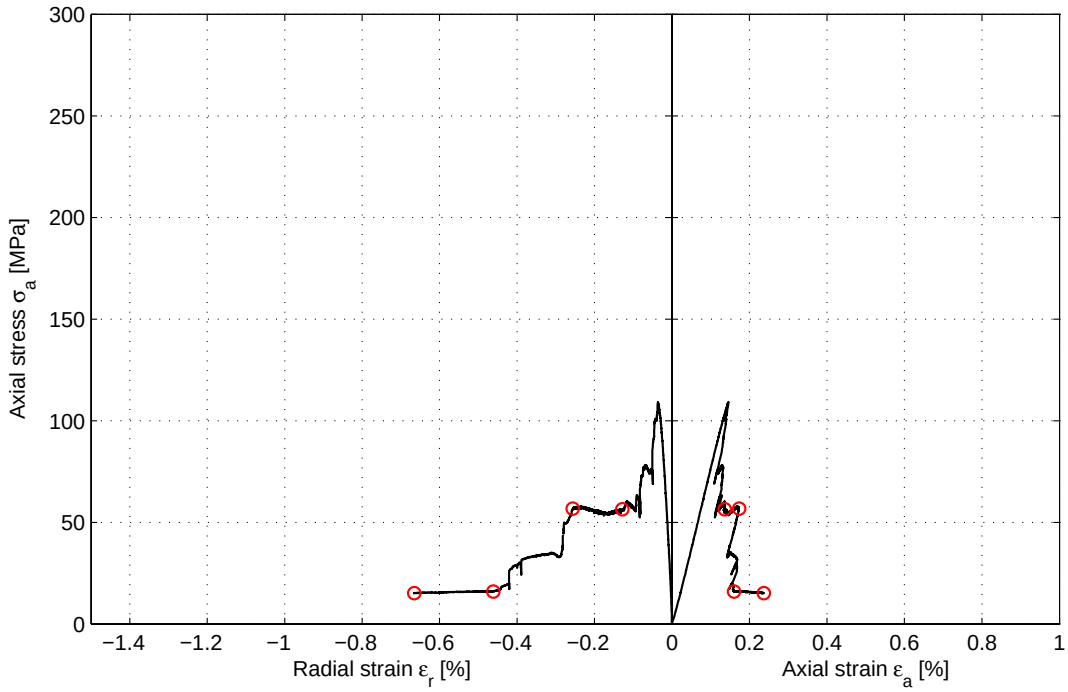

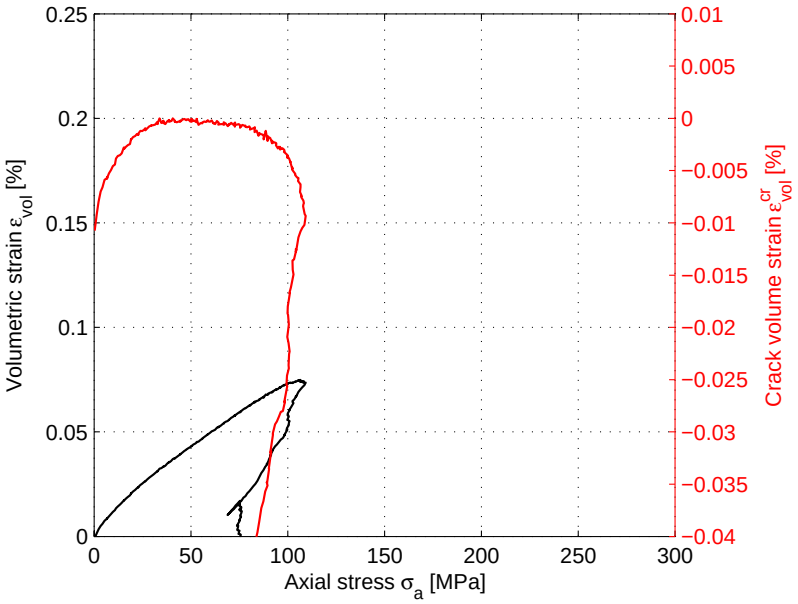

Specimen ID: KSH01A-113-18

Before mechanical test

After mechanical test

Diameter (mm)	Height (mm)	Density (kg/m^3)
49.5	118	2,780

Comments Multiple cracks in the vertical diagonal and horizontal directions. The test was restarted due to load oscillations after a sudden cracking.

Specimen ID: KSH01A−113−18

Youngs Modulus (E):	93	[GPa]
Poisson Ratio (ν):	0.317	[−]
Axial peak stress (σ_c):	158	[MPa]

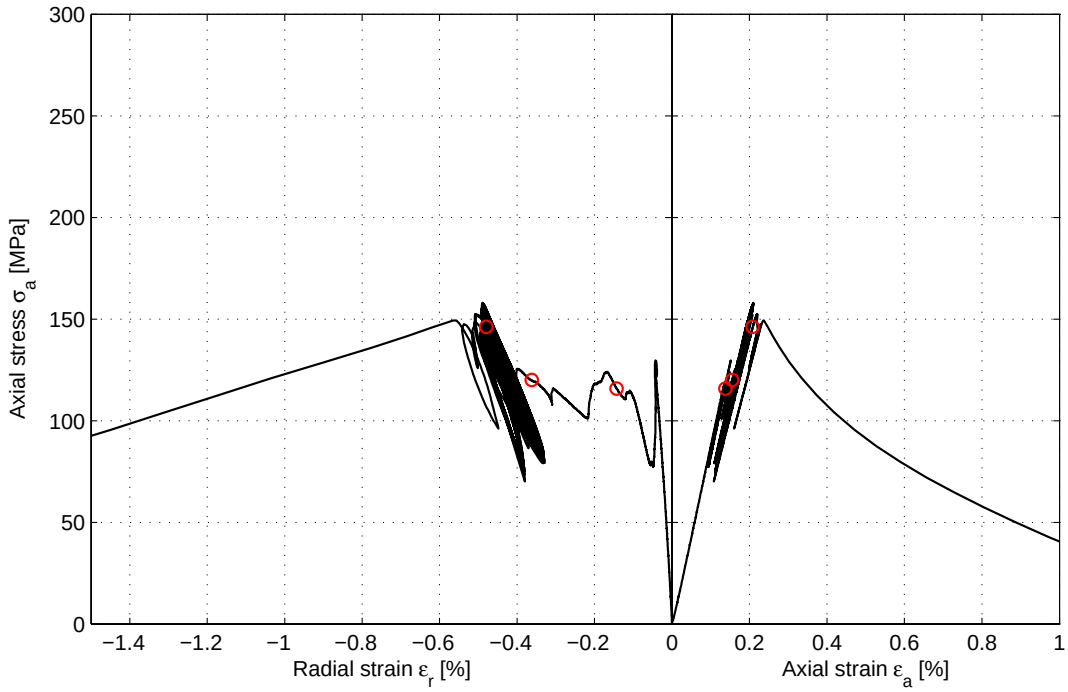

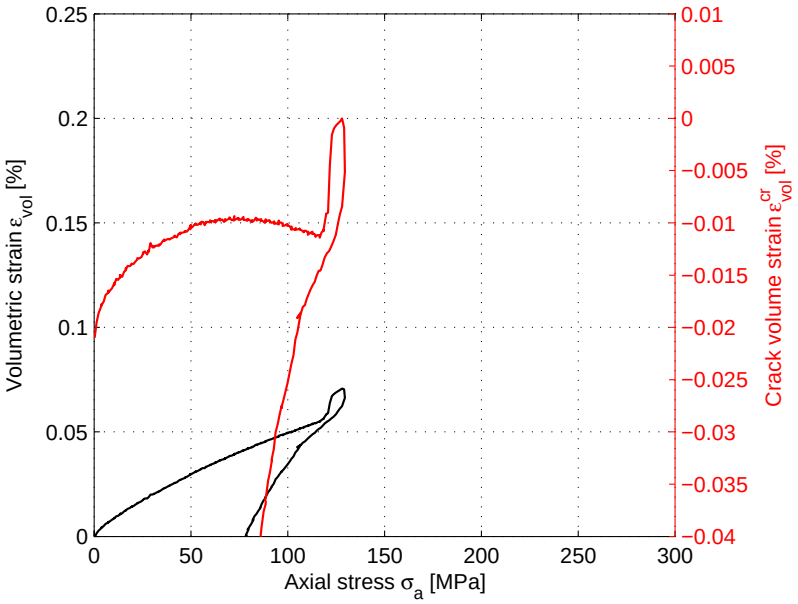

Specimen ID: KSH01A-113-19

Before mechanical test

After mechanical test

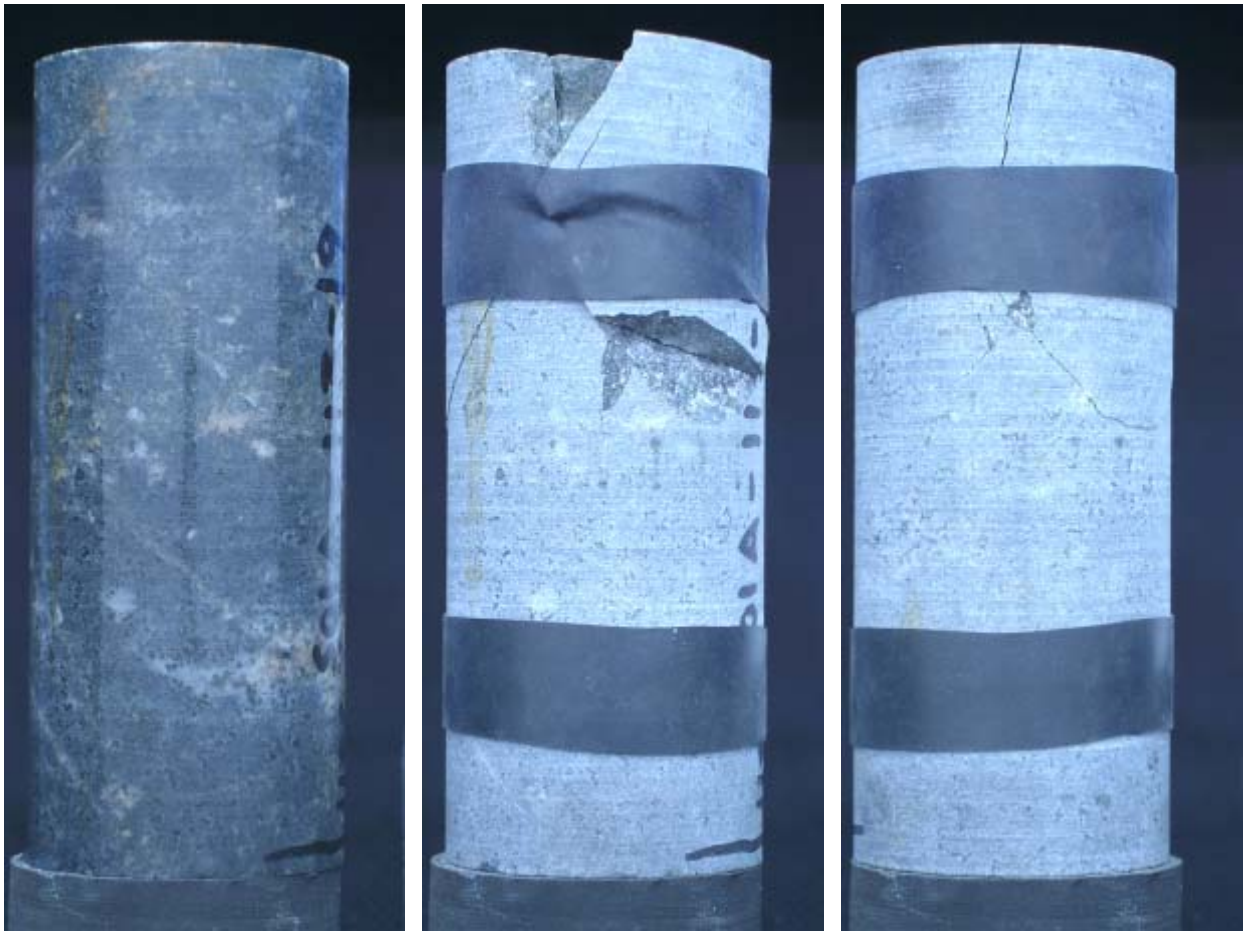

Diameter (mm)	Height (mm)	Density (kg/m^3)
49.5	124.6	2,770

Comments The cracking occurred in mainly one half of the specimen. A single crack seems to have started to develop through the specimen.

Specimen ID: KSH01A−113−19

Youngs Modulus (E):	103.9	[GPa]
Poisson Ratio (ν):	0.295	[−]
Axial peak stress (σ_c):	131.2	[MPa]

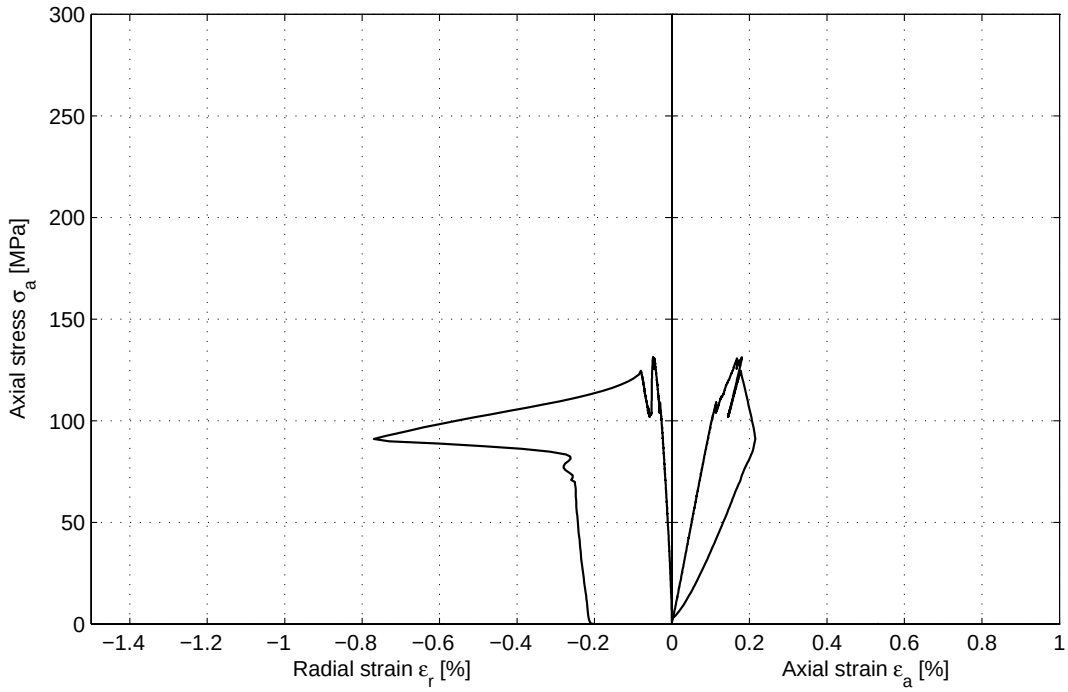

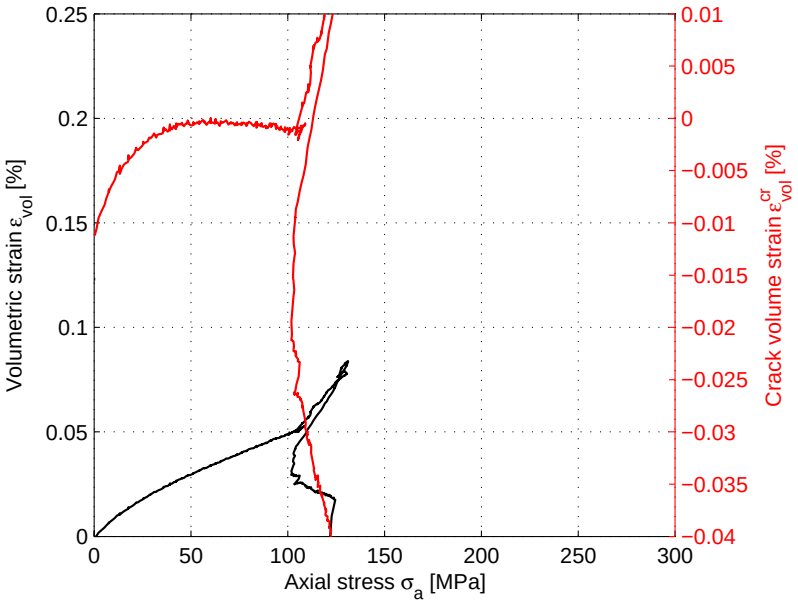

Specimen ID: KSH01A-113-21

Before mechanical test

After mechanical test

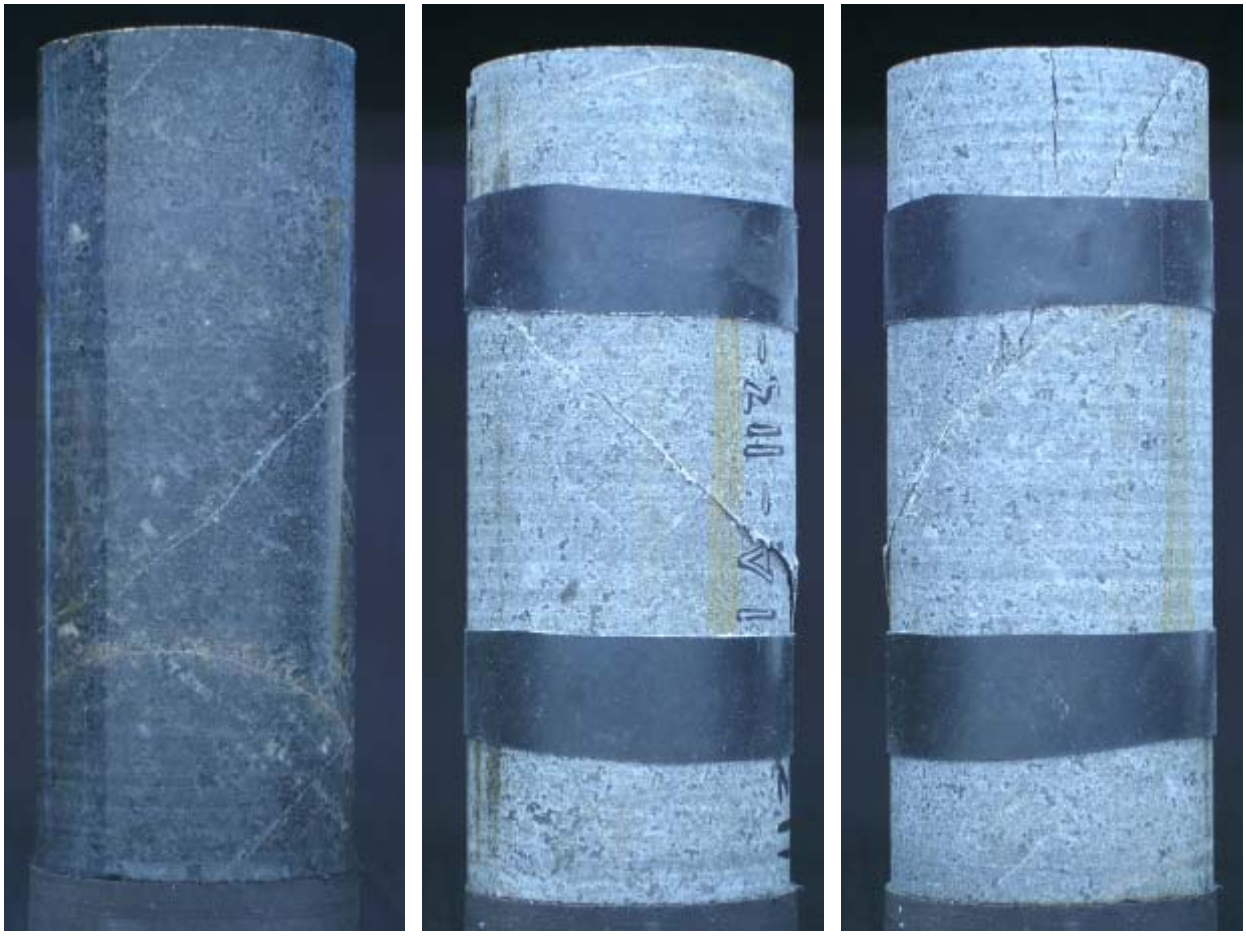

Diameter (mm)	Height (mm)	Density (kg/m^3)
50.1	127.5	2,810

Comments A diagonal crack was developed in a weakness zone in the rock structure. The test was restarted after compete unloading due to a large radial expansion.

Specimen ID: KSH01A−113−21

Youngs Modulus (E):	75.4	[GPa]
Poisson Ratio (ν):	0.302	[−]
Axial peak stress (σ_c):	181.6	[MPa]

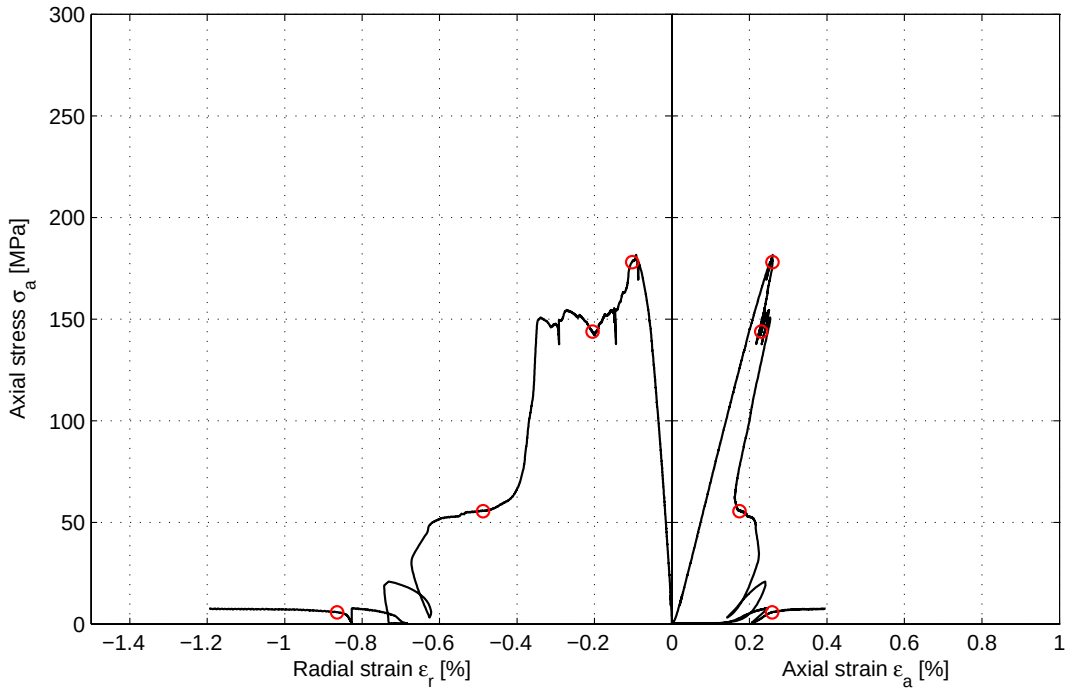

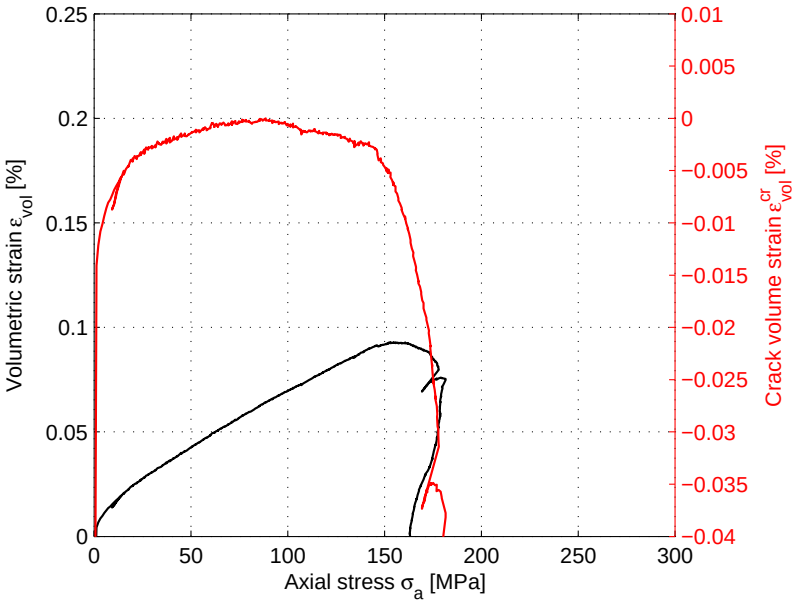

Specimen ID: KSH01A-113-22

Before mechanical test

After mechanical test

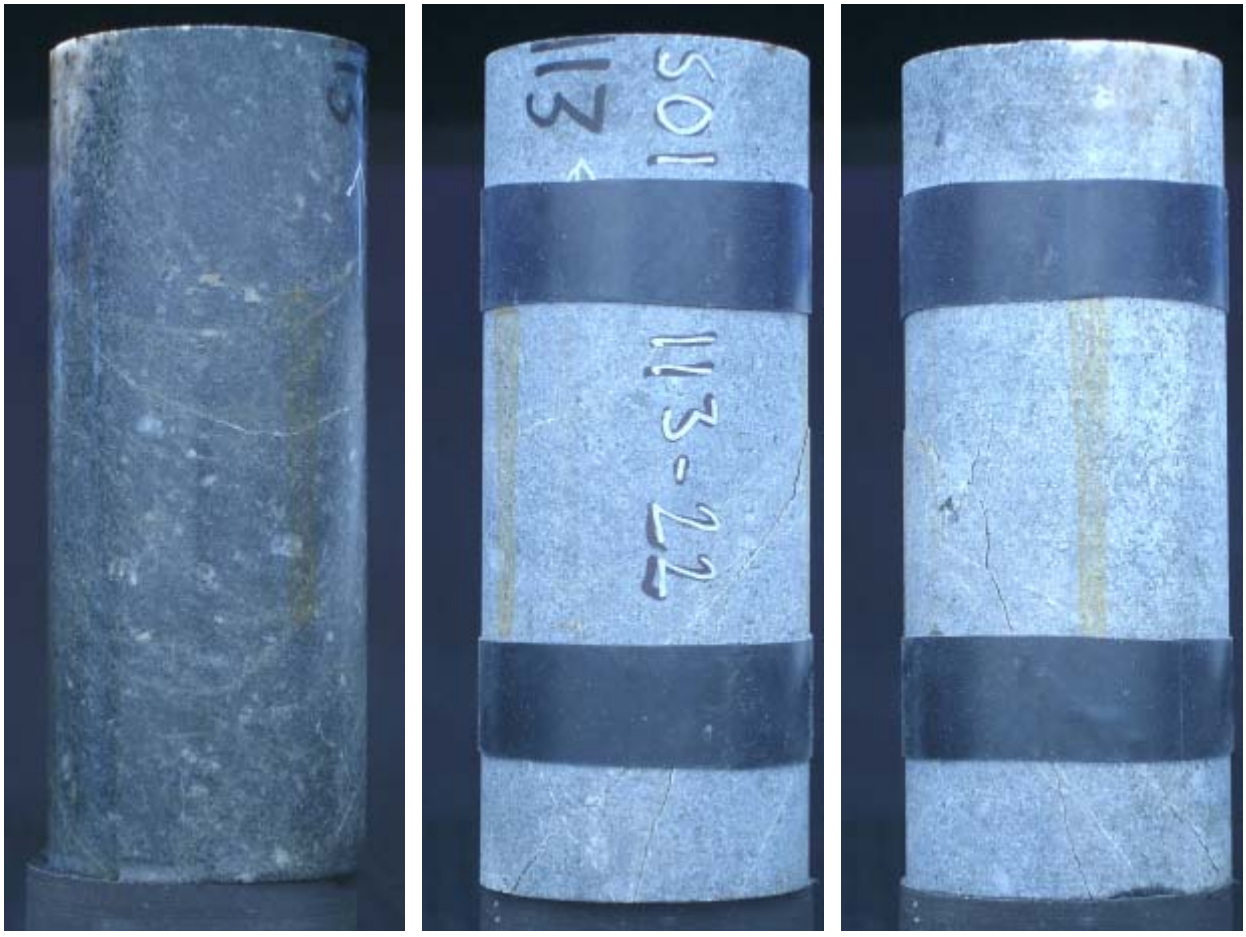

Diameter (mm)	Height (mm)	Density (kg/m^3)
50.1	127.6	2,800

Comments A diagonal crack was developed in a weakness zone in the rock structure. The test was restarted due to load oscillations after a sudden cracking.

Specimen ID: KSH01A−113−22

Youngs Modulus (E):	85	[GPa]
Poisson Ratio (ν):	0.249	[−]
Axial peak stress (σ_c):	91.9	[MPa]

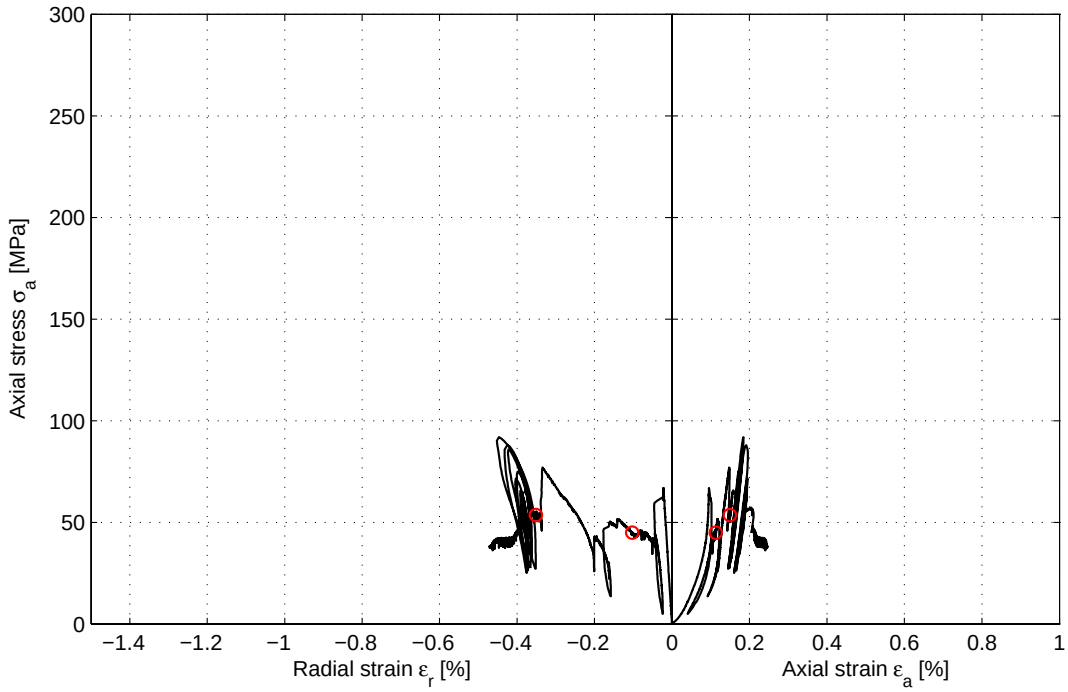

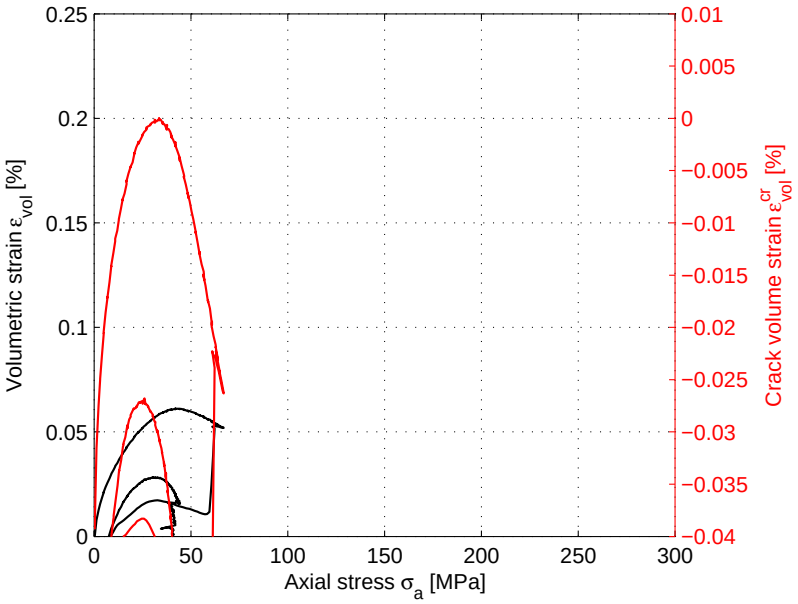

Specimen ID: KSH01A-113-23

Before mechanical test

After mechanical test

Diameter (mm)	Height (mm)	Density (kg/m^3)
50.1	127.3	2,800

Comments A diagonal crack was developed in a weakness zone in the rock structure. The test was restarted due to load oscillations after a sudden cracking.

Specimen ID: KSH01A−113−23

Youngs Modulus (E):	80.2	[GPa]
Poisson Ratio (ν):	0.253	[−]
Axial peak stress (σ_c):	142.1	[MPa]

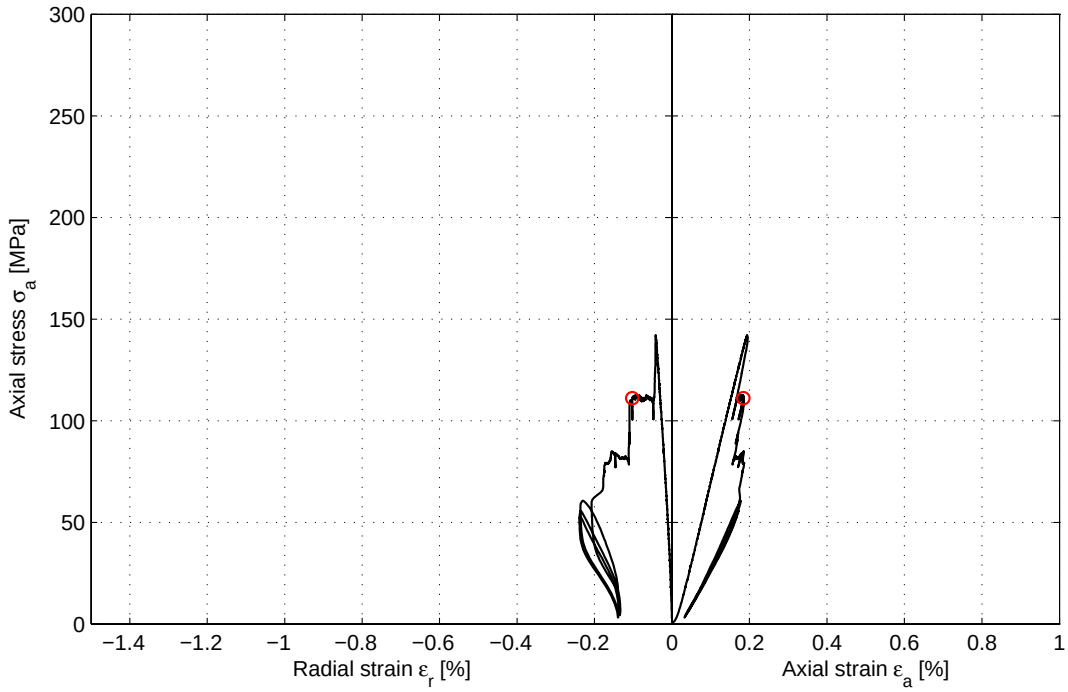

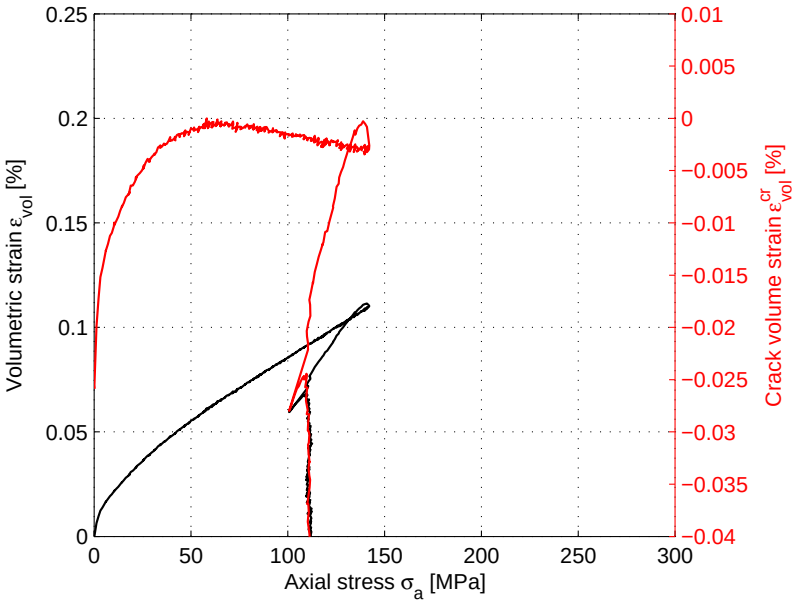

Specimen ID: KSH01A-113-24

Before mechanical test

After mechanical test

Diameter (mm)	Height (mm)	Density (kg/m^3)
50.1	123.5	2,790

Comments Vertical plus diagonal crackings are observed. The test was restarted due to load oscillations after a sudden cracking.

Specimen ID: KSH01A−113−24

Youngs Modulus (E):	76.6	[GPa]
Poisson Ratio (ν):	0.271	[−]
Axial peak stress (σ_c):	229.5	[MPa]

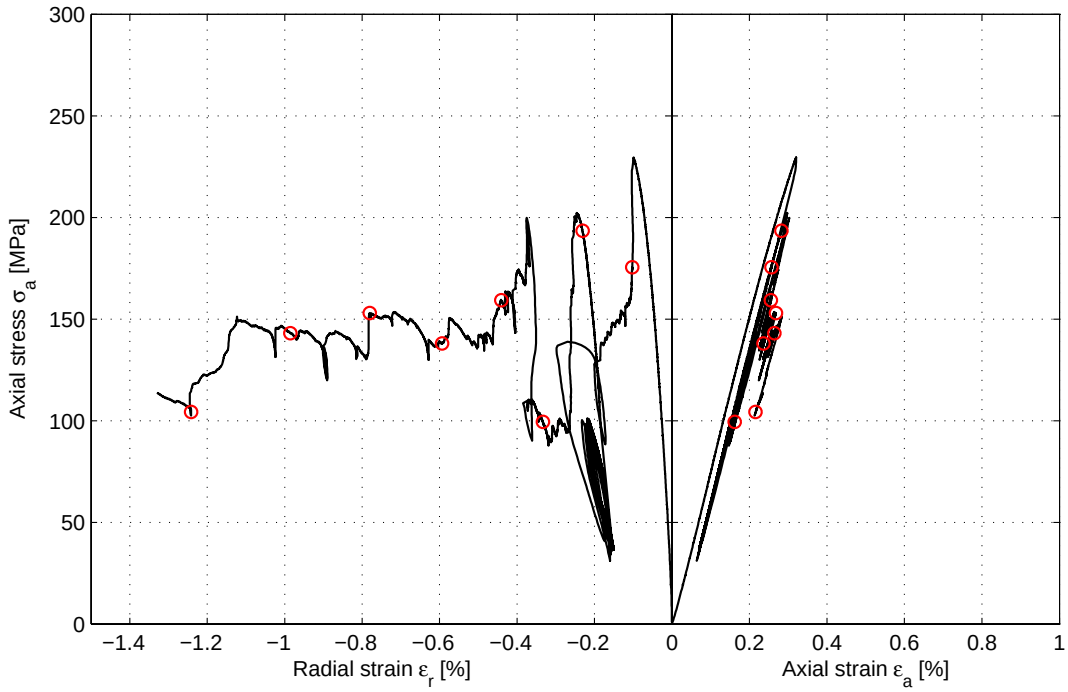

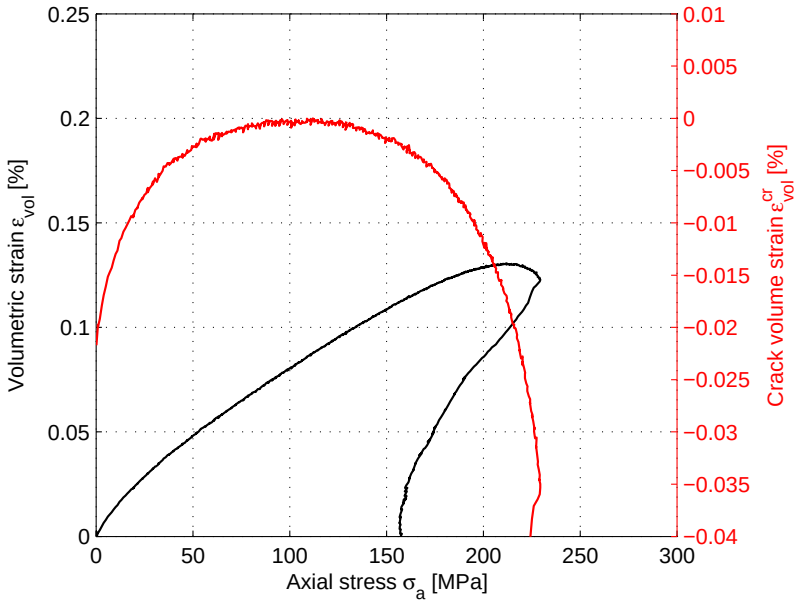

Specimen ID: KSH01A-113-25

Before mechanical test

After mechanical test

Diameter (mm)	**Height (mm)**	**Density (kg/m^3)**
50.1	127.1	2,790

Comments Vertical plus diagonal cracking are observed.

Specimen ID: KSH01A−113−25

Youngs Modulus (E):	97	[GPa]
Poisson Ratio (ν):	0.272	[−]
Axial peak stress (σ_c):	171.5	[MPa]

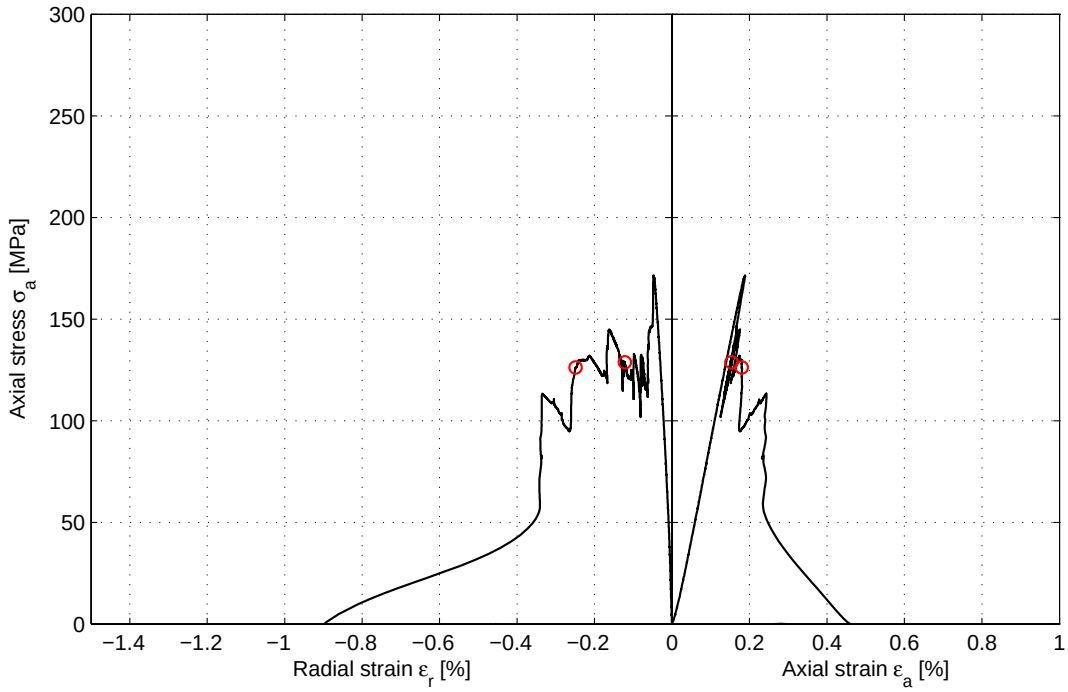

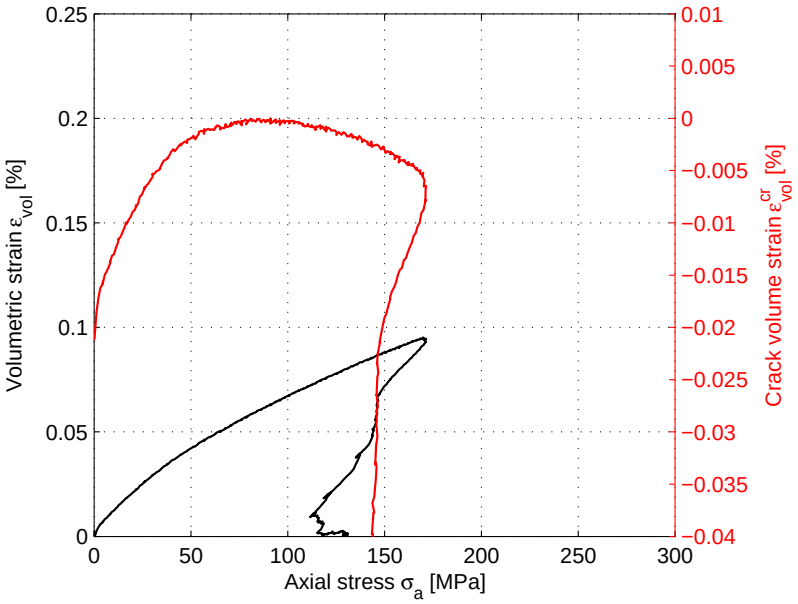

Specimen ID: KSH01A-113-28

Before mechanical test

After mechanical test

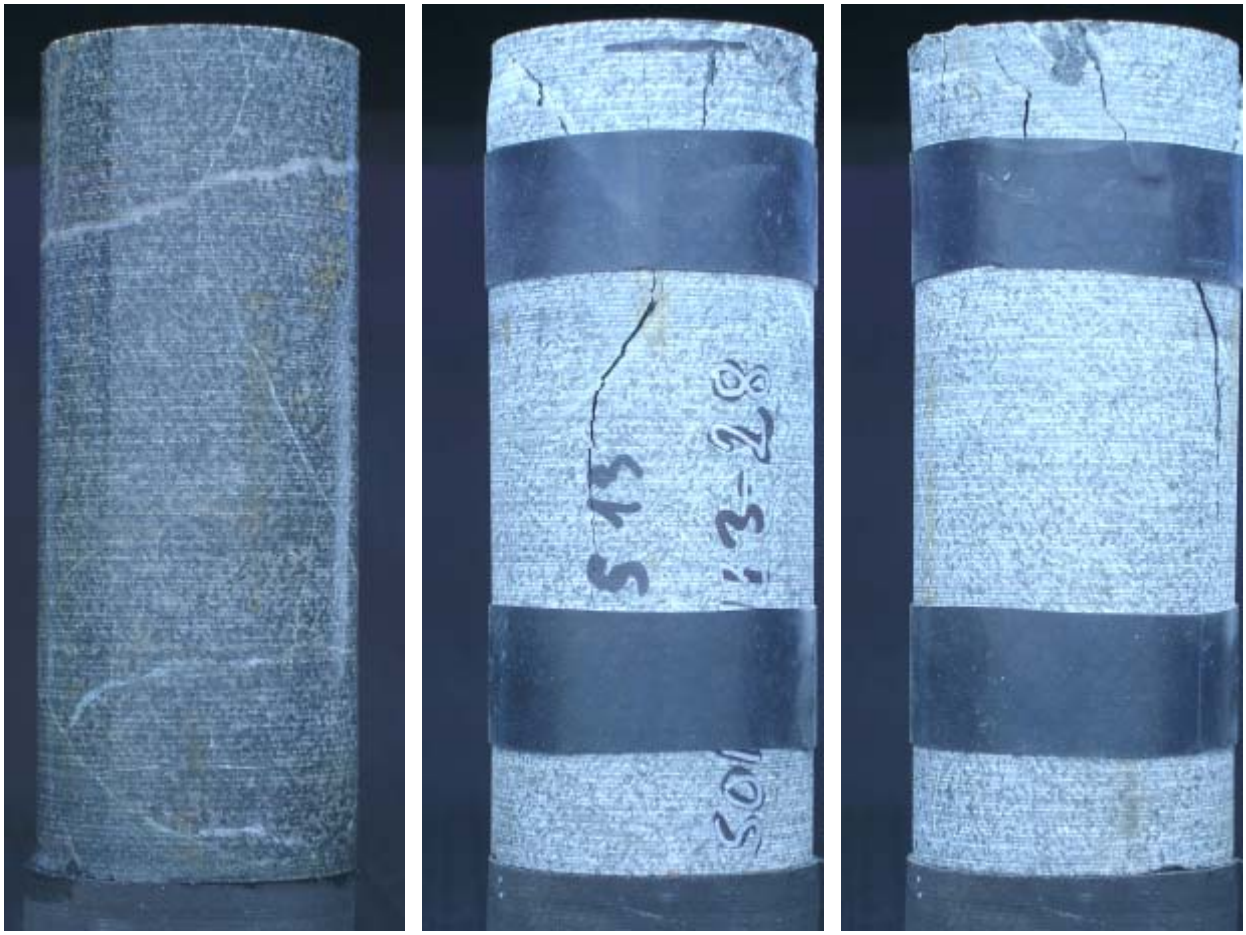

Diameter (mm)	Height (mm)	Density (kg/m^3)
50.1	127.6	2,830

Comments Diagonal cracks were developed in weakness zones in the rock structure. A wedge formed piece was formed in the upper end of the core. A second loading was probably obtained due to new loading surfaces that came into contact.

Specimen ID: KSH01A−113−28

Youngs Modulus (E):	82.9	[GPa]
Poisson Ratio (ν):	0.223	[−]
Axial peak stress (σ_c):	141.6	[MPa]

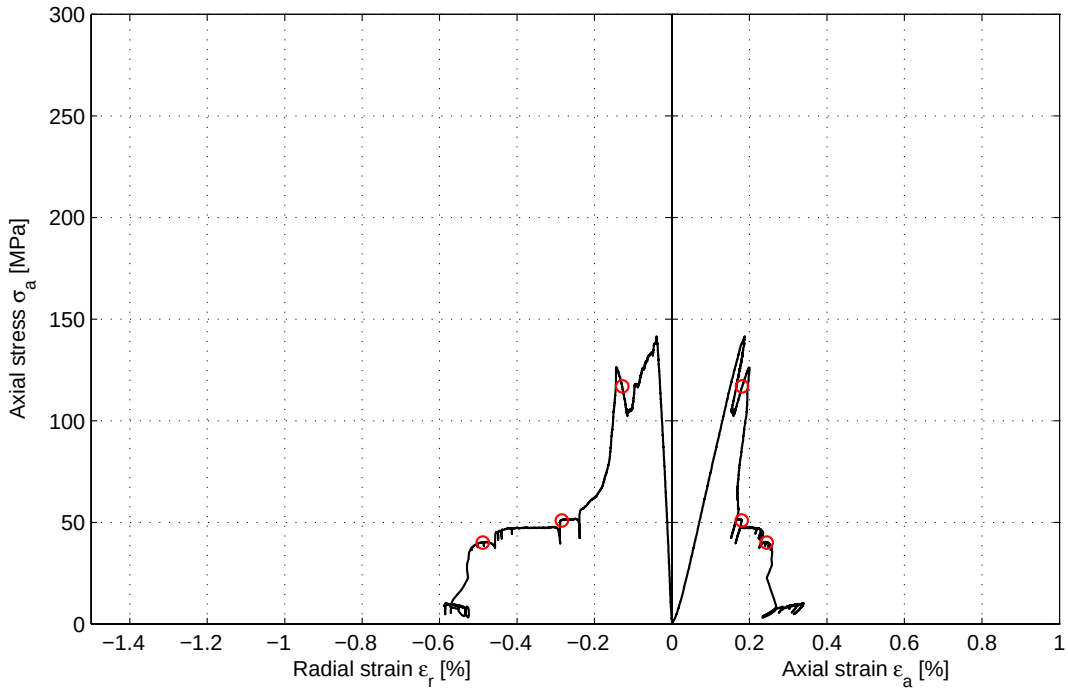

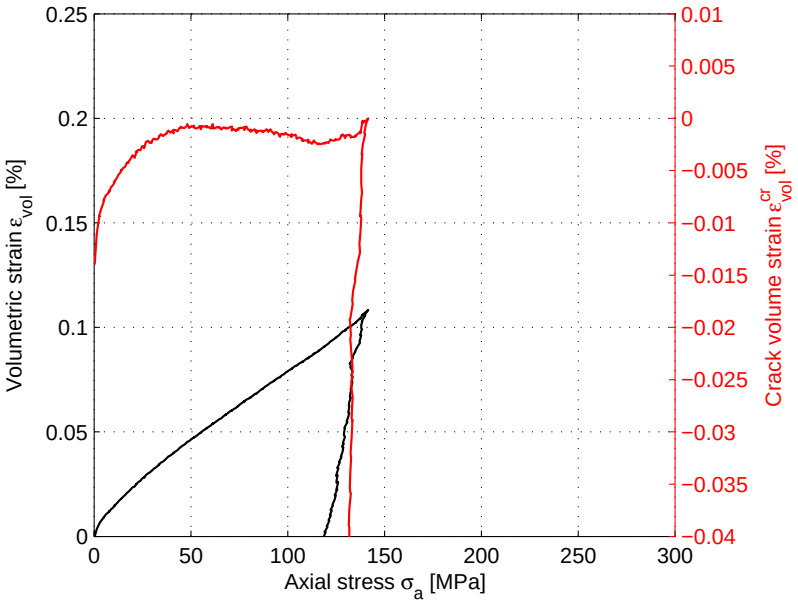

Specimen ID: KSH01A-113-29

Before mechanical test

After mechanical test

Diameter (mm)	Height (mm)	Density (kg/m^3)
50.1	127.1	2,830

Comments A diagonal crack was developed and a shear type of failure was obtained.

Specimen ID: KSH01A−113−29

Youngs Modulus (E):	74.3	[GPa]
Poisson Ratio (ν):	0.264	[−]
Axial peak stress (σ_c):	133.1	[MPa]

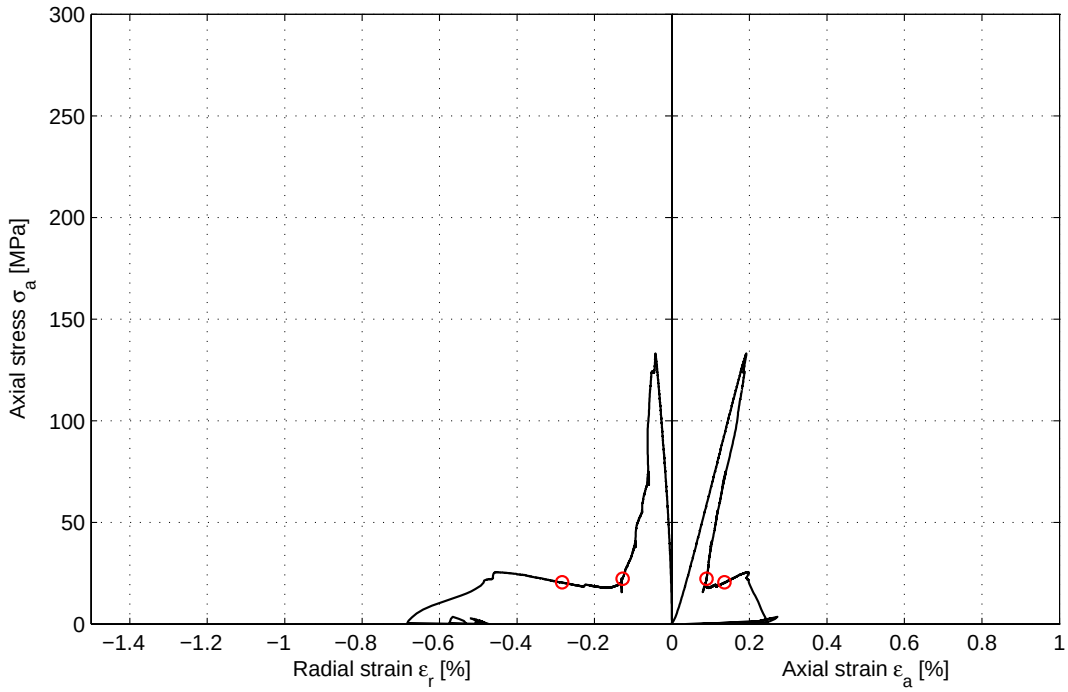

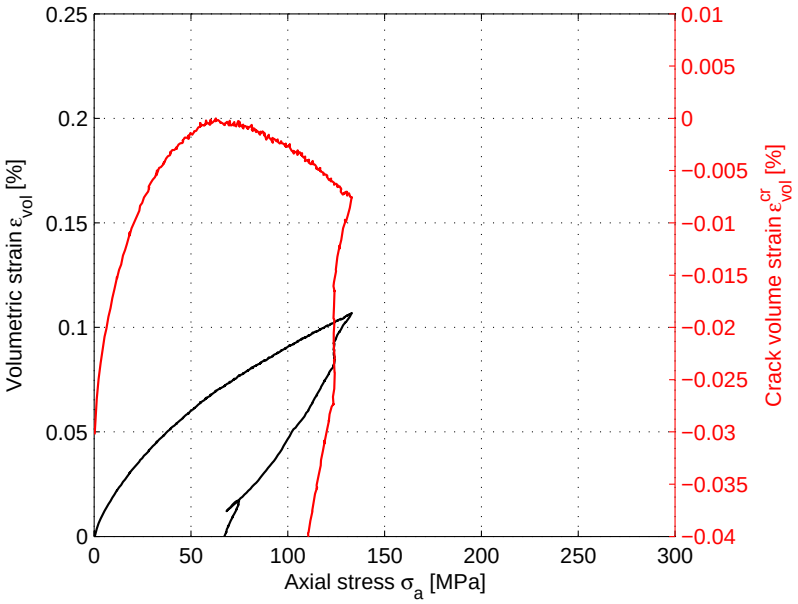

Specimen ID: KSH01A-113-30

Before mechanical test

After mechanical test

Diameter (mm)	Height (mm)	Density (kg/m^3)
50.1	127.5	2,840

Comments A crack was developed through the diameter of one of the end surfaces on the specimen. This resulted in an uneven loading as one side deformed more than the other side of the crack.

Specimen ID: KSH01A−113−30

Youngs Modulus (E):	82.6	[GPa]
Poisson Ratio (ν):	0.244	[−]
Axial peak stress (σ_c):	177.6	[MPa]

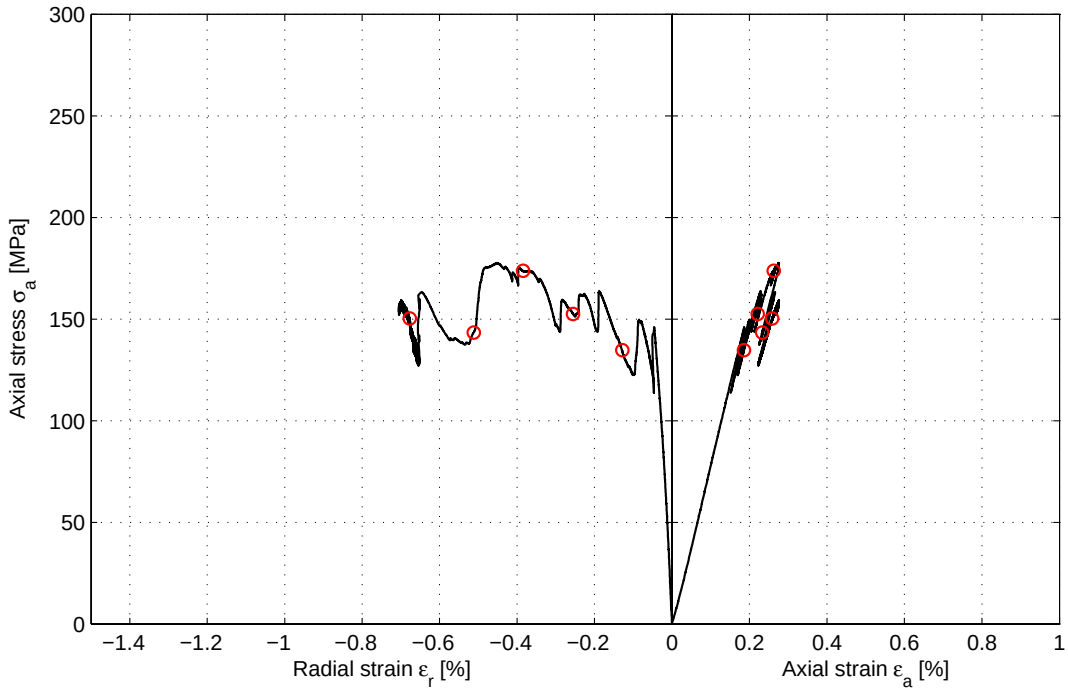

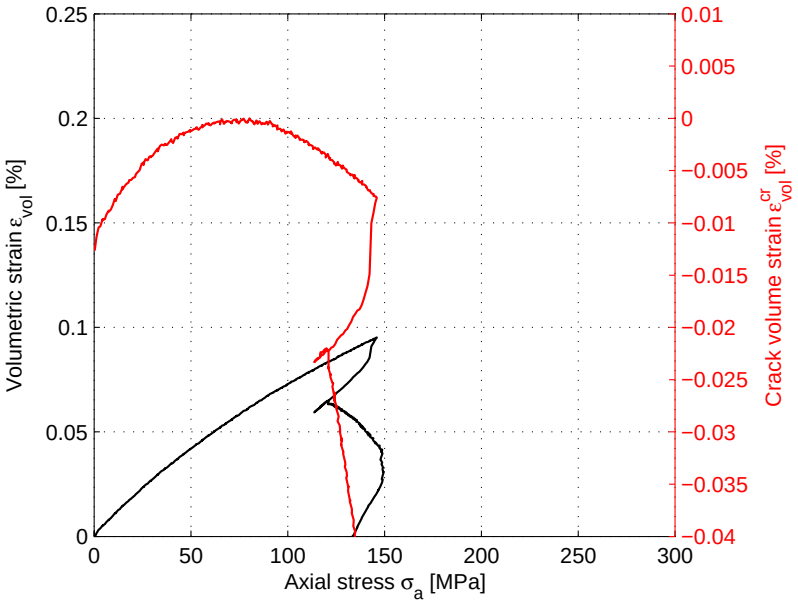

Specimen ID: KSH01A-113-31

Before mechanical test

After mechanical test

Diameter (mm)	Height (mm)	Density (kg/m^3)
50.1	127.3	2,830

Comments A crack was developed through the diameter of one of the end surfaces on the specimen. This resulted in an uneven loading as one side deformed more than the other side of the crack. The load started to oscillate after a sudden cracking and the test was stopped.

Specimen ID: KSH01A−113−31

Youngs Modulus (E):	80.6	[GPa]
Poisson Ratio (ν):	0.242	[−]
Axial peak stress (σ_c):	160.2	[MPa]

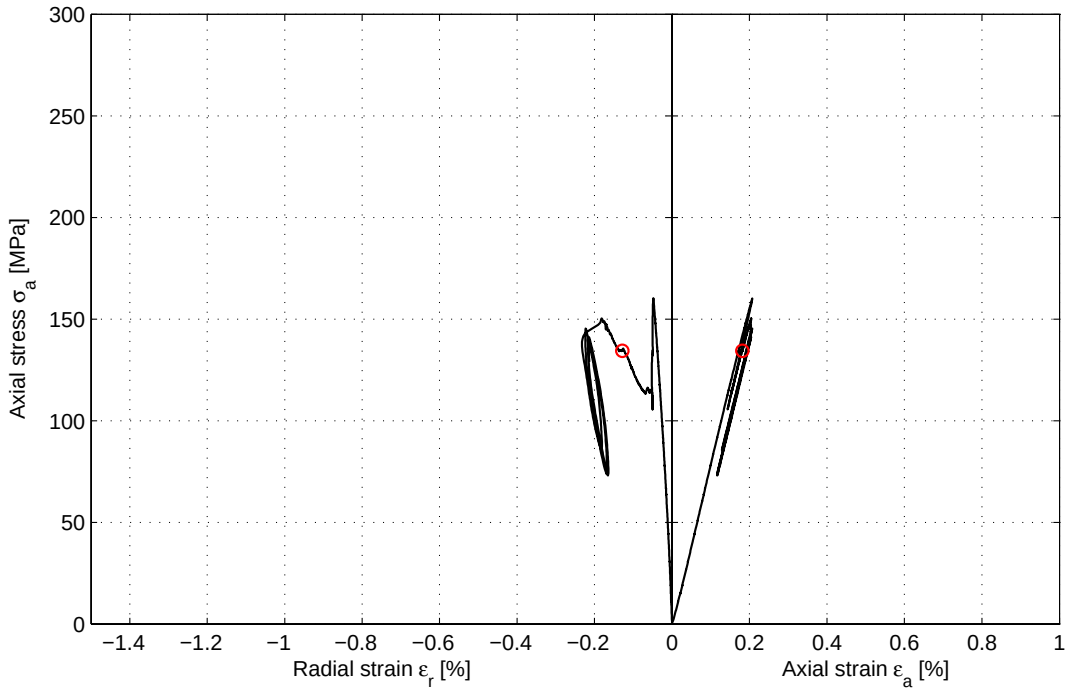

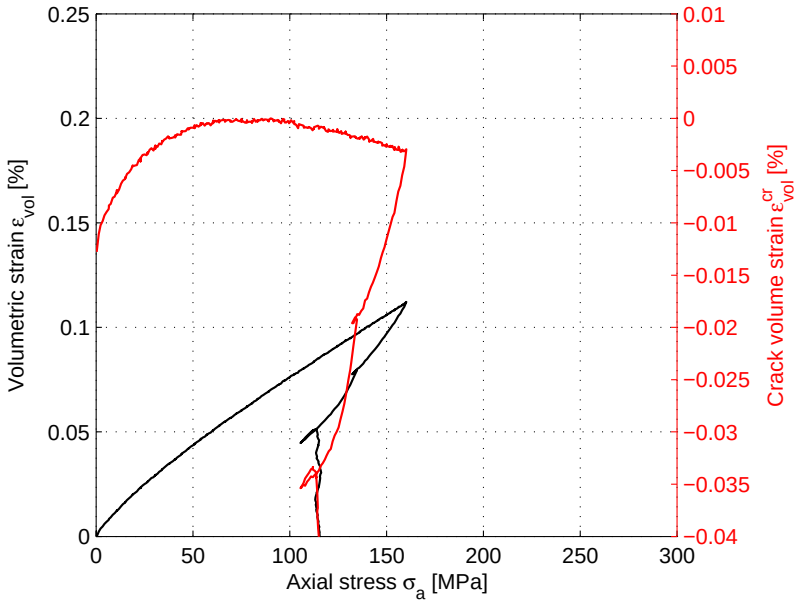

Specimen ID: KSH01A-113-32

Before mechanical test

After mechanical test

Diameter (mm)	Height (mm)	Density (kg/m^3)
50.1	127.2	2,830

Comments A crack was developed through the diameter of one of the end surfaces on the specimen. A shear type of failure was obtained.

Specimen ID: KSH01A−113−32

Youngs Modulus (E):	79	[GPa]
Poisson Ratio (ν):	0.192	[−]
Axial peak stress (σ_c):	118.3	[MPa]

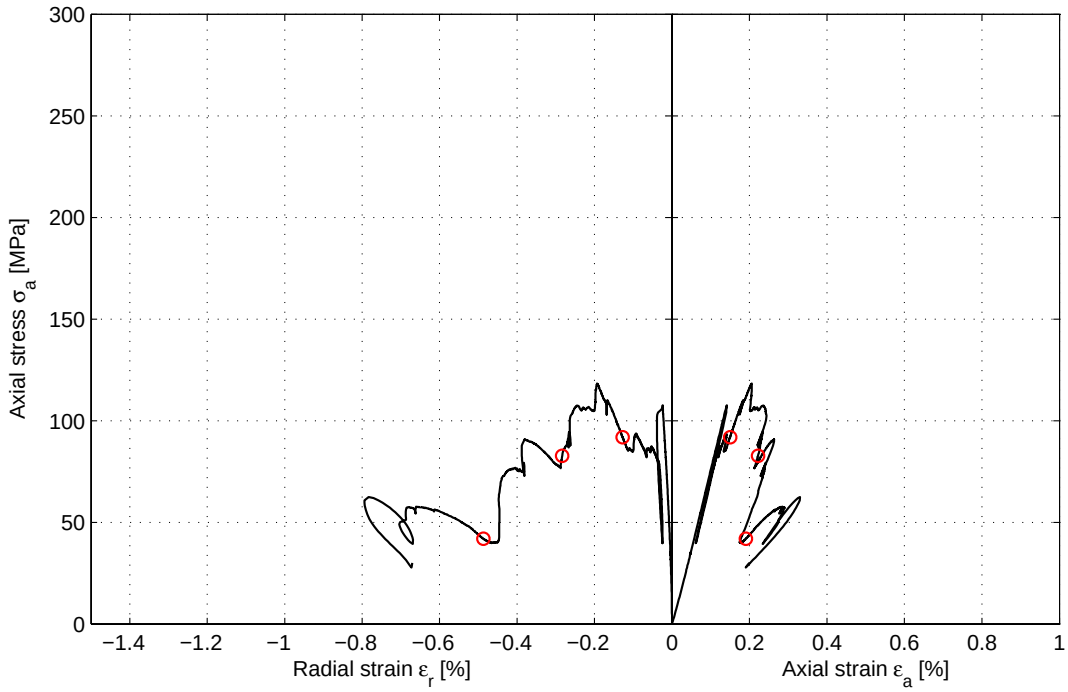

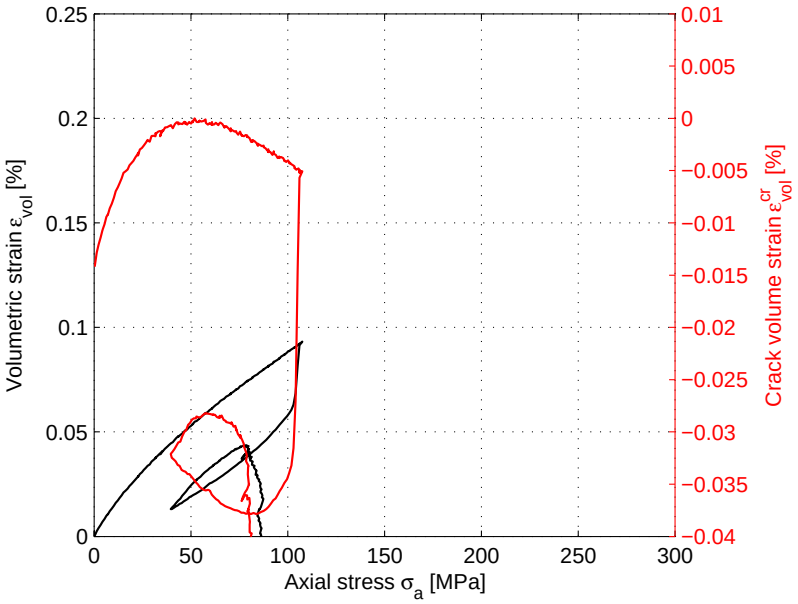

5.2 Results for the entire test series

A summary of the test results is shown in Tables 5-1 and 5-2. SKB has reviewed all results and excluded data that are not representative for the homogenous rock material, cf. Table 5-1. The density, uniaxial compressive strength, the tangent Young's modulus and the tangent Poisson ratio versus the depth, at which the samples are taken, are shown in Figures 5-1 to 5-4.

Table 5-1. Summary of results. The results in parenthesises denote results that are not representative for the homogenous rock material as defects in the specimens were observed.

Identification	Density (kg/m^3)	Compressive Strength (MPa)	Young's modulus (GPa)	Poisson ratio (–)	K_{system} (MN/m)	Comments
KSH01A-113-1	2,770	158.3	68.7	0.31	11.41	
KSH01A-113-3	2,770	167.7	66.0	0.33	13.74	
KSH01A-113-5	2,780	170.4	66.7	0.27	12.52	
KSH01A-113-7	2,790	192.9	82.9	0.32	8.39	
KSH01A-113-9	2,810	186.0	78.6	0.33	9.15	
KSH01A-113-14	2,780	(151.6)	81.7	0.19	13.10	Weakness zone
KSH01A-113-15	2,780	246.8	84.3	0.25	8.59	
KSH01A-113-17	2,780	109.3	78.5	0.24	10.59	Shear failure
KSH01A-113-18	2,780	(158.0)	93.0	0.32	6.92	Multiple cracks
KSH01A-113-19	2,770	(131.2)	103.9	0.29	4.33	Failure in sealed fracture
KSH01A-113-21	2,810	181.6	76.8	0.17	20.70	
KSH01A-113-22	2,800	(91.9)	(85.0)	(0.25)	1.07	Failure in sealed fracture
KSH01A-113-23	2,800	142.1	80.2	0.25	10.91	
KSH01A-113-24	2,790	229.5	76.6	0.27	12.44	
KSH01A-113-25	2,790	171.5	97.0	0.27	4.91	
KSH01A-113-28	2,830	141.6	82.9	0.22	8.39	
KSH01A-113-29	2,830	133.1	74.3	0.26	6.26	
KSH01A-113-30	2,840	177.6	82.6	0.24	11.72	
KSH01A-113-31	2,830	160.2	80.6	0.24	9.36	
KSH01A-113-32	2,830	(118.3)	79.0	0.19	10.74	Failure in sealed fracture

Table 5-2. Calculated mean values and standard deviation (Std dev) of the results. The results in parenthesises in Table 5-1 are excluded in the calculations.

	Density (kg/m^3)	Compressive Strength (MPa)	Young's modulus (GPa)	Poisson ratio (–)
Mean value (299–320 m)	2,784	175.0	72.6	0.31
Mean value (398–414 m)	2,778	178.0	88.3	0.26
Mean value (486–498 m)	2,798	181.2	82.6	0.24
Mean value (699–709 m)	2,832	153.1	79.9	0.23
Mean value (All levels)	2,798	171.2	80.8	0.26
Std dev (299–320 m)	16.7	14.1	7.7	0.02
Std dev (398–414 m)	4.5	97.2	10.3	0.05
Std dev (486–498 m)	8.4	36.3	9.7	0.05
Std dev (699–709 m)	4.5	19.9	3.5	0.03
Std dev (All levels)	23.3	35.1	9.5	0.05

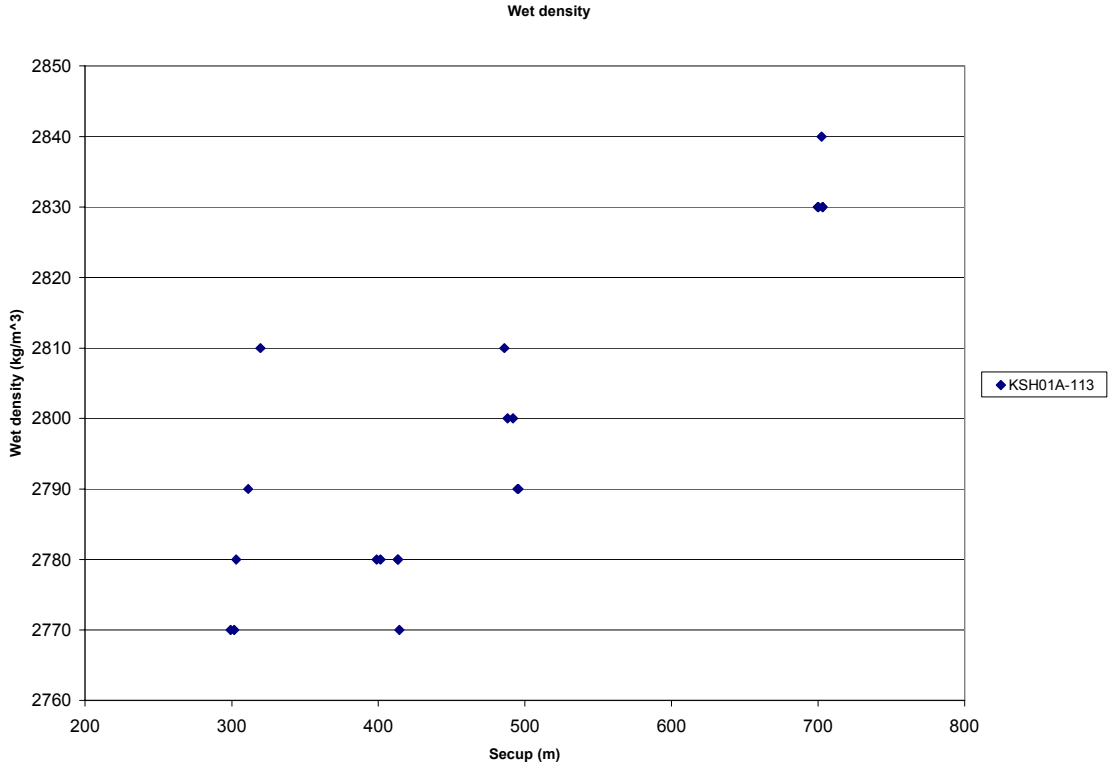

Figure 5-1. *Density versus depth at which the samples are taken in the borehole.*

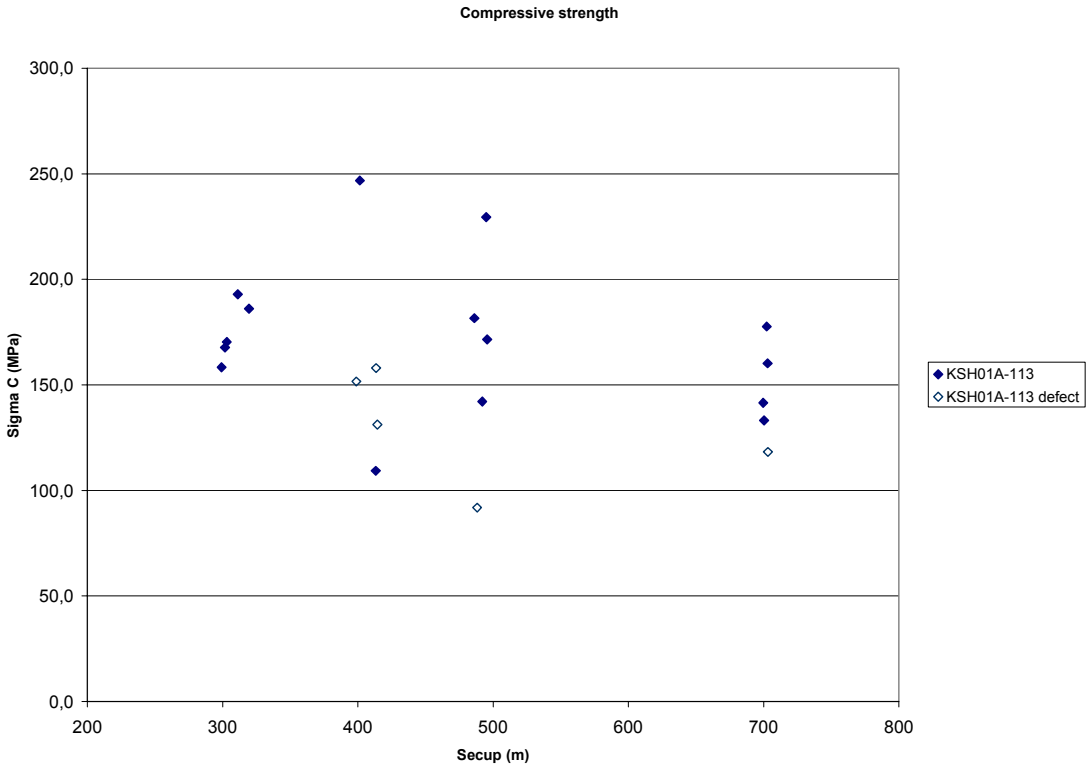

Figure 5-2. *Uniaxial compressive strength versus depth at which the samples are taken in the borehole.*

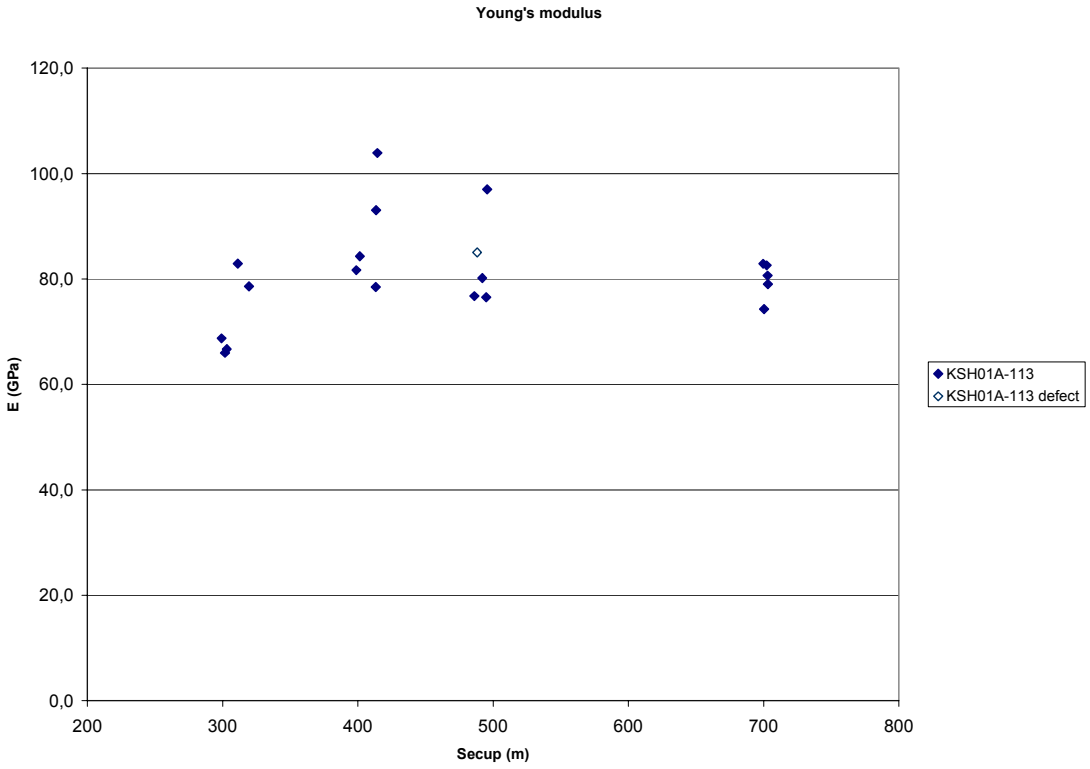

Figure 5-3. *Tangent Young's modulus versus depth at which the samples are taken in the borehole.*

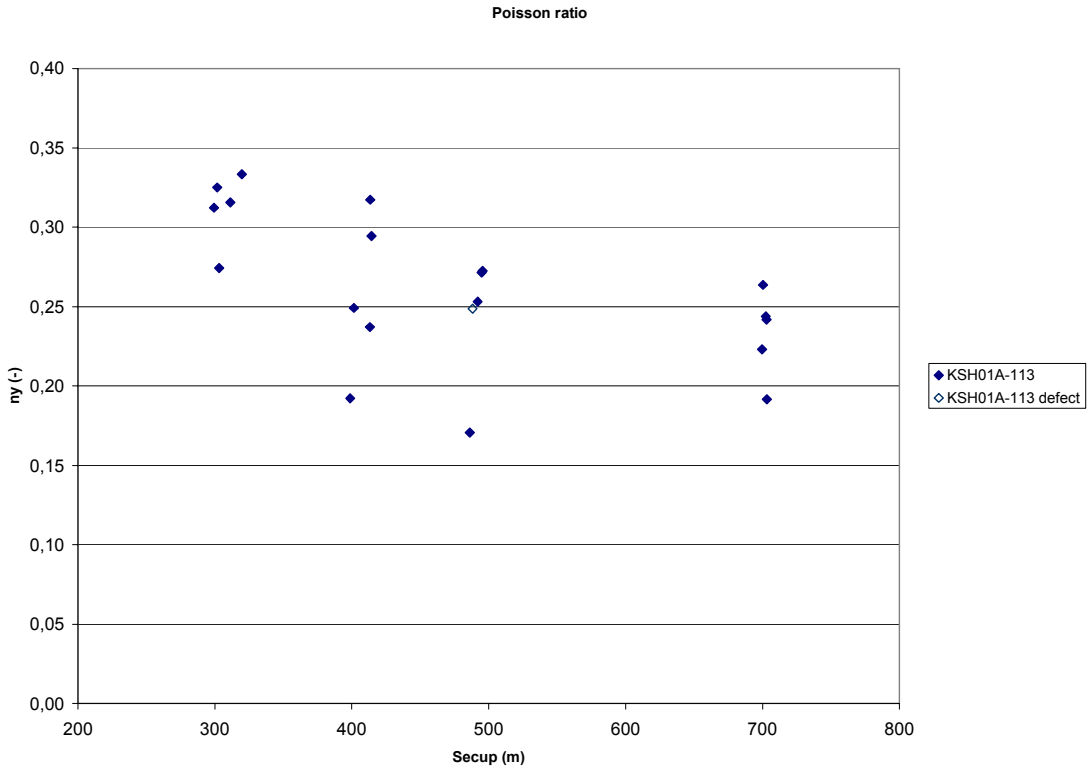

Figure 5-4. *Tangent Poisson ratio versus depth at which the samples are taken in the borehole.*

5.3 Discussion

The testing was conducted according to the method description with some deviations. It was observed that there was an error in the calibration of the LVDTs at the time for the testing. The LVDTs were therefore recalibrated and a correction of the measured data could be made. This implied that axial and circumferential strains have been determined within an accuracy of 2.7%, which is larger than what is specified in the ISRM-standard /1/. Further, double systems for measuring the axial deformation have been used, which is beyond the method description. This was conducted as development of the test method specially aimed for high-strength brittle rock. It must be remarked that some tests were restarted after complete unloading caused by a registration of a sudden radial expansion due to cracking. This was done in order to obtain further results in the post-failure region and but only in cases when the test just had entered the post failure-region and when it was judged that the specimen still had a large part of the load bearing capacity left. The radial strain feedback implies that the system responds with an unloading when an instantaneous radial expansion of the specimen takes place due to cracking. Moreover, the load started to oscillate in some tests after a crack was developed. An improper setting of the parameter setting of the feed-back control implying a too small stability margin allowed the oscillations to start.

The activity plan was followed with no departures with the exception of that specimen KSH01A-113-19 (secup 414.44 m) replaced specimen KSH01A-113-16 (secup 412.41 m) as it was cracked.

References

/1/ **ISRM, 1999.** Draft ISRM suggested method for the complete stress-strain curve for intact rock in uniaxial compression. Int. J. Rock. Mech. Min. Sci. 36(3), pp. 279–289.

/2/ **Martin C D, Chandler N A, 1994.** The progressive fracture of Luc du Bonnet granite, Int. J. Rock. Mech. Min. Sci. & Geomech. Abstr. 31(6), pp. 643–659.

/3/ **Eberhardt E, Stead D, Stimpson B, Read R S, 1998.** Identifying crack initiation and propagation thresholds in brittle rock. Can. Geotech. J. 35, pp. 222–233.

/4/ **ASTM 4543-01, 2001.** Standard practice for preparing rock core specimens and determining dimensional and shape tolerance.

/5/ **ISRM, 1979.** Suggested Method for Determining Water Content, Porosity, Density, Absorption and Related Properties and Swelling and Slake-durability Index Properties. Int. J. Rock. Mech. Min. Sci. & Geomech. Abstr. 16(2), pp. 141–156.

/6/ **SS-EN 13755.** Natural stone test methods – Determination of water absorption at atmospheric pressure.

/7/ **Stråhle A, 2001.** Definition och beskrivning av parametrar för geologisk, geofysisk och bergmekanisk kartering av berg. SKB R-01-19, Svensk Kärnbränslehantering AB. In Swedish.

/8/ **MATLAB, 2002.** The Language of Technical computing. Version 6.5. MathWorks Inc.

Appendix A

The following equations describe the calculation of radial strains when using a circumferential deformation device, see Figure A-1.

$$\varepsilon_r = \frac{\Delta C}{C_i}$$

where

$C_i = 2\ \pi R_i$ = initial specimen circumference

$$\Delta C = \text{change in specimen circumference} = \frac{\pi \cdot \Delta X}{\sin\left(\frac{\theta_i}{2}\right) + \left(\pi - \frac{\theta_i}{2}\right)\cos\left(\frac{\theta_i}{2}\right)}$$

and

ΔX = change in LVDT reading = $X_i - X_f$

(X_i = initial chain gap; X_f = current chain gap)

$$\theta_i = \text{initial chord angle} = 2\pi - \frac{L_c}{R_i + r}$$

L_c = chain length (measured from center of one end roller to center of other end roller)

r = roller radius

R_i = initial specimen radius

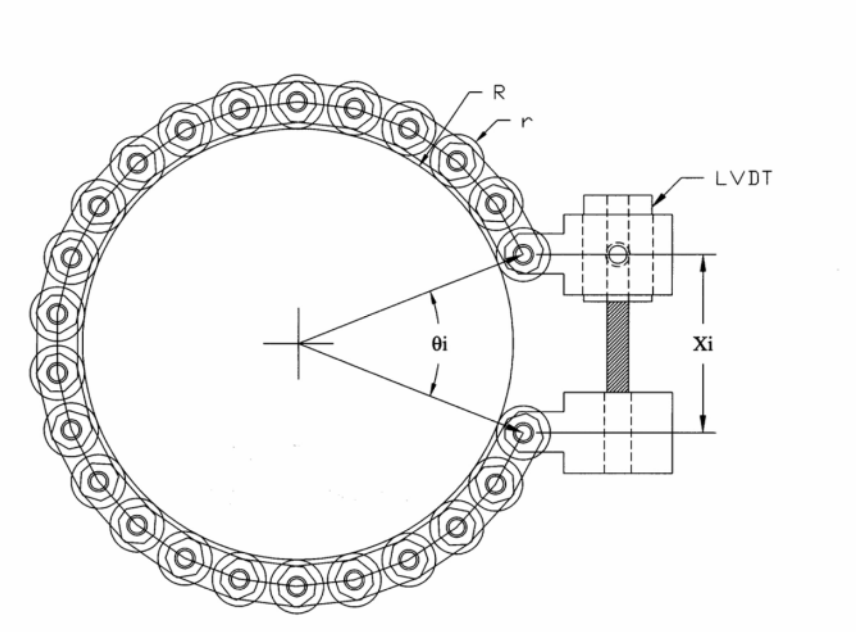

Figure A-1. *Chain for radial deformation measurement.*

Appendix B

This Appendix contains results showing the unprocessed data and values on the computed system stiffness K_{system} that was used for the data processing, cf. Section 4.4. In addition graphs showing the volumetric strain ε_{vol} versus the axial strain ε_a and the actual radial strain rate $d\varepsilon_r/dt$ versus time are also displayed.

Specimen ID: KSH01A−113−01

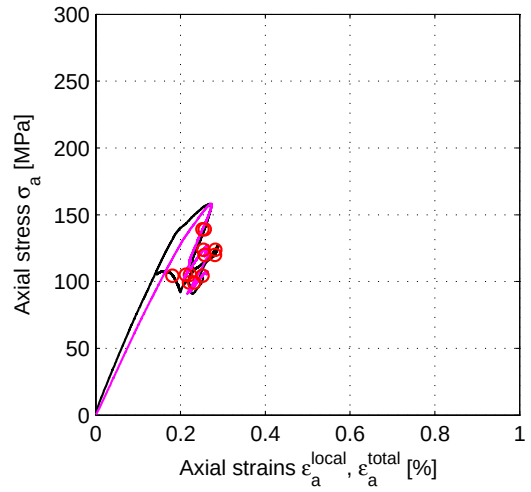

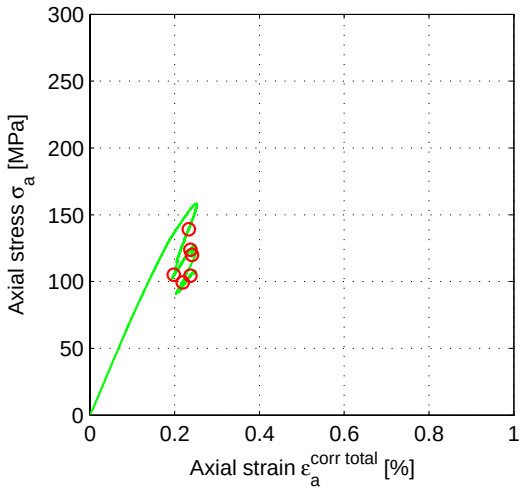

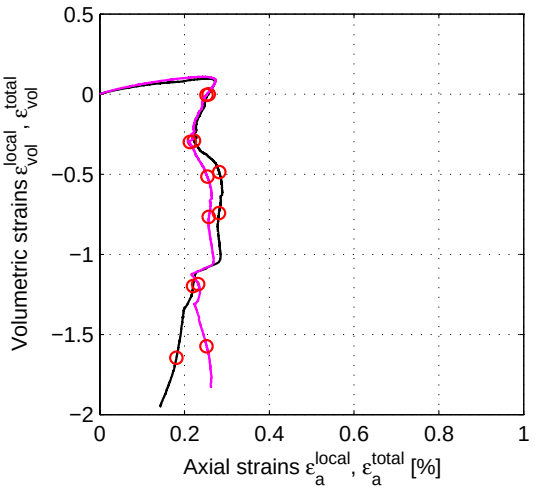

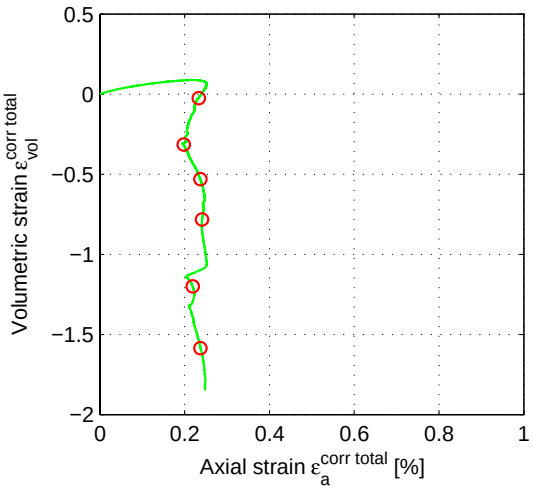

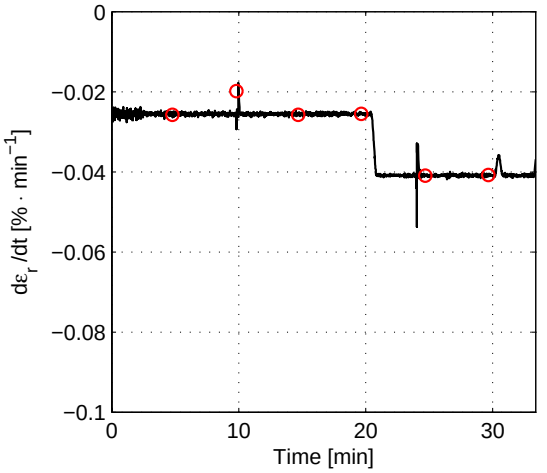

Explanation to curves above:

Based on local deformation (black)

Based on total deformation (mangenta)

Based on corrected deformation (green)

Calculated system stiffness:

K_{system} = 11.4098 [MN/m]

Specimen ID: KSH01A−113−03

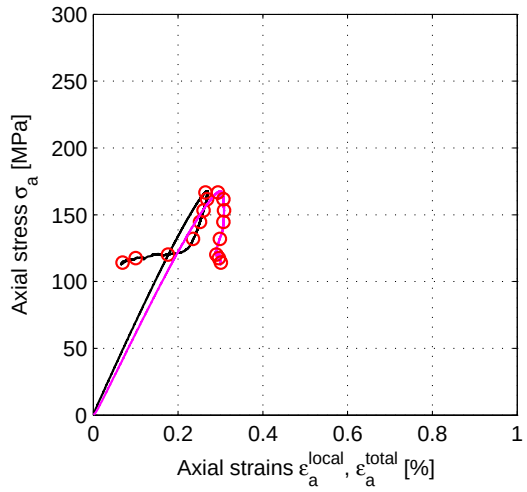

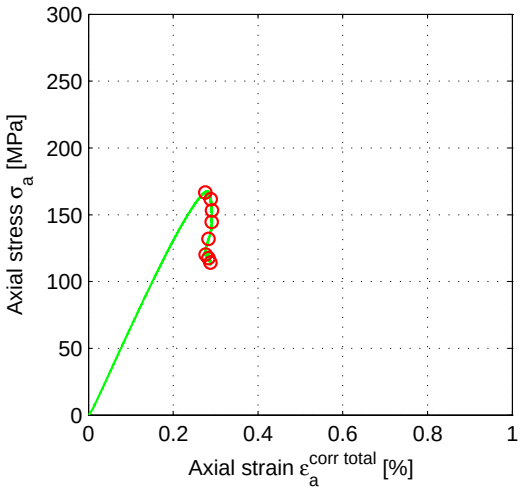

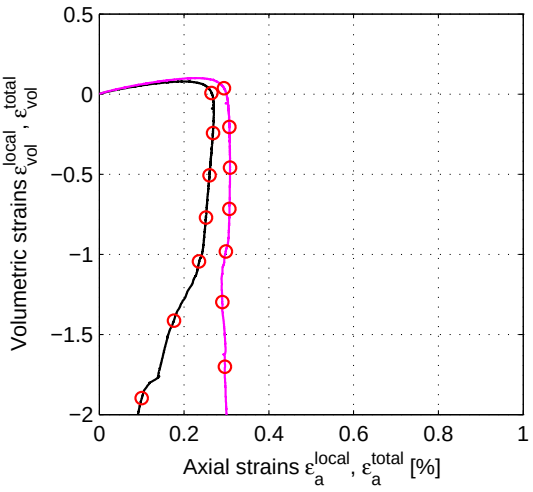

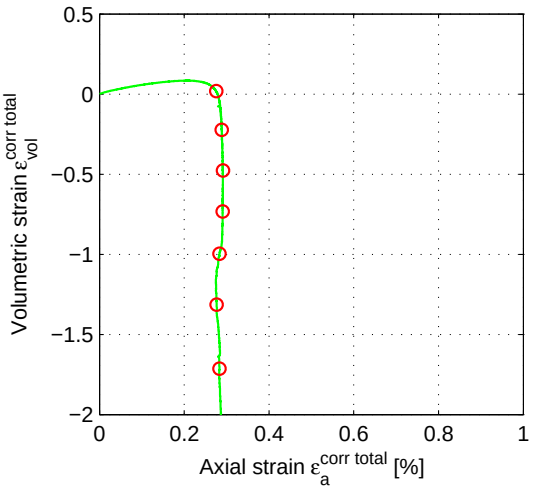

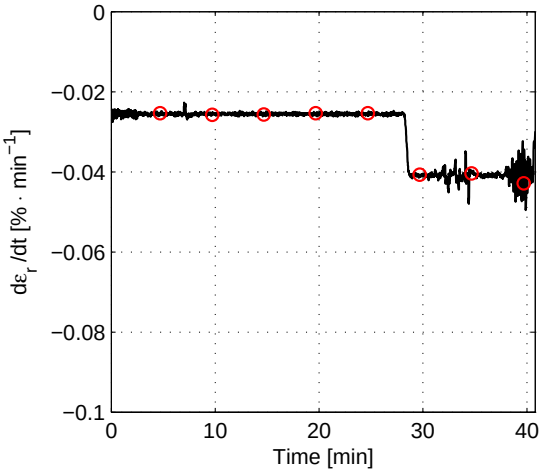

Explanation to curves above:

Based on local deformation (black)

Based on total deformation (mangenta)

Based on corrected deformation (green)

Calculated system stiffness:

K_{system} = 13.7352 [MN/m]

Specimen ID: KSH01A−113−05

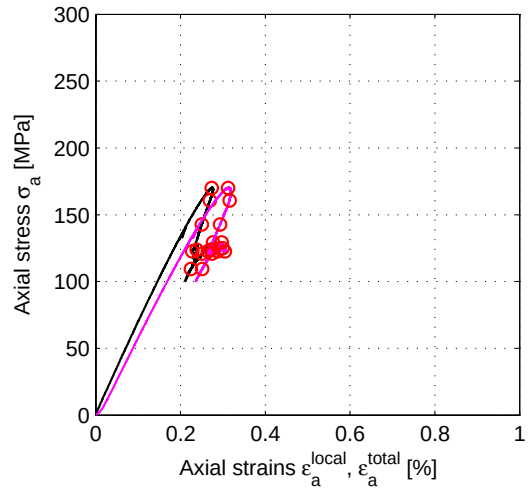

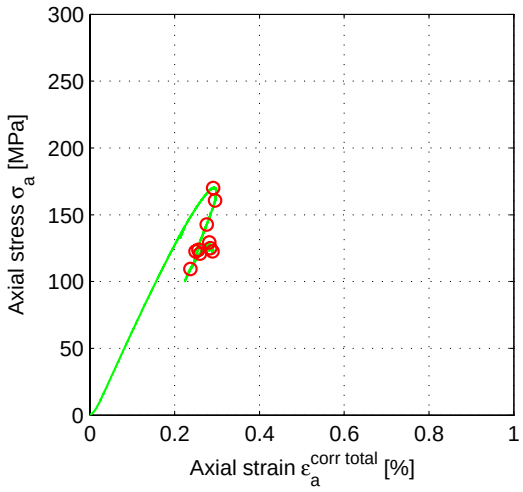

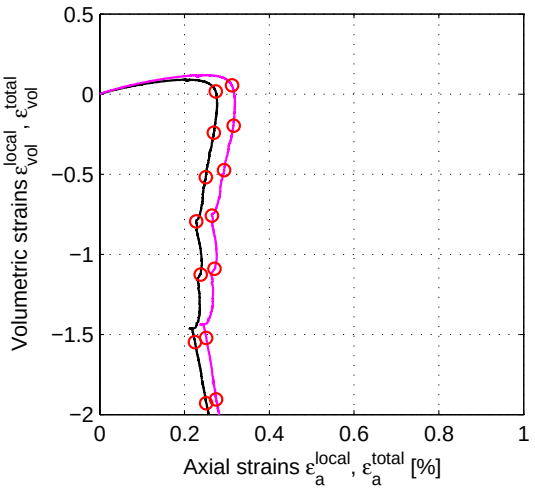

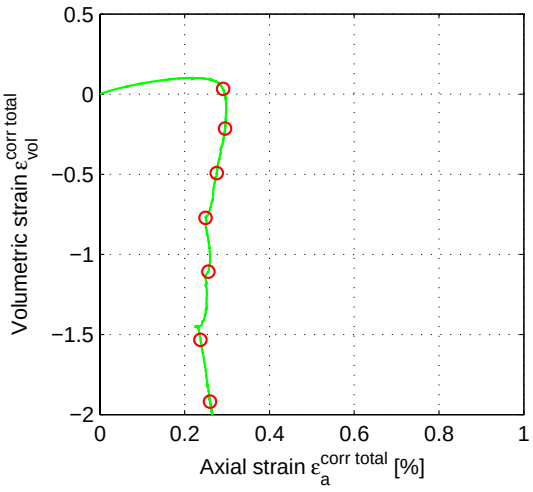

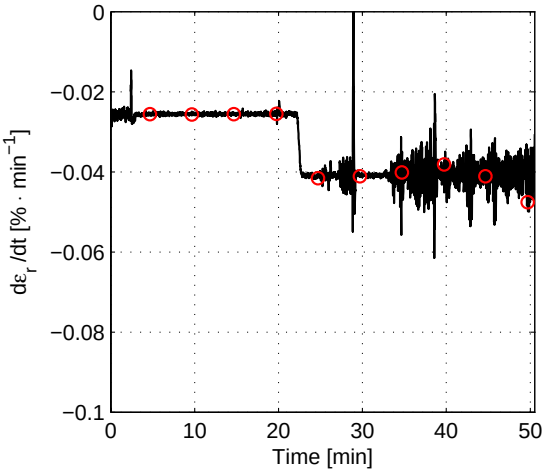

Explanation to curves above:

Based on local deformation (black)

Based on total deformation (mangenta)

Based on corrected deformation (green)

Calculated system stiffness:

K_{system} = 12.5223 [MN/m]

Specimen ID: KSH01A−113−07

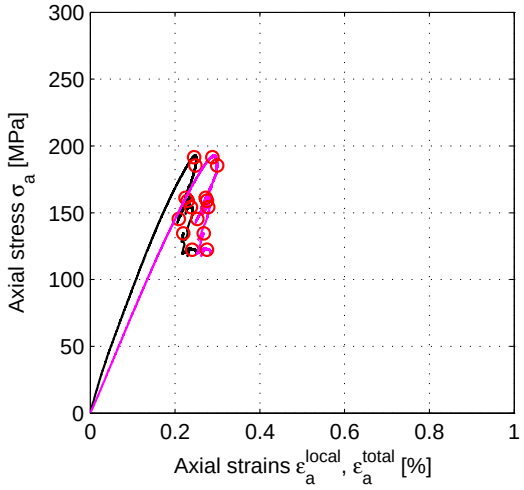

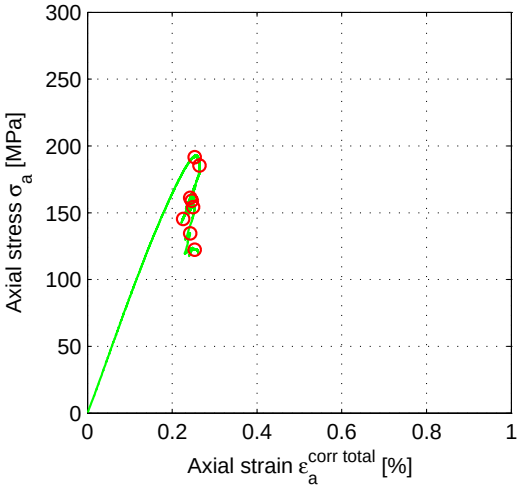

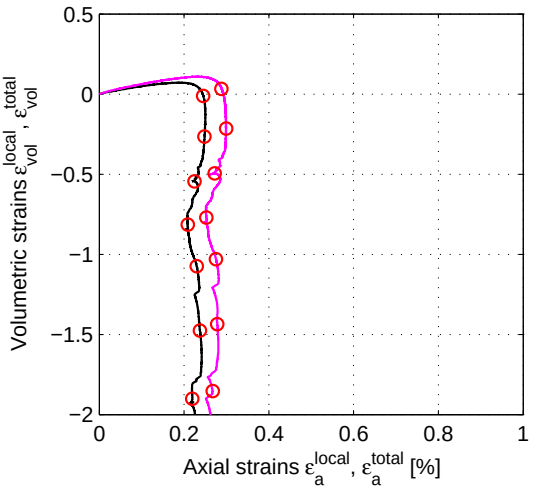

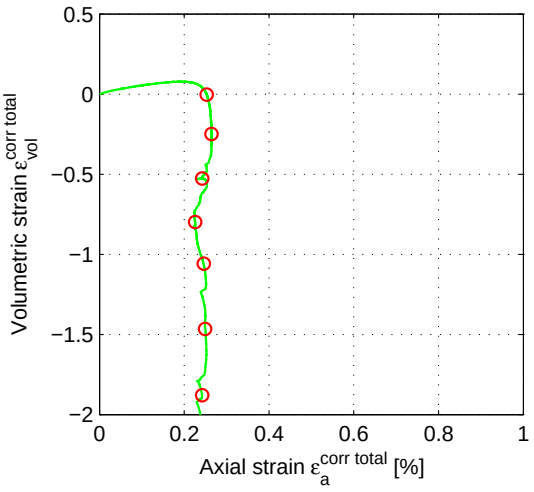

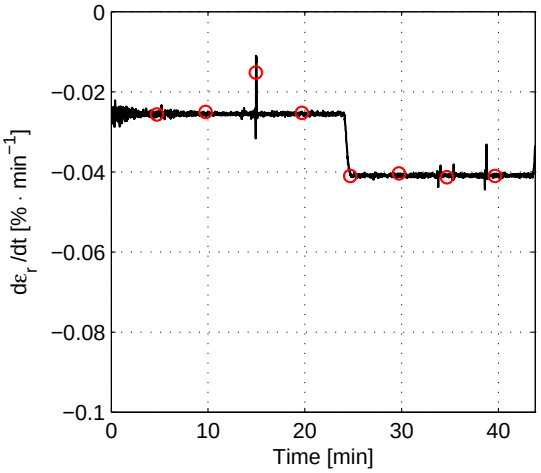

Explanation to curves above:

Based on local deformation (black)

Based on total deformation (mangenta)

Based on corrected deformation (green)

Calculated system stiffness:

K_{system} = 8.3893 [MN/m]

Specimen ID: KSH01A−113−09

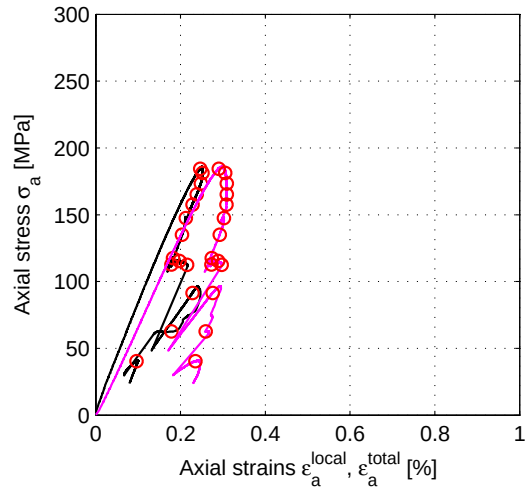

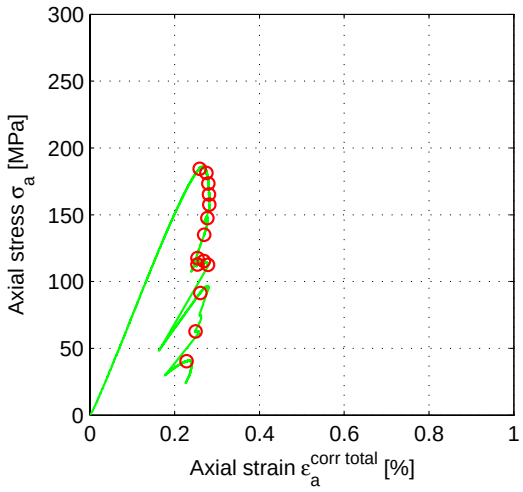

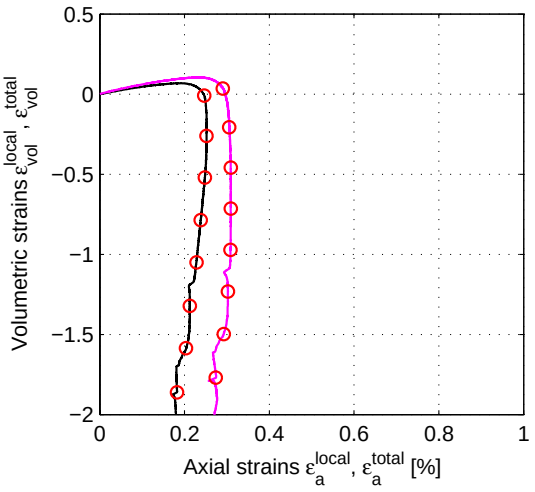

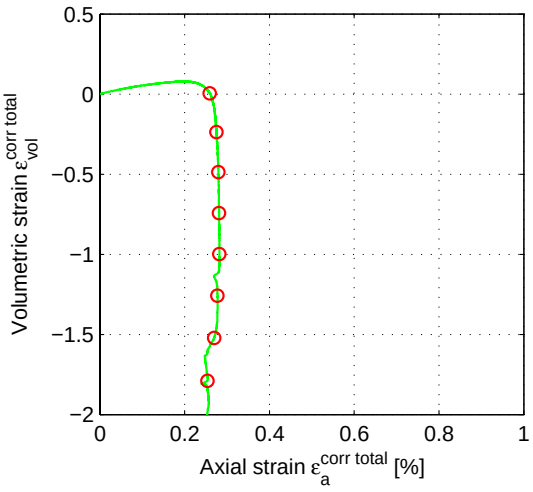

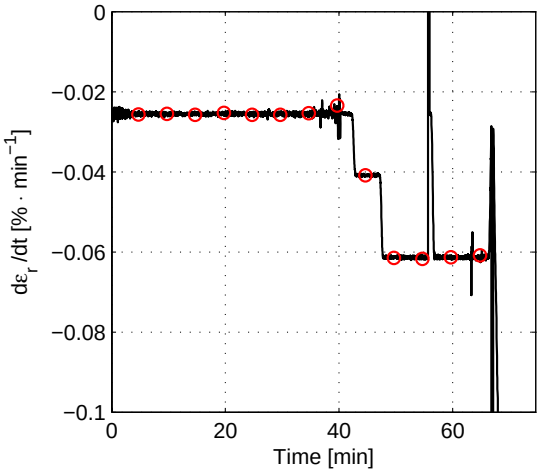

Explanation to curves above:

Based on local deformation (black)

Based on total deformation (mangenta)

Based on corrected deformation (green)

Calculated system stiffness:

K_{system} = 9.1546 [MN/m]

Specimen ID: KSH01A−113−14

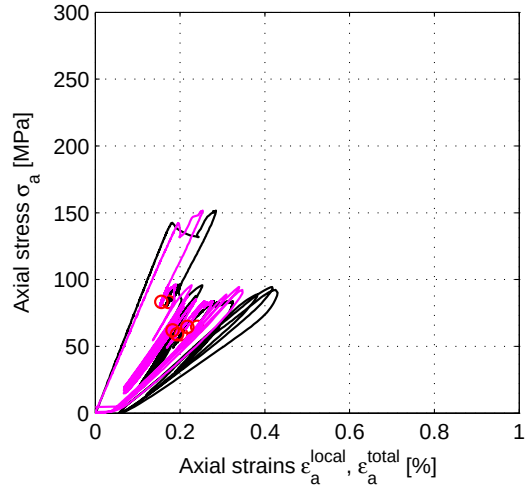

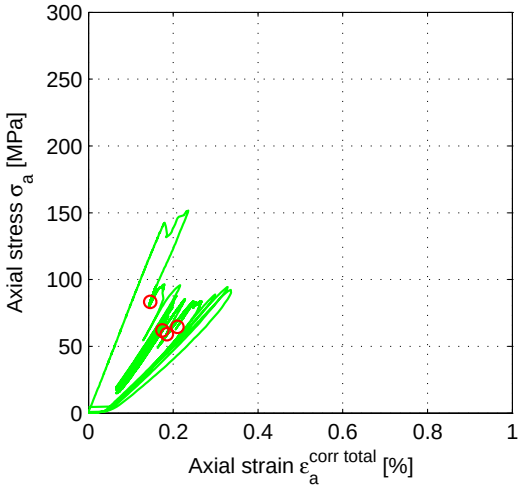

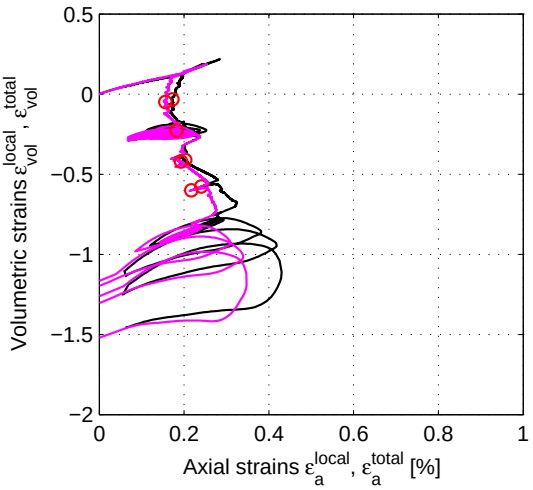

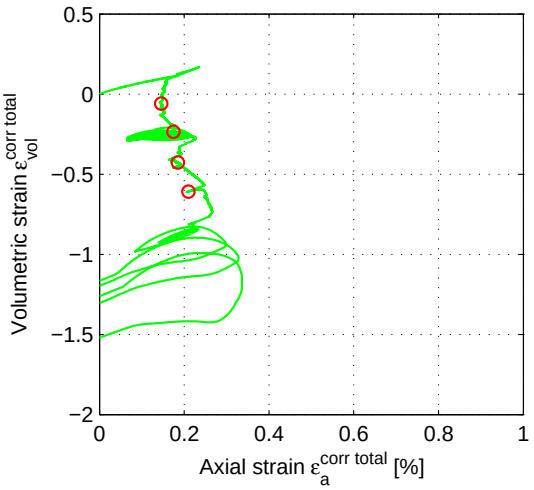

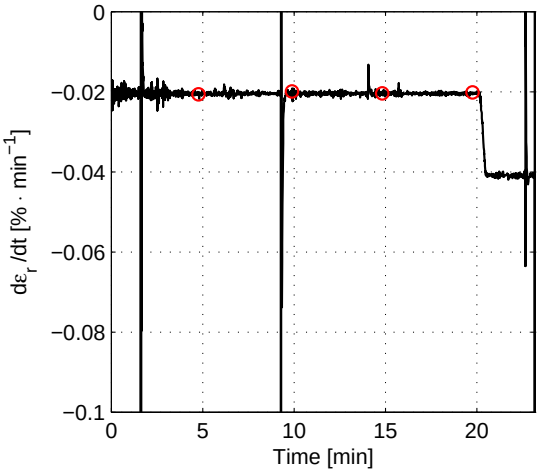

Explanation to curves above:

Based on local deformation (black)

Based on total deformation (mangenta)

Based on corrected deformation (green)

Calculated system stiffness:

K_{system} = 13.1013 [MN/m]

Specimen ID: KSH01A−113−15

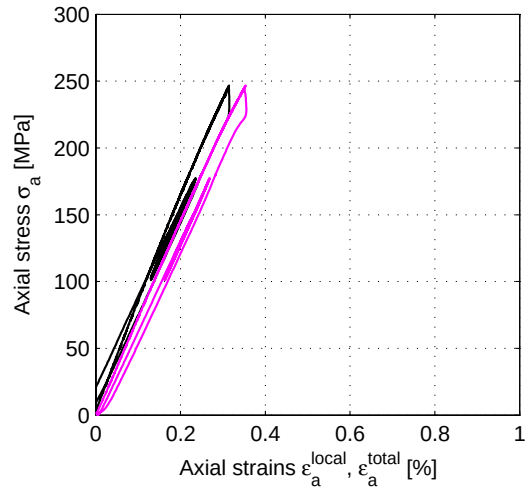

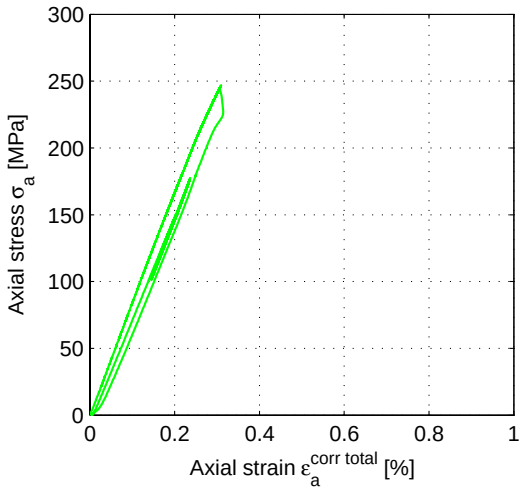

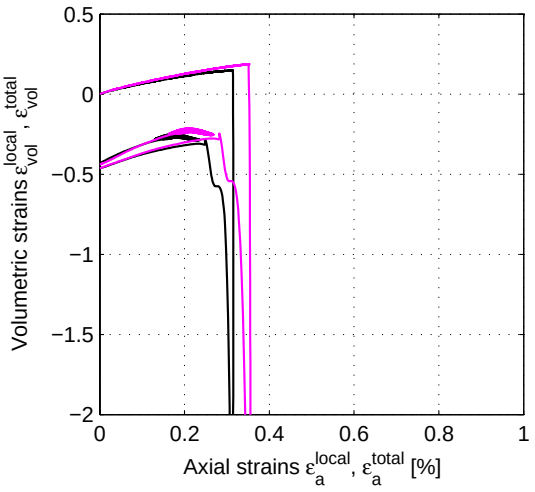

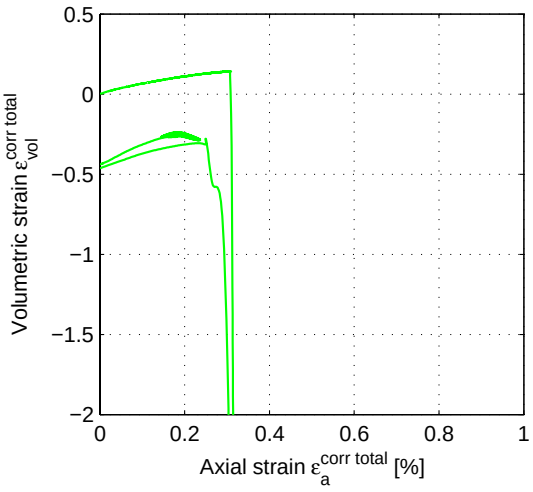

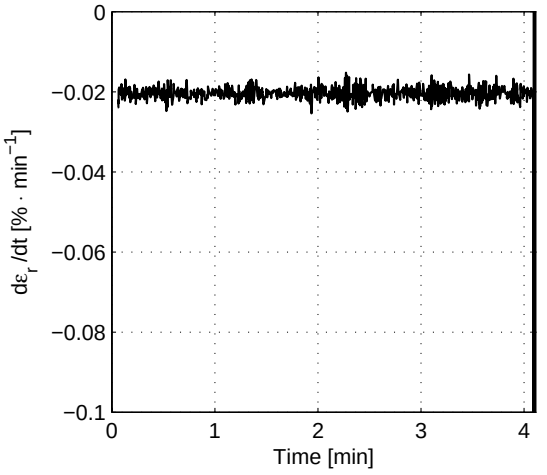

Explanation to curves above:

Based on local deformation (black)

Based on total deformation (mangenta)

Based on corrected deformation (green)

Calculated system stiffness:

K_{system} = 8.5902 [MN/m]

Specimen ID: KSH01A−113−17

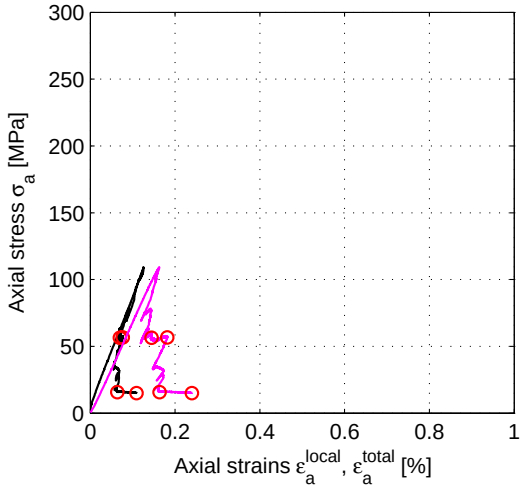

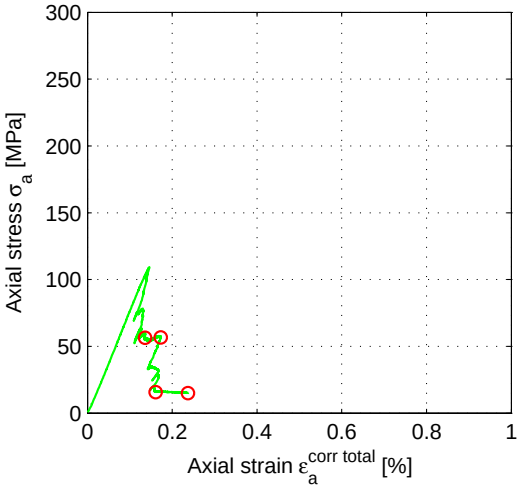

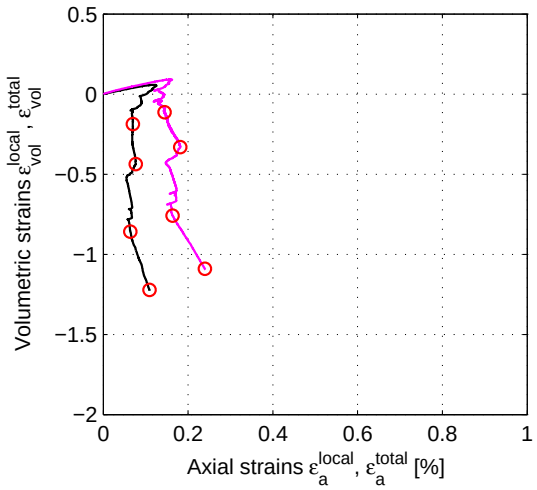

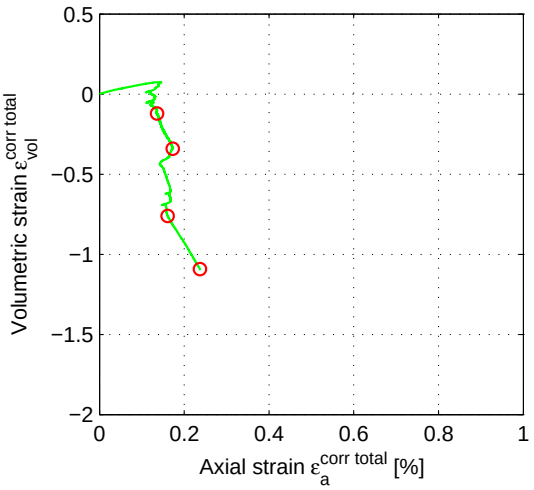

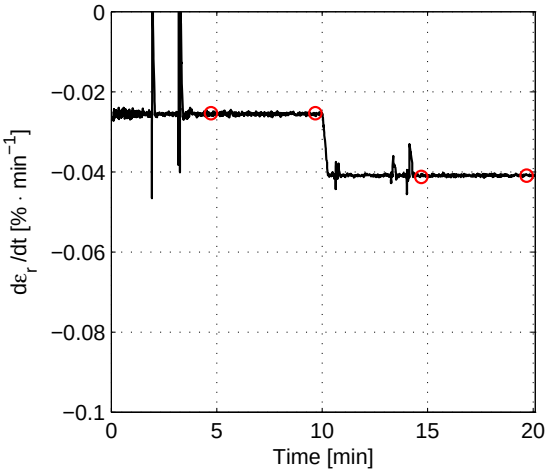

Explanation to curves above:

Based on local deformation (black)

Based on total deformation (mangenta)

Based on corrected deformation (green)

Calculated system stiffness:

K_{system} = 10.5927 [MN/m]

Specimen ID: KSH01A−113−18

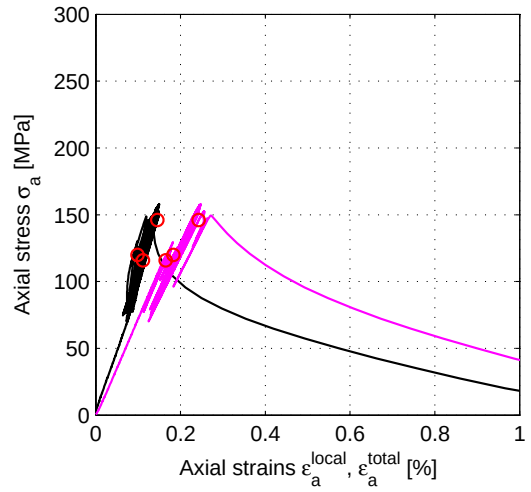

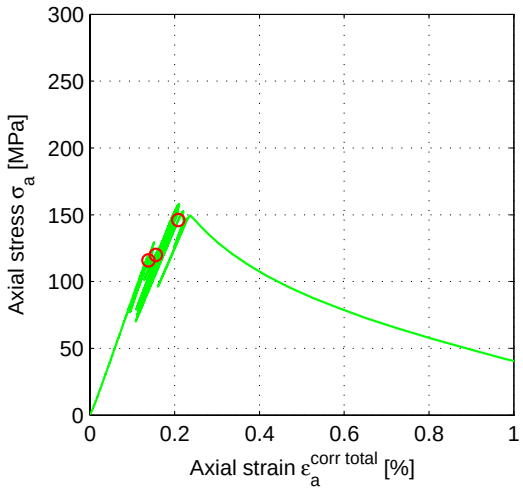

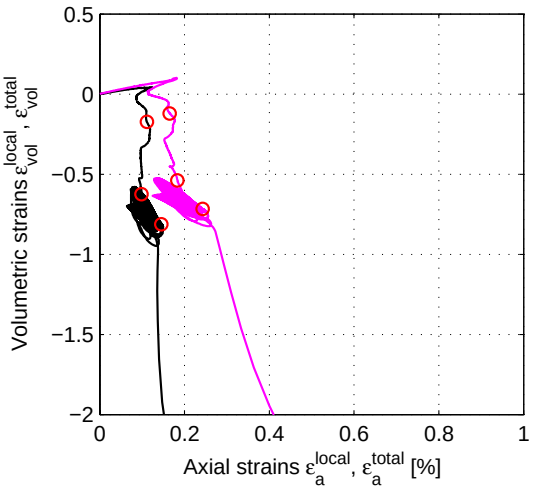

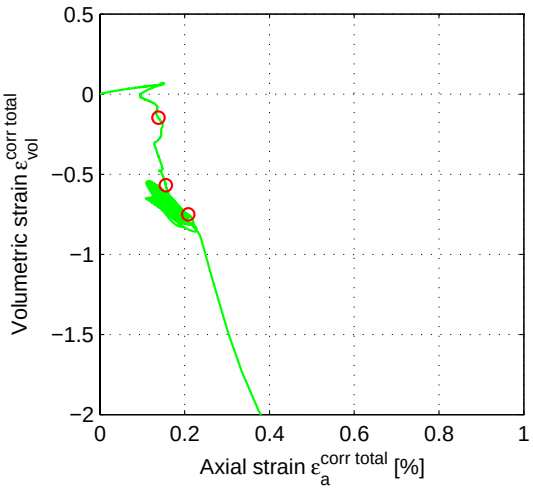

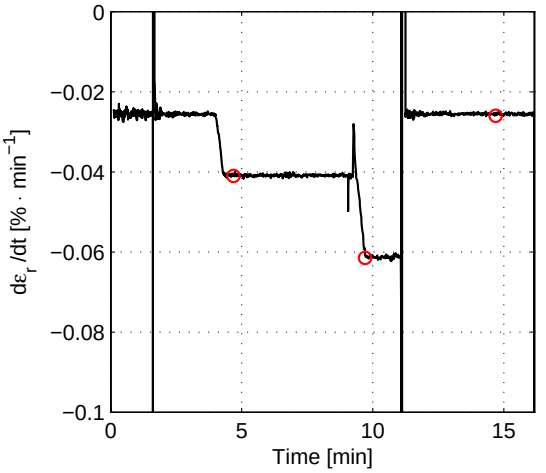

Explanation to curves above:

Based on local deformation (black)

Based on total deformation (mangenta)

Based on corrected deformation (green)

Calculated system stiffness:

K_{system} = 6.9183 [MN/m]

Specimen ID: KSH01A−113−19

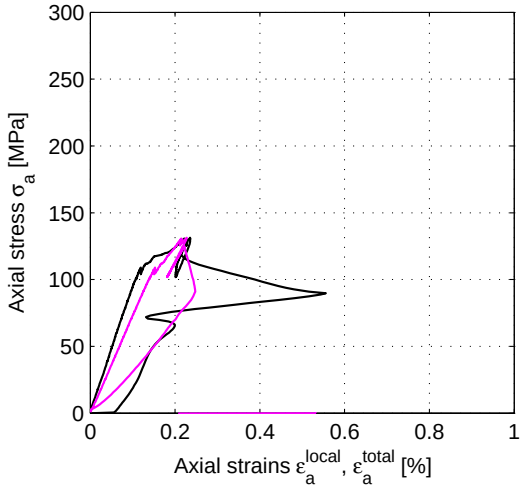

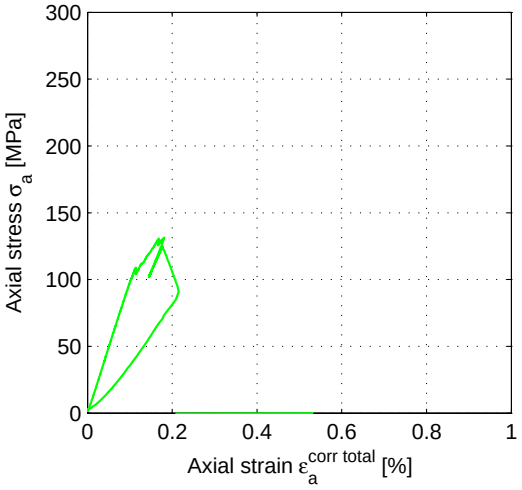

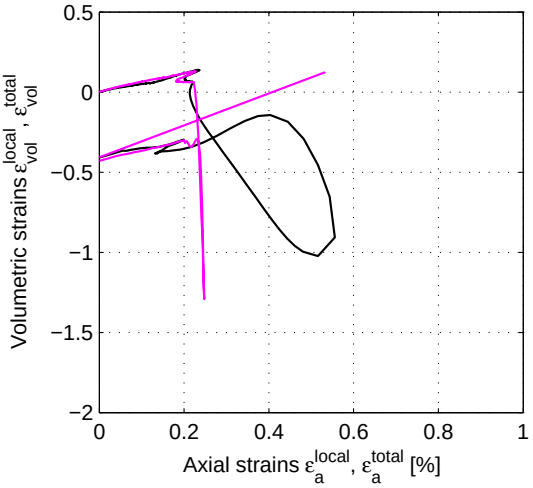

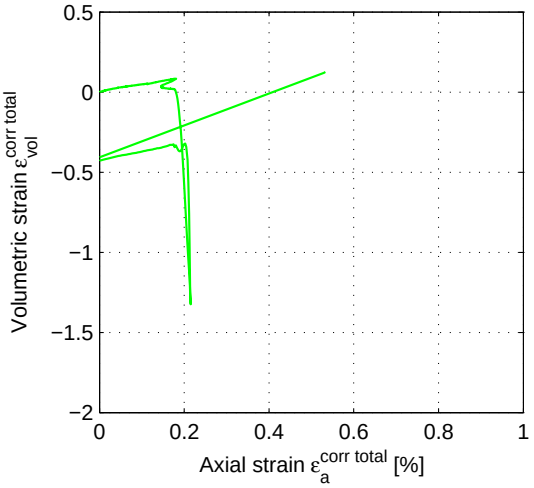

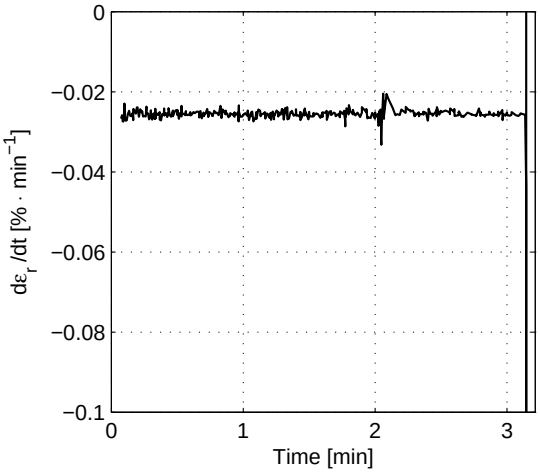

Explanation to curves above:

Based on local deformation (black)

Based on total deformation (mangenta)

Based on corrected deformation (green)

Calculated system stiffness:

K_{system} = 4.3341 [MN/m]

Specimen ID: KSH01A−113−21

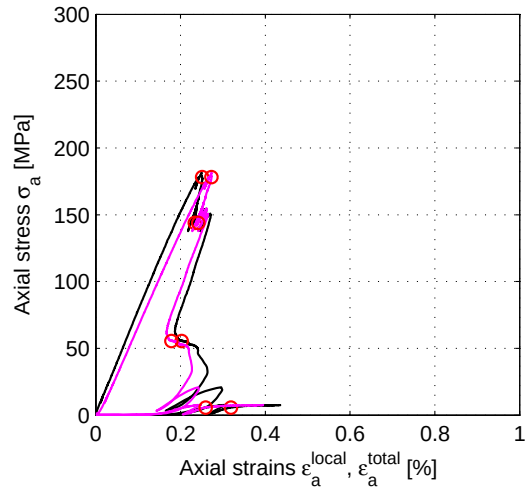

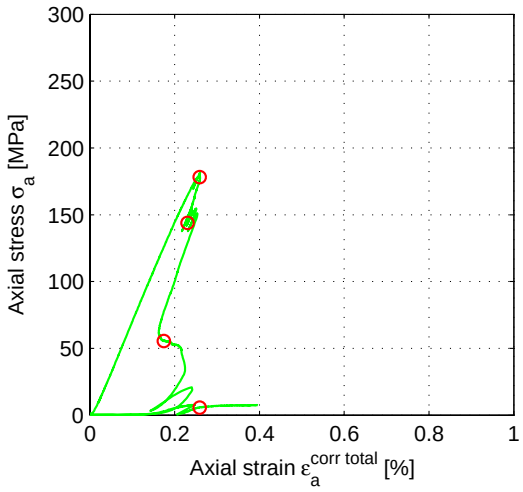

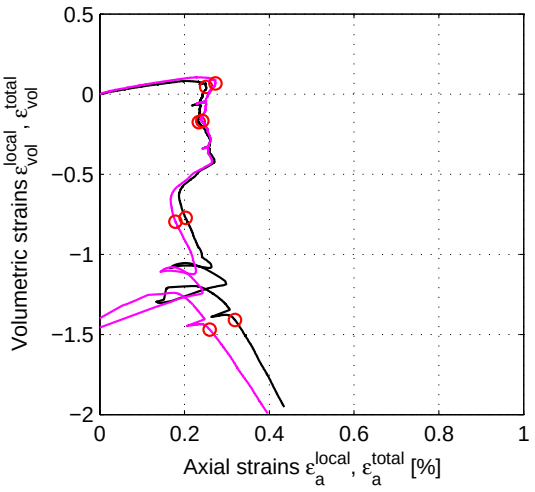

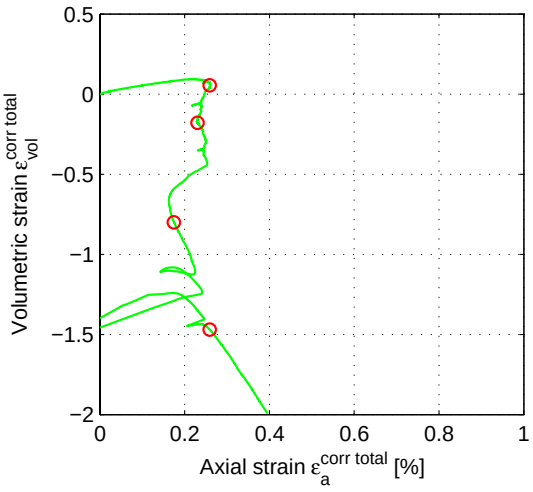

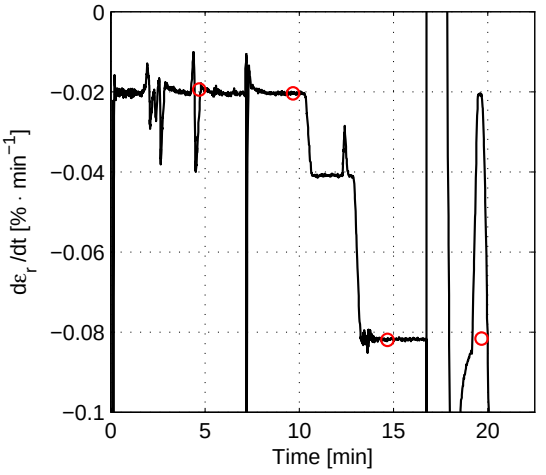

Explanation to curves above:

Based on local deformation (black)

Based on total deformation (mangenta)

Based on corrected deformation (green)

Calculated system stiffness:

K_{system} = 20.6956 [MN/m]

Specimen ID: KSH01A−113−22

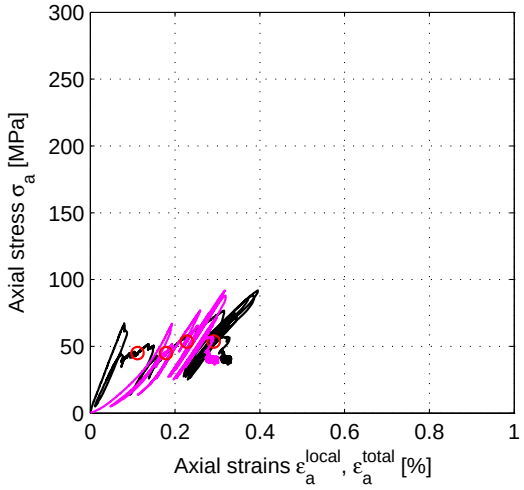

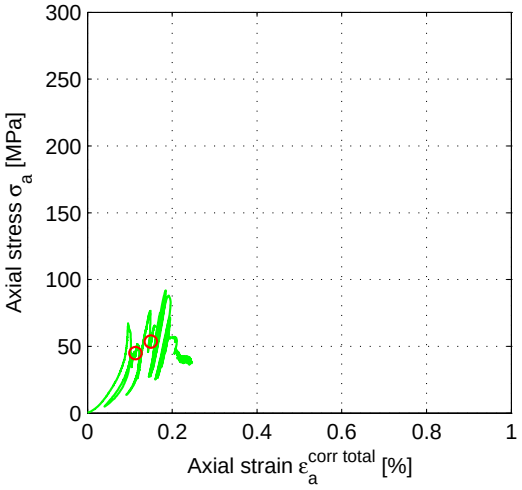

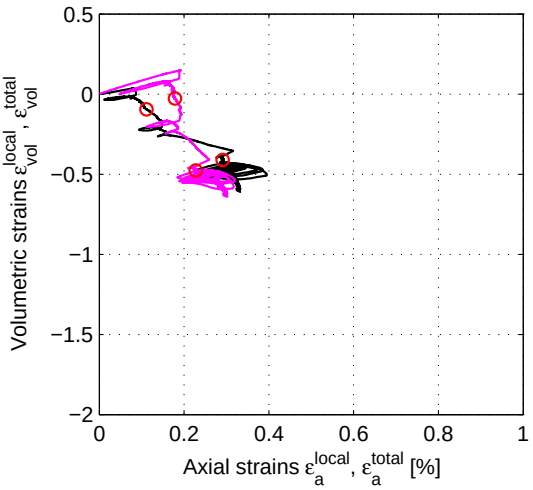

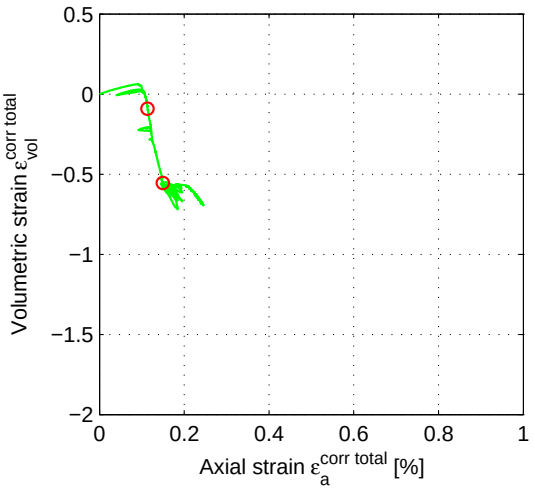

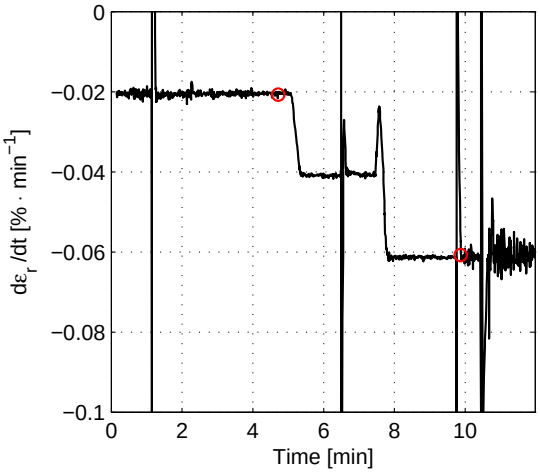

Explanation to curves above:

Based on local deformation (black)

Based on total deformation (mangenta)

Based on corrected deformation (green)

Calculated system stiffness:

K_{system} = 1.0666 [MN/m]

Specimen ID: KSH01A−113−23

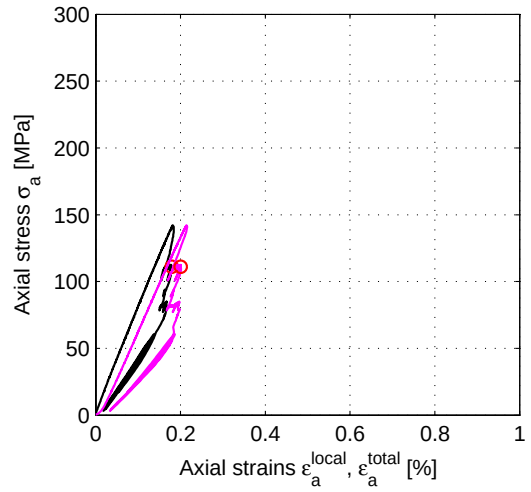

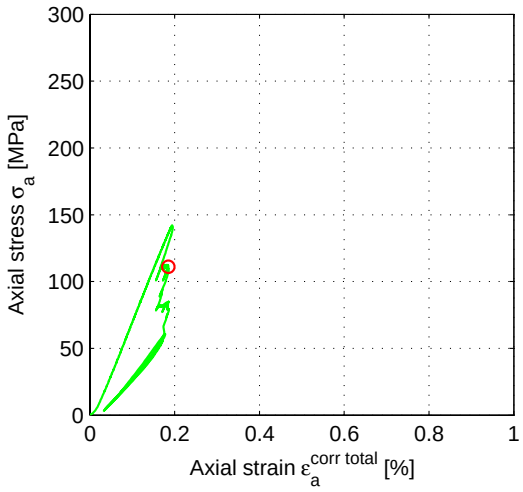

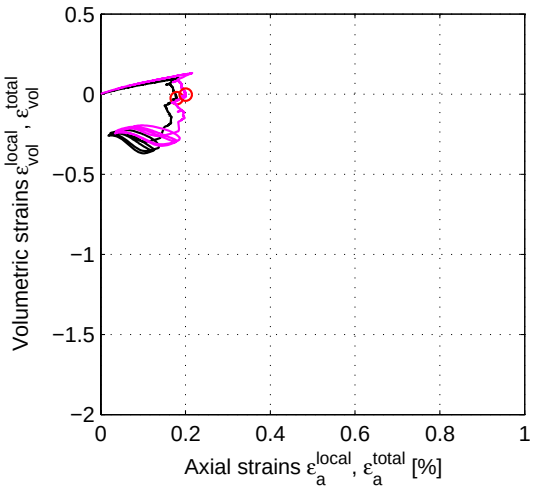

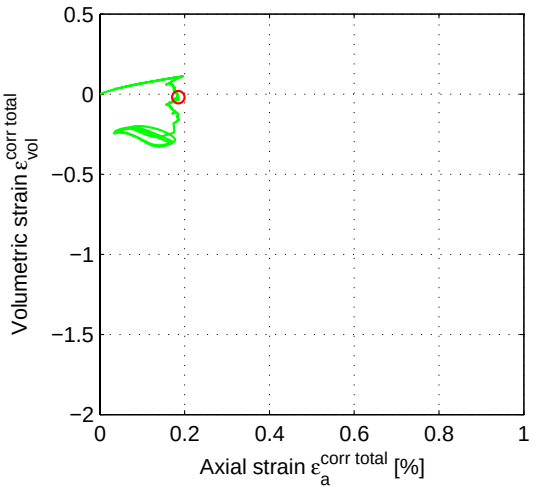

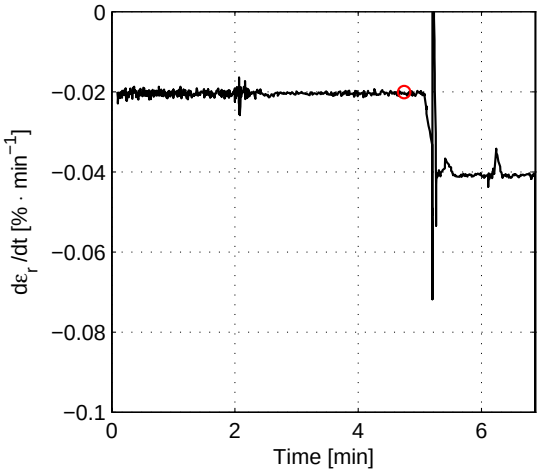

Explanation to curves above:

Based on local deformation (black)

Based on total deformation (mangenta)

Based on corrected deformation (green)

Calculated system stiffness:

K_{system} = 10.9135 [MN/m]

Specimen ID: KSH01A−113−24

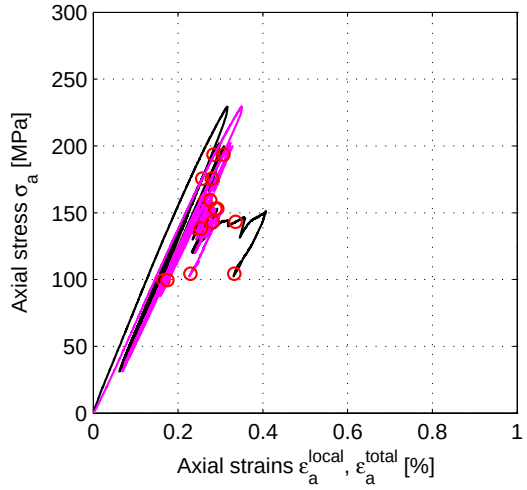

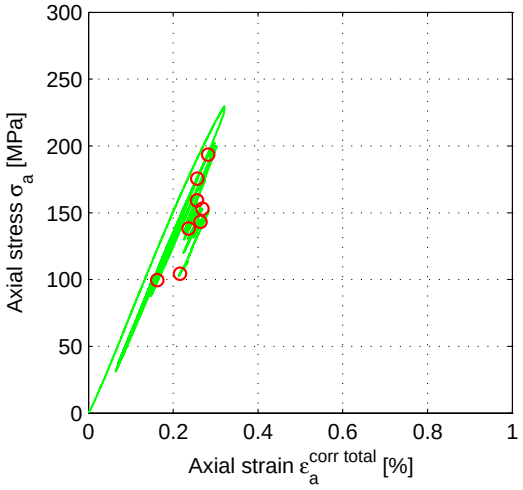

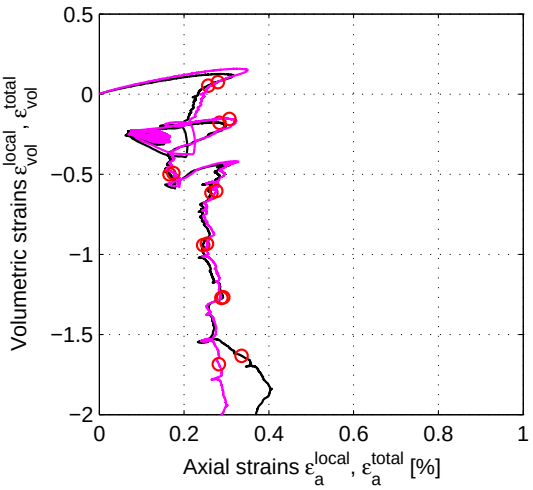

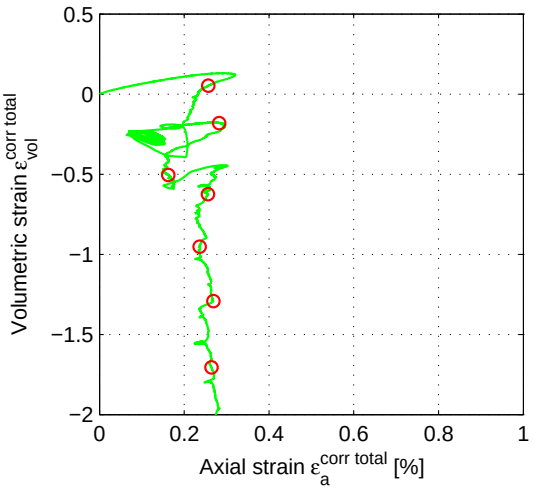

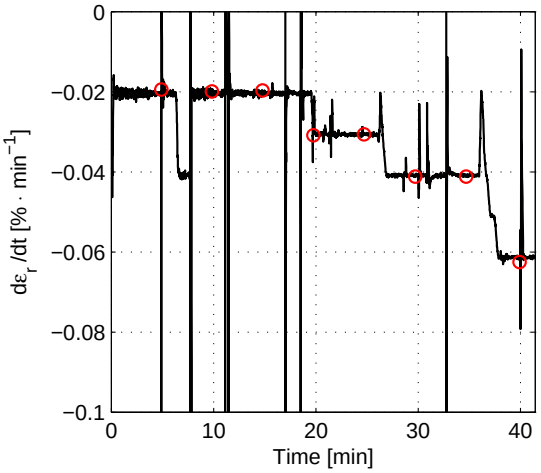

Explanation to curves above:

Based on local deformation (black)

Based on total deformation (mangenta)

Based on corrected deformation (green)

Calculated system stiffness:

K_{system} = 12.443 [MN/m]

Specimen ID: KSH01A−113−25

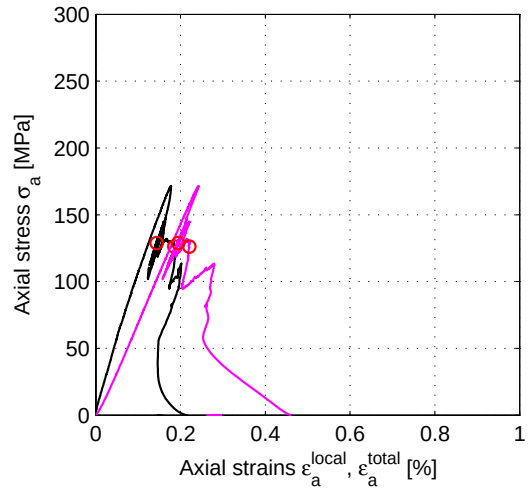

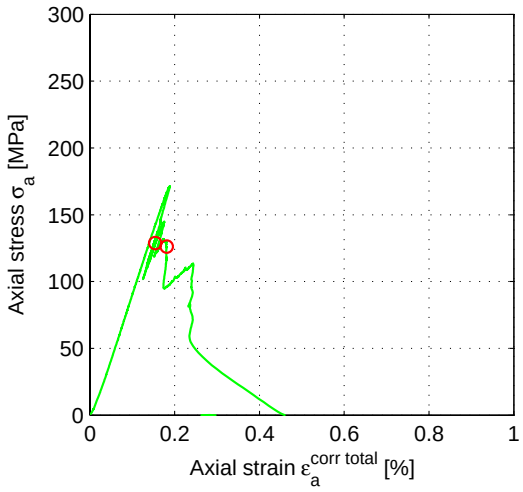

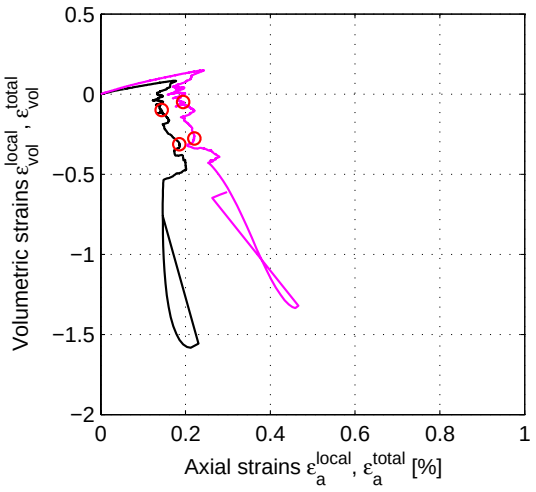

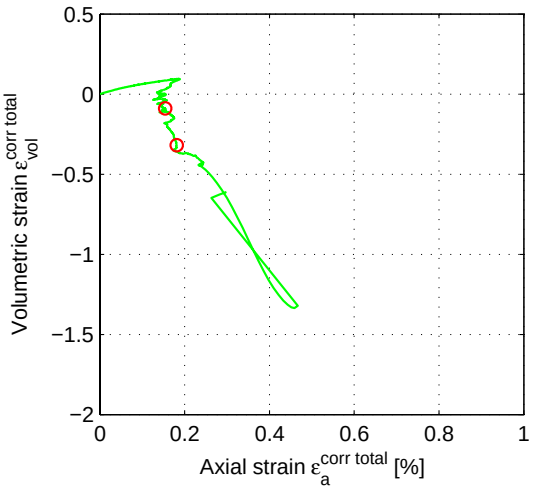

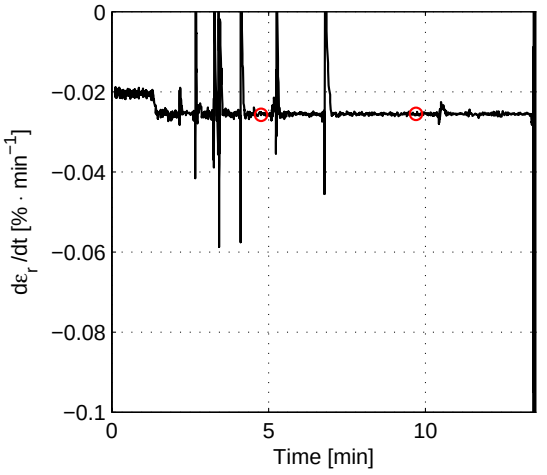

Explanation to curves above:

Based on local deformation (black)

Based on total deformation (mangenta)

Based on corrected deformation (green)

Calculated system stiffness:

K_{system} = 4.9127 [MN/m]

Specimen ID: KSH01A−113−28

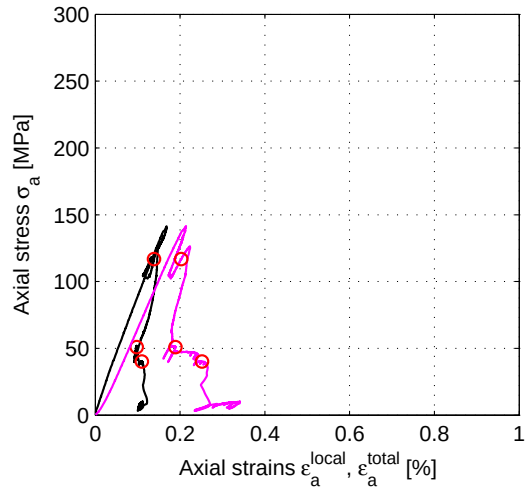

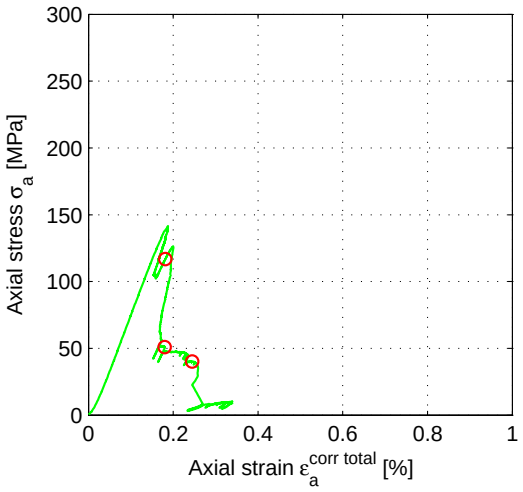

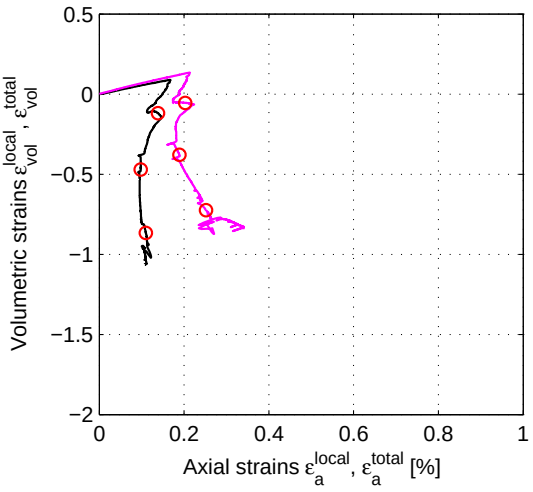

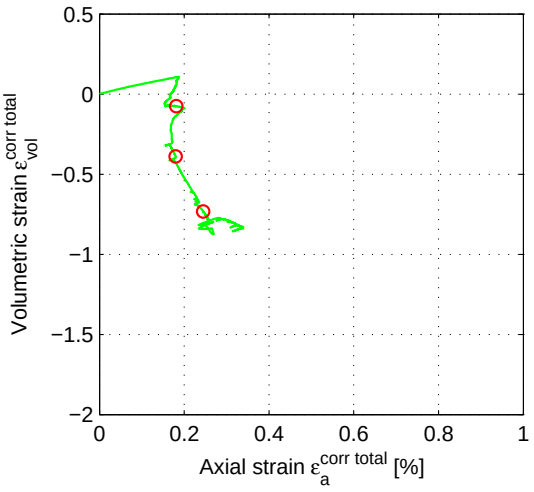

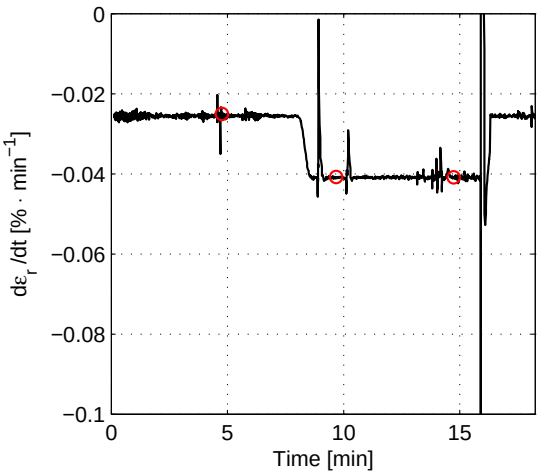

Explanation to curves above:

Based on local deformation (black)

Based on total deformation (mangenta)

Based on corrected deformation (green)

Calculated system stiffness:

K_{system} = 8.3898 [MN/m]

Specimen ID: KSH01A−113−29

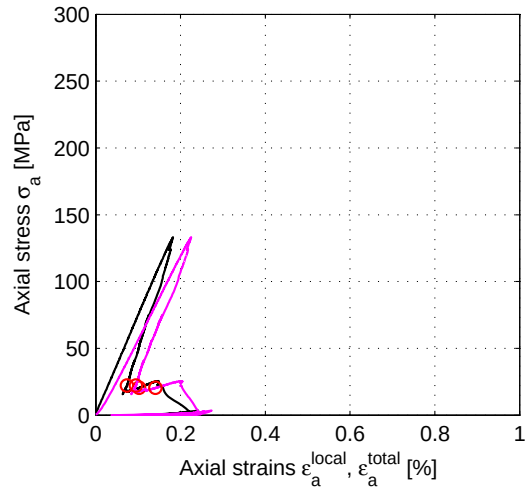

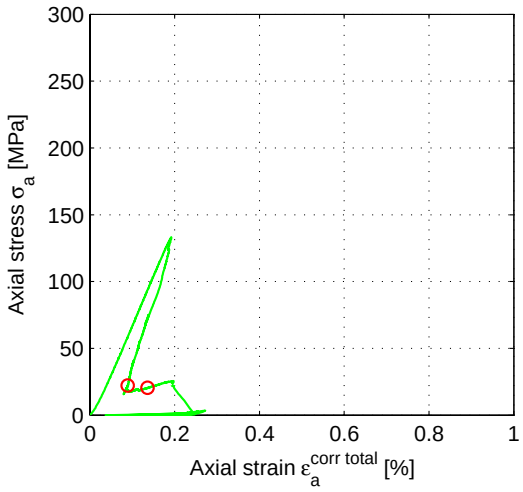

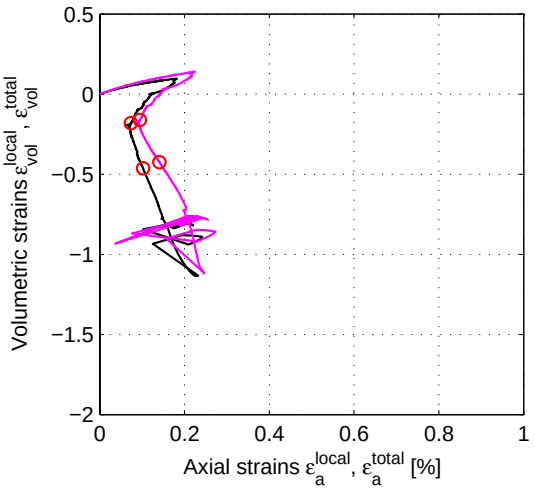

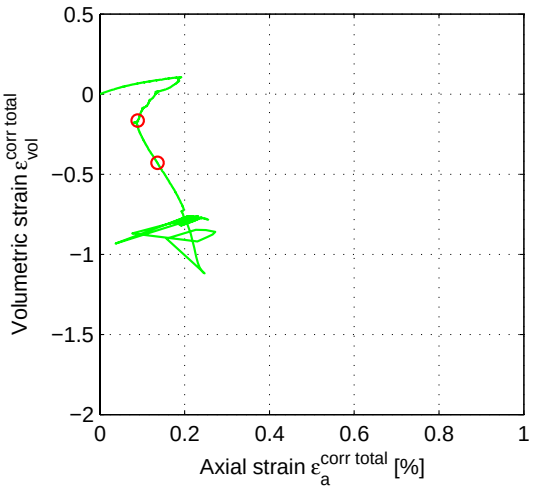

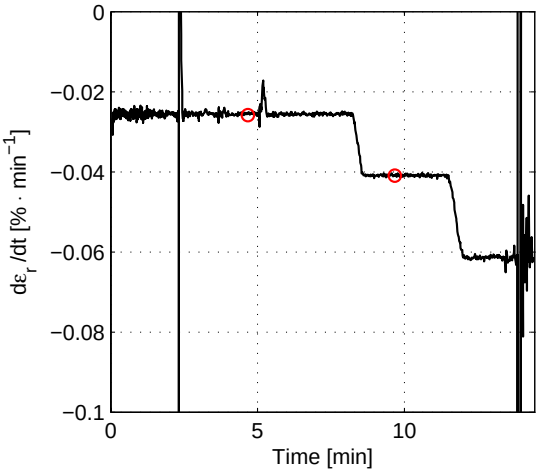

Explanation to curves above:

Based on local deformation (black)

Based on total deformation (mangenta)

Based on corrected deformation (green)

Calculated system stiffness:

K_{system} = 6.2605 [MN/m]

Specimen ID: KSH01A−113−30

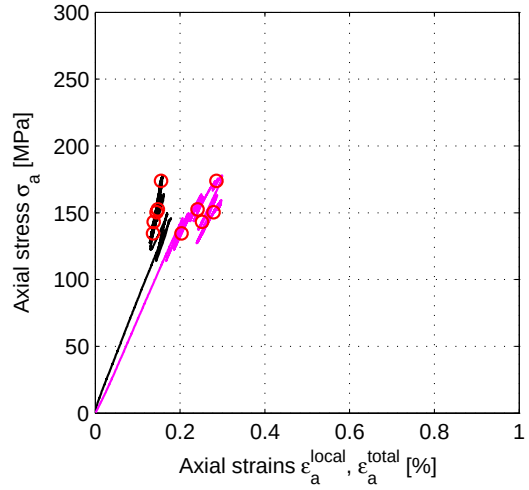

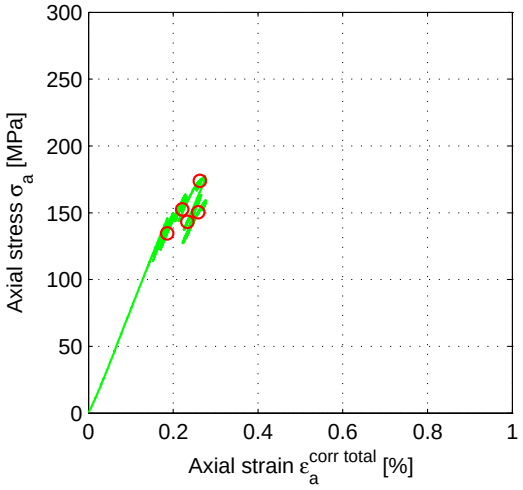

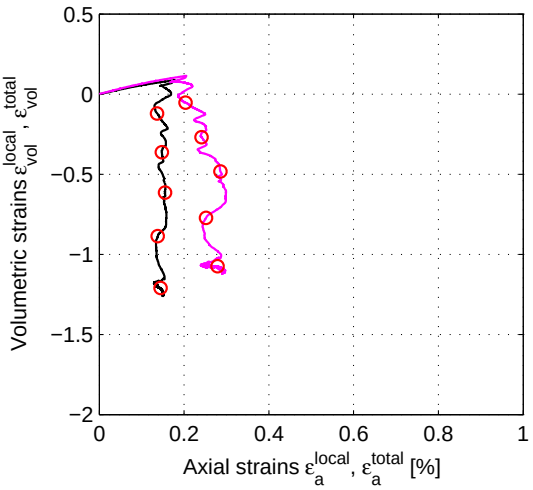

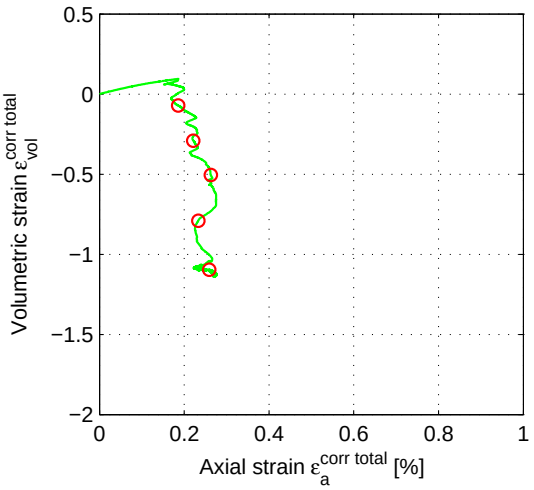

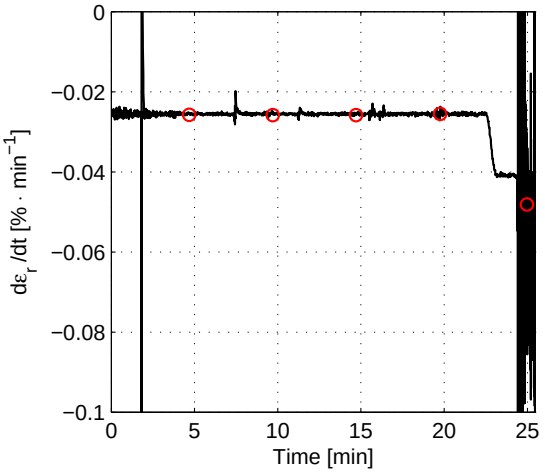

Explanation to curves above:

Based on local deformation (black)

Based on total deformation (mangenta)

Based on corrected deformation (green)

Calculated system stiffness:

K_{system} = 11.7183 [MN/m]

Specimen ID: KSH01A−113−31

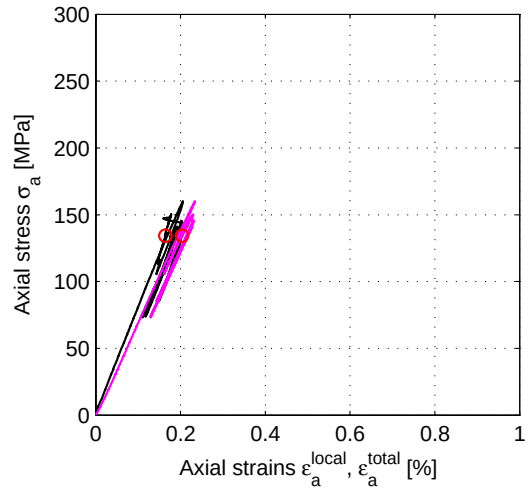

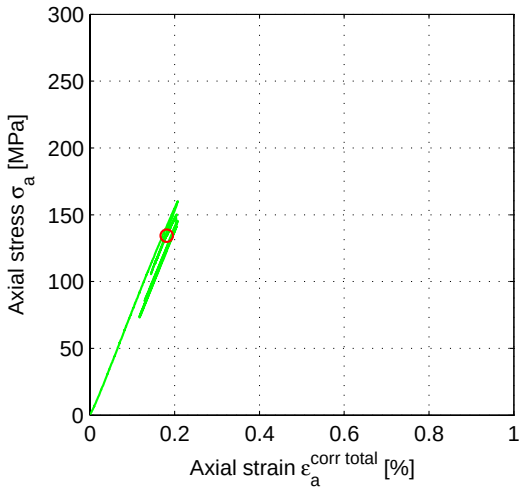

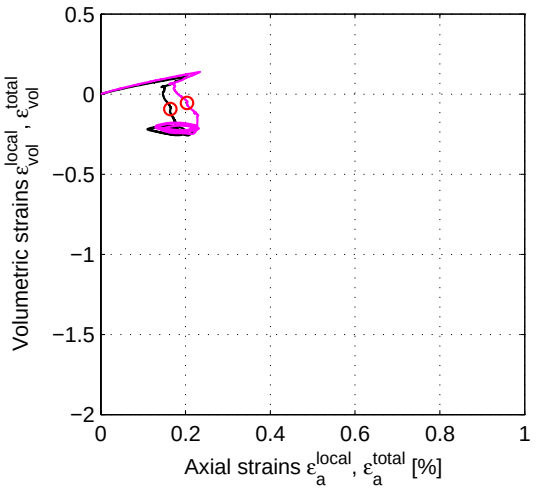

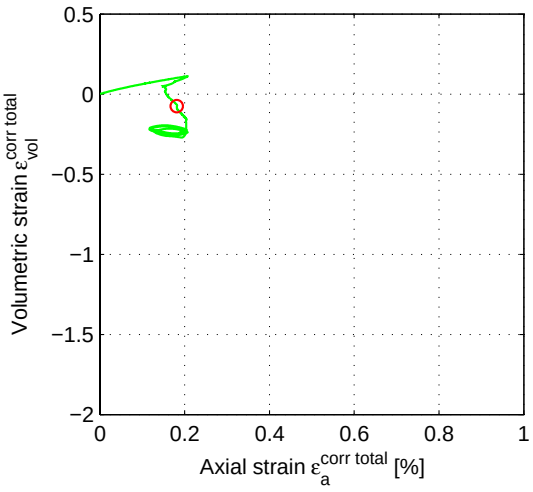

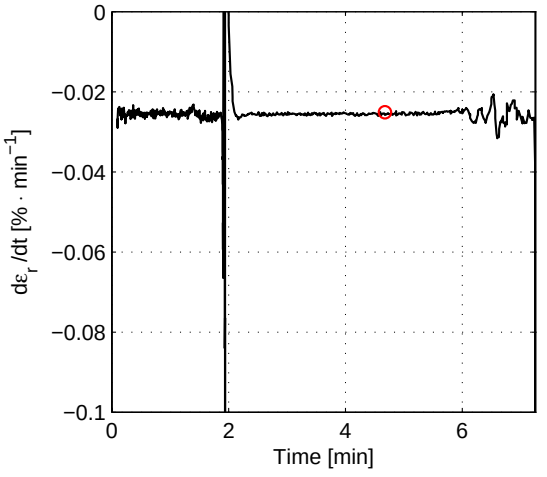

Explanation to curves above:

Based on local deformation (black)

Based on total deformation (mangenta)

Based on corrected deformation (green)

Calculated system stiffness:

K_{system} = 9.3602 [MN/m]

Specimen ID: KSH01A−113−32

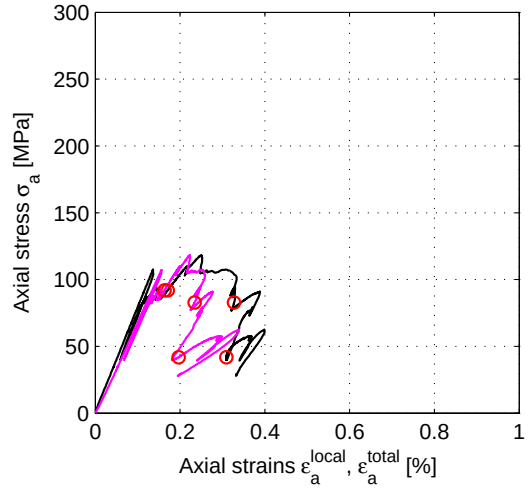

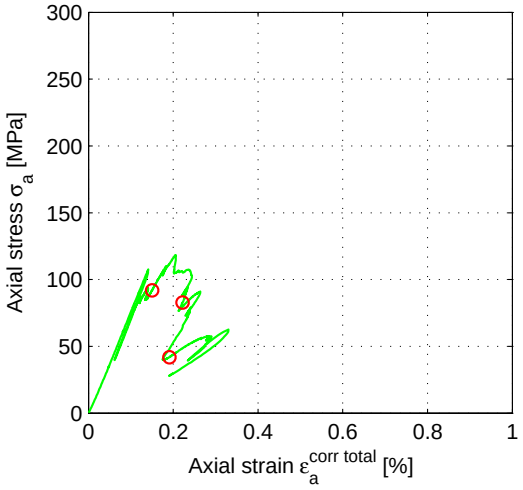

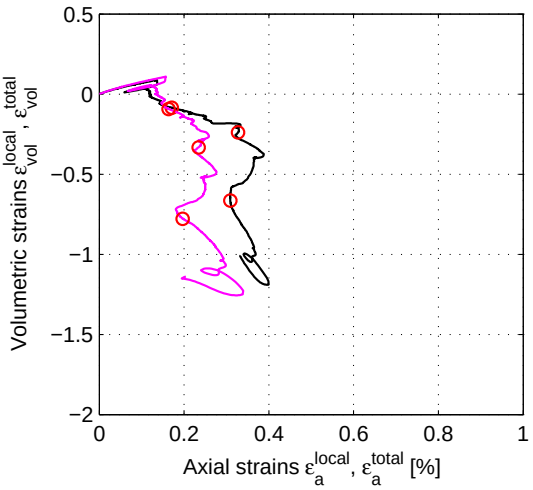

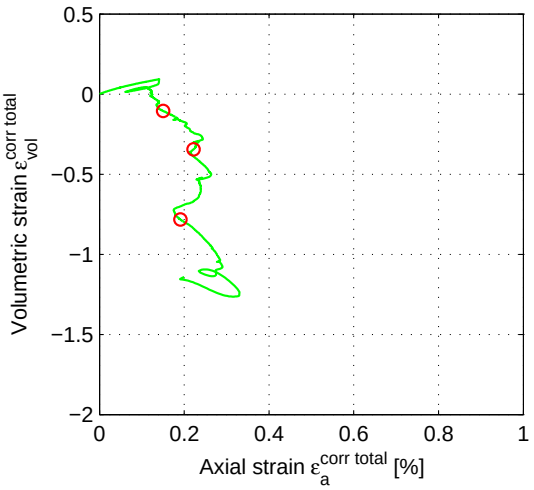

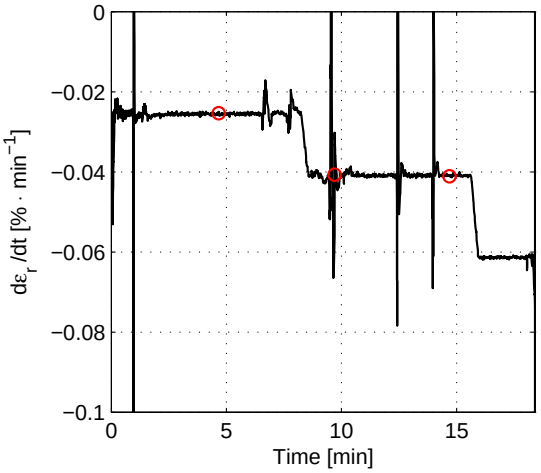

Explanation to curves above:

Based on local deformation (black)

Based on total deformation (mangenta)

Based on corrected deformation (green)

Calculated system stiffness:

K_{system} = 10.7387 [MN/m]